Microbial-driven phosphate flux via polyphosphate accumulation in the benthic layer

Dissertation

to obtain the degree of

Doctor of Natural Sciences (Dr. rer. nat.)

from the Faculty of Mathematics and Natural Sciences

at the University of Rostock, Germany

Submitted by

Simeon Enyi Choo

born in the Republic of Singapore

Hanseatic and University City of Rostock, March 2023

https://doi.org/10.18453/rosdok_id00004393

Date of Submission: 14.04.2023

Date of Defense: 07.07.2023

Reviewers:

Prof. Dr. Heide Schulz-Vogt

Geomicrobiology, Department of Biological Oceanography

Leibniz Institute for Baltic Sea Research Warnemünde

Prof. Dr. Andreas Schramm

Microbiology, Department of Biology

Aarhus University

Sometimes just getting up and carrying on is brave and magnificent.

-Charlie Mackesy, *The Boy, The Mole, The Fox and The Horse*

Table of Contents

Summary

Polyphosphate is believed to contribute significantly to the phosphorus cycle in certain environments. In recent decades, an increasing number of studies have suggested that polyphosphate-accumulating organisms could influence the aquatic phosphorus flux in both the water column and the benthic layer. However, it is still not clearly understood how the storage of polyphosphate by these organisms affect the PO_4^{3-} concentration in the water. Therefore, this thesis aims to assess the impact of a polyphosphate-accumulating microbial mat on dissolved PO_4^{3-} concentration in the natural environment, compute the relationship between microbial PO_4^{3-} uptake and polyphosphate accumulation by constructing a mass balance, as well as determine the effect of stressors on PO_4^{3-} uptake and the storage of polyphosphate. We explored these objectives by implementing three work packages: (1) Carrying out an incubation experiment with environmental short peat core samples to demonstrate the effect of a polyphosphate-accumulating microbial mat on the phosphate flux at the benthic layer under various environmental conditions, (2) acclimating and enriching the microbial mat in the lab, and subsequently (3) carrying out an incubation experiment with the enriched microbial mat samples to determine the relationship between microbial PO_4^{3-} uptake and polyphosphate accumulation, again under different conditions. The focal sampling site in this doctoral study was Karrendorfer Wiesen, a rewetted peatland on the German Baltic Sea coast. Declines in bottom water PO_4^{3-} concentration were recorded in treatments where a microbial mat had formed (summer and winter) but not in the mat-deficient fall treatment. The mats were densely populated with polyphosphate-rich *Lyngbya* sp. filaments. To examine the effect of the mat on ambient PO_4^{3-} concentration, pieces of microbial mat were collected from the study site and grown in a lab culture. Incubations were then carried out to determine the phosphorus response of the cultured mat under varying conditions, and a phosphorus budget was constructed to relate the contribution of microbial polyphosphate to the difference in dissolved PO_4^{3-} concentration over time. These results reveal that microbial polyphosphate storage is capable of significantly influencing the phosphorus flux, which has implications for the phosphorus cycle, especially in highly eutrophic regions.

Zusammenfassung

Man geht davon aus, dass Polyphosphat in bestimmten Umgebungen wesentlich zum Phosphorkreislauf beiträgt. In den letzten Jahrzehnten haben immer mehr Studien gezeigt, dass polyphosphatakkumulierende Organismen den Phosphorfluss im Wasser sowohl in der Wassersäule als auch in der benthischen Schicht beeinflussen könnten. Es ist jedoch immer noch nicht klar, wie die Speicherung von Polyphosphat durch diese Organismen die PO_4^{3-}-Konzentration im Wasser beeinflusst. Ziel dieser Arbeit ist es daher, die Auswirkungen einer polyphosphatakkumulierenden mikrobiellen Matte auf die Konzentration von gelöstem PO_4^{3-} in der natürlichen Umgebung zu bewerten, die Beziehung zwischen mikrobieller PO_4^{3-}-Aufnahme und Polyphosphatakkumulation durch Erstellung einer Massenbilanz zu berechnen sowie die Auswirkungen von Stressfaktoren auf die PO_4^{3-}-Aufnahme und die Speicherung von Polyphosphat zu bestimmen. Diese Ziele wurden in drei Arbeitspaketen verfolgt: (1) Durchführung eines Inkubationsexperiments mit kurzen Torf-kernen aus der Umwelt, um die Wirkung einer polyphosphatakkumulierenden Bakterienmatte auf den Phosphatfluss in der benthischen Schicht unter verschiedenen Umweltbedingungen zu untersuchen, (2) Akklimatisierung und Anreicherung der mikrobiellen Matte im Labor und anschließend (3) Durchführung eines Inkubationsexperiments mit den angereicherten mikrobiellen Matteproben, um die Beziehung zwischen mikrobieller PO_4^{3-}-Aufnahme und Polyphosphatakkumulation, wiederum unter verschiedenen Bedingungen, zu bestimmen. Die Probenahmestelle in dieser Doktorarbeit waren die Karrendorfer Wiesen, ein wiedervernässtes Moorgebiet an der deutschen Ostseeküste. Ein Rückgang der PO_4^{3-}-Konzentration im Bodenwasser wurde bei den Ansätzen festgestellt, bei denen sich eine mikrobielle Matte gebildet hatte (Sommer und Winter), nicht jedoch bei dem Herbst-Ansatz ohne Matte. Die Matten waren dicht mit polyphosphatreichen *Lyngbya* sp.-Filamenten besiedelt. Um die Auswirkung der Matte auf die PO_4^{3-}-Konzentration in der Umgebung eindeutig zu untersuchen, wurden Stücke der mikrobiellen Matte von der Untersuchungsstelle entnommen und als Laborkultur gezüchtet. Anschließend wurden Inkubationen durchgeführt, um die Phosphorreaktion der kultivierten Matte unter verschiedenen Bedingungen zu untersuchen, und es wurde ein Phosphorbudget erstellt, um den Beitrag von mikrobiellem Polyphosphat zu den Unterschieden in der Konzentration von gelöstem PO_4^{3-} im Laufe der Zeit in Beziehung zu setzen. Diese Ergebnisse zeigen, dass die mikrobielle Polyphosphatspeicherung in der Lage ist, den Phosphorfluss erheblich zu beeinflussen, was sich auf den Phosphorkreislauf auswirkt, insbesondere in stark eutrophierten Regionen.

1 Introduction

1.1 Phosphorus cycling in sediments

Phosphorus (P) is generally considered to be the limiting nutrient in the aquatic environment. For this reason, the availability of P controls the growth of primary producers such as plants and algae as well as microorganisms which assimilate P for growth, in turn providing a source of P for other organisms higher up in the food chain. Aquatic sediments are a settling ground for both labile and refractory P fractions, whether organic or inorganic (Sundby et al. 1992). Refractory forms of P are permanently buried, while labile forms of P such as those loosely bound to sediment, soluble reactive phosphate (SRP), and metal-bound P can be transformed via changes in reduction potential, pH as well as kinetics (James et al. 2002). Other labile forms such as labile organic P are broken down via organic matter degradation (Harrison 1982). While microbial-driven organic matter degradation is a major driver of P release in the sediments, the process of redox-sensitive P adsorption-desorption can have a dominant role in calcium (Ca) carbonate and iron (Fe) oxide-rich sediment (Gonsiorczyk et al. 1998). The coupling of the elemental cycles is a strong driver of P release, especially in seasonally hypoxic or anoxic environments. Under oxic conditions, dissolved inorganic P can precipitate as Fe or Ca-bound P in the sediment, while anoxic conditions lead to the reductive dissolution of metal ions and the desorption of P (Yu et al. 2017).

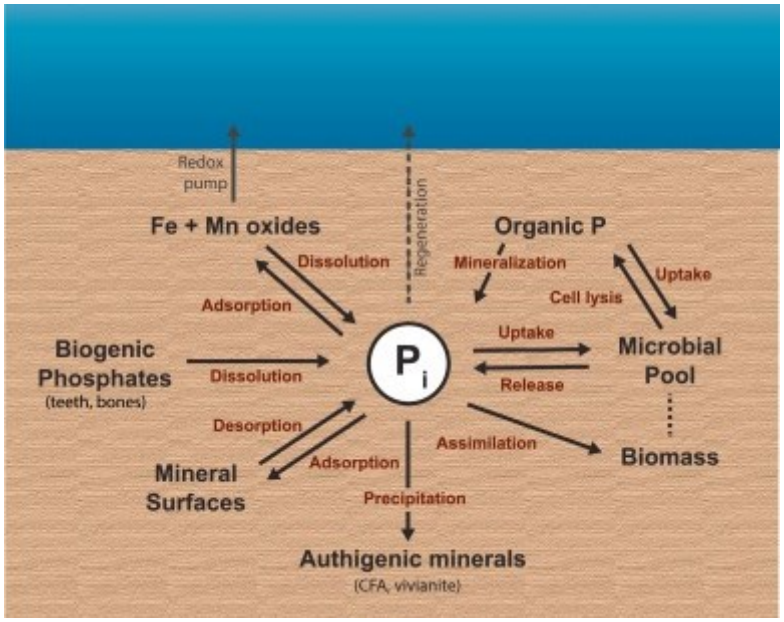

Fig. 1. General overview of the P cycle in marine sediments. Dissolved inorganic P is referred to as P_i, and CFA refers to authigenic carbonate fluorapatite. Figure credit: Defforey & Paytan 2018

Phosphorus which is released from both organic matter degradation and reduced metal compounds can ultimately precipitate in either temporary or more permanent P sinks (Fig. 1). The temporary burial of P is mainly believed to be in the form of P adsorbed to metal compounds such as Fe oxyhydroxides and calcite, which is then desorbed during progressively reducing conditions (Defforey & Paytan 2018, Sulu-Gambari et al. 2018). On the other hand, permanent sinks for P in marine sediments can be in the form of authigenic carbonate fluorapatite and phosphorite (Delaney 1998, Joshi et al. 2015, Sulu-Gambari et al. 2018), while in brackish systems, authigenic P forms such as manganese (Mn) phosphate and Fe-P can be significantly present in the form of vivianite, if sulfide levels are low (Wilfert et al. 2020, Kubeneck et al. 2021).

1.2 Role of microbial P-fixation in P cycling

Nonetheless, our current understanding of the contributors to the P cycle is still inadequate. Over the last few decades, several studies have indicated the role of microbial P-fixation in sedimentary P cycling. For instance, benthic bacteria might stimulate P regeneration and burial in the surface sediment layer by converting organic P from settling particles into refractory organic P such as inositol hexakisphosphates (Gächter & Meyer 1993, Ingall & Jahnke 1997, Jørgensen et al. 2011). The P cycle is also regulated by the accumulation and metabolism of microbial polyphosphate (polyP); however, this contribution is still understudied (Dale et al. 2016). Nevertheless, there is increasing interest in understanding the effect of microbial phosphorus accumulation and release on the P flux in the sediment surface layer. PolyP-accumulating bacteria can take up large amounts of P and accumulate it as polyP. The accumulated polyP is mainly stored in membrane-bound organelles called acido-calcisomes; and with polyP being an inorganic polymer composed of multiple phosphate residues joined together by high-energy phosphoanhydride bonds, the acidocalcisomes function as an energy source (ATP generation) or PO_4^{3-} reservoir during periods of P deprivation (Sanz-Luque et al. 2020). In certain regions such as the Benguela Upwelling System, microorganisms such as the large sulfur bacteria *Thiomargarita namibiensis* can take up and accumulate a huge amount of inorganic P under anoxic conditions, by utilizing stored nitrate as the primary electron acceptor (Schulz & Schulz 2005). The accumulated inorganic P is subsequently precipitated on stored polyP, resulting in crystallization to hydroxyapatite (Goldhammer et al. 2010). Furthermore, the release of P by populations of *T. namibiensis* was able to generate sharp spikes in porewater PO_4^{3-} concentration of close to 300 μmol L^{-1}, which

could create a suitable condition for the precipitation of hydroxyapatite and the subsequent formation of phosphorite deposits in the sediment (Schulz & Schulz 2005).

In other regions such as the Black Sea and Lake Pavin, magnetotactic bacteria are postulated to contribute to the P flux in the water column and sediment, respectively (Rivas-Lamelo et al. 2017, Schulz-Vogt et al. 2019). A bacterial phosphate shuttle has been proposed within the suboxic zone in the waters of the Black Sea, where large magnetotactic bacteria take up PO_4^{3-} at the upper layer, subsequently releasing it at the lower boundary of the suboxic zone. It is suggested that this process contributes significantly to the phosphorus peak at the lower boundary since these bacteria are estimated to have a 100× larger polyP storage capacity than average-sized bacteria such as *Sulfurimonas gotlandica*. In addition to size, the microbial quantity might also influence aquatic P concentration. PolyP-accumulating filamentous cyanobacteria of the genus *Lyngbya* (the main bacteria examined in this doctoral study) form dense algal blooms (Arthur et al. 2009), which could potentially sequester a significant amount of PO_4^{3-} from the water column.

1.3 Challenges in determining microbial polyP contribution to the P cycle

Several studies have proposed that microbial polyP cycling represents a significant contribution to the aquatic P cycle. In a modified diagenetic model, P burial was ~30% lower in sediments without a polyP-driven microbial P pump when compared to the baseline model (Dale et al. 2016). In certain aquatic environments, polyP also made up a noticeable proportion of total P in the surface sediment (Sannigrahi & Ingall 2005, Watson et al. 2018). However, the extent to which microbial polyP accumulation and breakdown influence the P cycle remains unknown.

To the best of our knowledge, a constructed mass-balance budget relating microbial polyP to PO_4^{3-} uptake is still lacking, mainly a result of a shortage of reasonably simple and accurate polyP quantification methods. For example, ^{31}P Nuclear Magnetic Resonance Spectroscopy (NMR) is one of the most common methods for polyP quantification (Hupfer et al. 1995). However, the instrumentation is expensive, large sample sizes and high sample concentrations are required, and the sensitivity of this method in certain sample types (e.g., metal cation-bound polyP in solid granules) might be low (Hupfer & Lewandowski 2008, Christ et al. 2020).

In general, an initial polyP extraction and purification step is also required for most quantification methods, especially for protocols with low specificity for polyP detection.

Complications can arise in this initial step, where for example, alkaline extractions might only partially extract polyP (Hupfer & Lewandowski 2008), even hydrolyzing or degrading polyP, resulting in shortened chain lengths (Ahlgren et al. 2011). The subsequent purification of extracted polyP can further decrease yields (Kulakova et al. 2011). In our current study, the main challenge faced during polyP extraction was overcoming the high resilience of the cyanobacterial cell wall. Therefore, our microbial mat samples underwent multiple cycles of freeze-thaw treatment to achieve sufficient cell lysis.

Moreover, the chain lengths of polyP molecules in both lab and environmental samples can vary widely, and only a portion of current methods can cover the measurement of all chain lengths in a sample (Christ et al. 2020). For example, methods including polyP-binding dyes (e.g., 4',6-diamidino-2-phenylindole or DAPI, toluidine blue O), polyacrylamide gel electrophoresis, light microscopy, and flow cytometry are only able to detect polyP molecules with chain lengths longer than 15 P-subunits, which might lead to an underestimation in the total polyP concentration in a sample.

Another challenge in polyP quantification is that not all methods have high specificity for polyP detection. High-specificity methods such as ^{31}P NMR, enzyme assays, and Raman microscopy can detect polyP unambiguously (Christ et al. 2020). Medium-specificity methods such as Fourier transform infrared spectroscopy, fluorescence spectroscopy, and flow cytometry can mostly detect polyP, but might also introduce matrix effects into the final result by co-quantifying other compounds. Low-specificity methods such as chromatography, end group titration, and capillary electrophoresis detect all components in a sample but are inefficient at discriminating between specific compounds. Currently, only 30% of methods display a high specificity, another 40% show medium specificity and the remainder have low specificity for polyP detection (Pokhrel et al. 2019, Christ et al. 2020).

1.4 Thesis focus

Microbial P cycling supports a significant portion of P turnover in wetlands. In recent years, the importance of microbial polyP in P cycling has gradually been acknowledged (McMahon & Read 2013, Dale et al. 2016, Li & Dittrich 2019); however, the extent to which the PO_4^{3-} concentration in bottom waters is affected by microbial PO_4^{3-} uptake and release at the sediment-water interface is still unknown. Furthermore, there is uncertainty about the impact of changing environmental conditions on this mechanism. In this thesis and as part of the Baltic TRANSCOAST project, we aimed to elucidate the effect of polyP accumulation in the

benthic microbial mat on the bottom water PO_4^{3-} concentration in a coastal peatland of the southern Baltic Sea. In work package (WP) 1, we investigated the effect of mat-forming bacteria on the benthic P flux in a rewetted coastal fen. During preliminary sampling, polyP-accumulating microbial mats were discovered at the surface peat layer, which mostly comprised filamentous cyanobacteria of the genus *Lyngbya*. The size of the mats showed seasonal variation: being the largest in February – June (winter – early summer), and greatly reduced in August – November (late summer – fall). Since the fen is exposed to varying environmental conditions, we examined the P response of the microbial mat under *in-situ*, elevated temperature, and oxygen-depleted conditions. Through a series of lab incubations of short peat cores (with overlying water), we showed that the presence of a microbial mat community could regulate the bottom water PO_4^{3-} concentration in the short-term, as well as mitigate increases in concentration via PO_4^{3-} release mechanisms such as organic matter remineralization and Fe-bound P release. An increase in microbial polyP content during PO_4^{3-} removal from the bottom water was also recorded, suggesting that microbial P sequestration affected bottom water PO_4^{3-} levels. Through DAPI-based fluorescence microscopy, we discovered that the bulk of polyP in the microbial mat was stored in filamentous cyanobacteria. To study the effect of the microbial mat on PO_4^{3-} concentration without interference from other P cycling mechanisms, we collected microbial mat samples from the study site to be established in a stable lab culture, as part of WP 2. Through the setting up of a stable culture, we were able to investigate the ability of the filament-rich microbial mat to take up and assimilate PO_4^{3-} as polyP under *in-situ* conditions as well as under elevated temperature and reduced salinity stressors in WP 3. From here, we constructed a mass-balance budget to determine the contribution of polyP accumulation to the removal of PO_4^{3-} from the microbial mat's environment, as well as understand how functional redundancy in the microbial mat community contributed to polyP accumulation under various stressors. Ultimately, this study proposes the role of the polyP-accumulating microbial mat as a significant biological sink in the aquatic P cycle amid varying environmental conditions.

2 Materials & Methods

2.1 Study site

The study site was a coastal fen located in Karrendorfer Wiesen, Germany (54.158°N, 13.393°E) (Fig. 2). It is a rewetted peatland covering an estimated 3.5 km^2, with the surrounding region dominated by a salt marsh (Bernhardt & Koch 2003, Seiberling & Stock 2009). Ever since a de-embankment of the fen in 1993, natural flood dynamics were re-established, allowing for frequent flooding of low-lying portions of the fen. This is aided by the fact that the fen is situated next to the Baltic Sea with the shortest distance of approximately 4 m, making it prone to irregular flooding, especially in stormy periods.

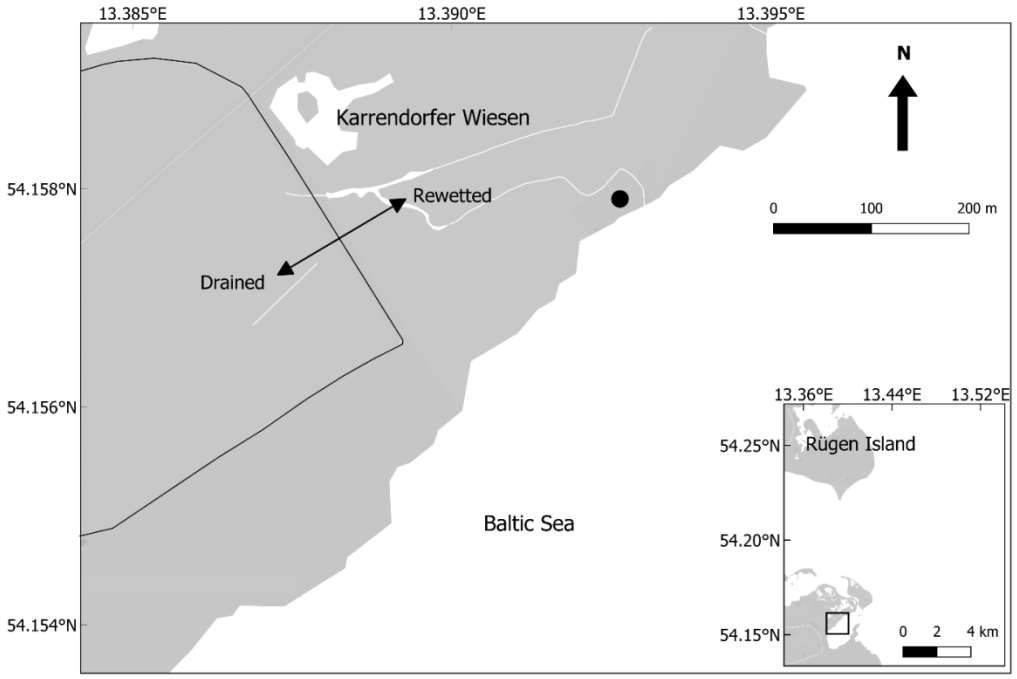

Fig. 2. Sampling area Karrendorfer Wiesen, located in the state of Mecklenburg-Western Pomerania, NE Germany. Short cores were collected at a fen peat (black dot) in the rewetted zone

For most of the year, the study site is fed by rainwater, except in late summer when precipitation is at its lowest. A mixture of marsh plant debris (e.g., reed stalks, spindly leaves) and peat soil constitute the fen's surface layer (Fig. 3). The site's temperature varies throughout the year, typically between 0 °C (winter) and 31 °C (summer). Our study data also indicated strong salinity fluctuations at the site, with 5.1 psu in late January and 18.7 psu in late July (Choo et al. 2022).

Fig. 3. Flooded study site in Karrendorfer Wiesen, which is surrounded by a salt marsh. The surface layer of the fen is covered by a mixture of marsh plant debris such as reed stalks and spindly leaves

2.2 Field sampling

2.2.1 Collection of short peat cores

At the study site, short peat cores were collected for the incubation experiments in winter (February 2020), summer (June 2020), and fall (October 2020). The temperature, dissolved oxygen, and conductivity of the bottom water were measured on-site using a Hach HQ40D Portable Multimeter, which includes a built-in function for salinity determination (Table 1). The acrylic tubes used to obtain the cores each had a length of 20 cm and an inner diameter of 7 cm. During core collection, a tube was manually drilled into the peat to an estimated depth of 10 cm. To minimize disturbances to the benthic layer, we jointly retrieved peat and supernatant water (mentioned as bottom water in this thesis) in the same tube.

An additional 8 short peat cores were jointly collected with the above-mentioned cores during the winter experiment, to determine the peat's total P and Fe content. From each core, the upper 1 cm peat layer was extracted, homogenized, and kept in a 50 mL Falcon tube. A sub-sample was then taken from each tube and weighed, then freeze-dried for 48 hours. The freeze-dried sub-sample was weighed to calculate water content and then homogenized using an agate mortar. Each sub-sample was taken as a replicate.

Table 1. Temperature, salinity, pH, and oxygen levels at the time of core collection at the study site in the winter, summer, and fall

Season	Temperature (°C)	Salinity (psu)	pH	Oxygen (µmol L^{-1})
Winter	5.9	5.8	7.3	422
Summer	15.2	11.5	5.6	238
Fall	13.7	7.8	6.9	338

2.2.2 Collecting microbial mat for laboratory cultivation

In late spring (May 2021), microbial mats were collected at 5 different points along the water's edge of the study site. The temperature, salinity, and oxygen content measured on-site were 7.6 °C, 9.5 psu, and 353 µmol L^{-1}, respectively. The mat pieces were then placed in 15 mL tubes (one tube for each collection point), and the tubes were filled up with water from the study site. The tubes were then brought back to the laboratory and incubated by a window at room temperature (19 – 22 °C) for a total of 10 days, to allow the mats to acclimatize to laboratory conditions. At the end of the incubation, only one tube displayed a slight enrichment of *Lyngbya* sp. filaments and was therefore used as the source culture for subsequent cultivation tests.

2.3 Incubation of short peat cores

Incubation of the short peat cores (with bottom water) took place in INFORS HT Multitron Pro incubation chambers for either 8 or 10-day periods, subject to various treatments (Table 2). The first day of incubation was denoted by Day 0. The water temperature at the time of core collection at the study site (during each season) was designated as the *in-situ* temperature during the incubations. The "*in-situ* temperature + 10 °C" treatment consisted of cores that were incubated at 10 °C higher than the *in-situ* temperature. In the fall, an oxygen-depleted incubation displaying a permanently reduced microbial mat was installed as a negative control, to determine the impact of reduced microbial PO_4^{3-} uptake on the bottom water PO_4^{3-} concentration. In each seasonal treatment, the *in-situ* temperature was: winter, 5 °C; summer, 15 °C; fall, 5 °C. Cores were set up in triplicates in each treatment (Fig. 4).

Table 2. Incubation treatments (8 – 10 days) of short cores collected in winter, summer, and fall in 2020 (n = 3) from Karrendorfer Wiesen, to examine the impact of elevated temperature and oxygen depletion on dissolved PO_4^{3-} turnover. OX: aerobic; OD: oxygen-depleted; number refers to temperature

Season	Treatment		
	Aerobic, *in-situ* temperature	**Aerobic, *in-situ* temperature + 10 °C**	**Oxygen-depleted, *in-situ* temperature**
Winter	WinterOX5	WinterOX15	WinterOD5
Summer	SummerOX15	SummerOX25	SummerOD15
Fall	-	-	FallOD5 (negative control)

Oxygenated conditions were maintained in aerobically-treated short cores via constant light exposure, to stimulate photosynthetic activity and oxygen production. Photosynthetic activity was limited within the peat layer of the core by concealing it with aluminum foil (Fig. 4). In oxygen-depleted treatment cores, hypoxic conditions were attained by bubbling pure nitrogen gas (N_2) for 20 – 25 min into the water column to reach an approximate oxygen concentration of 53 µmol L^{-1}, just before incubation began. The oxygen content in the cores was not tracked during the incubation; nevertheless, the cores were set in complete darkness to prevent photosynthetic activity and maintain oxygen-depleted conditions. To preserve oxygen-depleted conditions after daily bottom water sampling (12 mL), the water column was refilled with N_2-bubbled water derived from the study site. The top of the core was then capped with a glass lid and sealed with industrial-grade silicone to prevent gaseous exchange between the core and the external environment. Throughout the incubations, the pH of the 3 seasonal experiments ranged from 5.8 – 7.5. Cores in the summer treatment were incubated in the same manner as in the winter and fall treatments, except that the upper 1 cm layer of peat (including the microbial mat) was removed from all summer cores at the end of Day 2. Since we hypothesized that the mat could regulate the benthic dissolved P flux, the removal was carried out to investigate if a reduced microbial mat would result in an increased bottom water PO_4^{3-} concentration. In addition, the effects of a potential mat re-establishment could also be studied. After removal, 3 sub-samples were extracted from each summer core and visualized under light microscopy, to ensure that the microbial mat had been sufficiently removed.

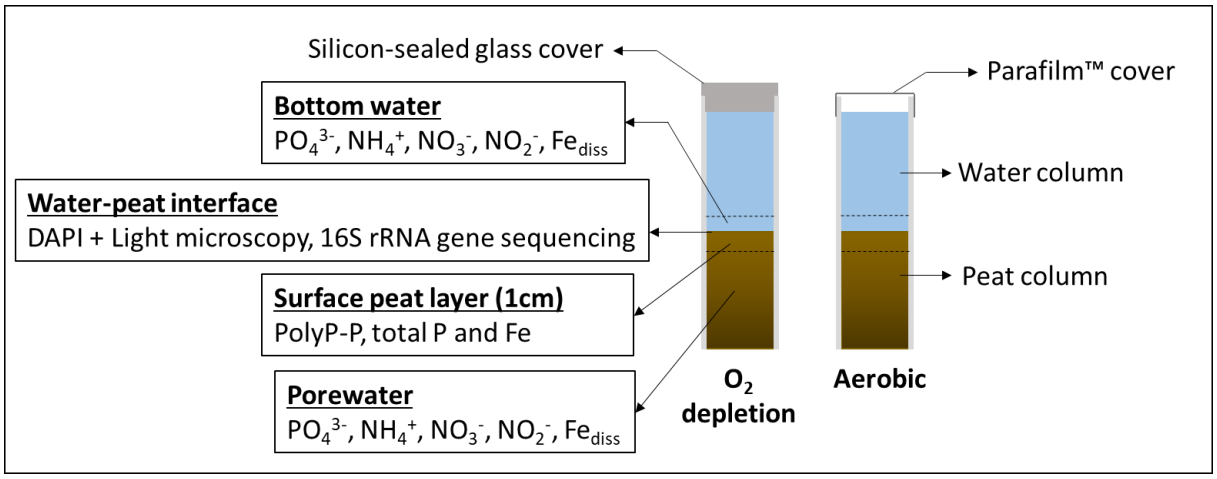

Fig. 4. Core features and the measured parameters. Bottom water, porewater, water-peat interface, and surface peat layer sub-samples were extracted on either a daily or one-time basis from all cores. In the summer treatment cores, the upper 1 cm peat layer was removed on Day 2 to eliminate a significant portion of the microbial mat, and trigger the release of porewater PO_4^{3-} to the bottom water. The peat and water depth in the cores ranged from 11−13 and 9−11 cm, respectively, during the study. Fe_{diss}: dissolved Fe

2.4 Sub-sampling of short peat cores

Winter treatment cores from both Day 0 and the last day were each sliced at peat depths of 0 – 0.7 cm and 0.7 – 1.4 cm to retrieve peat sub-samples, which were then homogenized. From each homogenized sub-sample, approximately 2 mL of peat was obtained for downstream microscopy, geochemical analyses, and polyP-P quantification. In all seasonal incubations, 12 mL of bottom water was extracted daily from each treatment core and filtered through a Whatman® glass microfiber filter (GF/F grade, 25 mm diameter), to be used for determining dissolved inorganic nutrients and Fe levels. Before extraction, the bottom water was gently homogenized with a flat-surfaced plastic stirrer, ensuring minimal disturbance to the surface peat layer. From the filtered bottom water, 2 mL was aliquoted into reaction tubes (volume: 2 mL), acidified with concentrated HNO_3 to 2 vol%, and stored at -20 °C for the subsequent measurement of dissolved P and Fe. The dissolved nutrient and Fe concentrations were later corrected for the decreasing water volume in the core.

Porewater samples (also for dissolved P and Fe measurement) were obtained on Day 0 and the last day of incubation. The porewater was extracted at peat depths of 0.8 cm and 1.5 cm, using rhizons (Seeberg-Elverfeldt et al. 2005; Rhizon CSS 19.21.23F pore size 0.15 µm, Rhizosphere Research Products), and treated in the same manner as the bottom water aliquots.

2.5 Nutrient measurement and analysis

2.5.1 Dissolved inorganic nutrient measurements

A colorimetric measurement was done on bottom water and porewater samples to determine the concentrations of dissolved PO_4^{3-}, ammonium (NH_4^+), nitrate (NO_3^-), and nitrite (NO_2^-) (Hansen & Koroleff 1999). The measurement was conducted with a Seal Analytical QuAAtro constant flow analyzer, with a precision of 2.0% PO_4^{3-} and 3.1% NO_x (i.e., NO_3^- + NO_2^-) (Krause et al. 2021).

2.5.2 Calculation of diffusive PO_4^{3-} fluxes

The bottom water and porewater PO_4^{3-} values (Table 3) were used to calculate the PO_4^{3-} diffusive flux from the surface peat layer into the overlying bottom water, by applying Fick's First Law. The PO_4^{3-} diffusion coefficients were corrected for temperature, salinity, and porosity (Fig. S1) (Boudreau 1997, Berg et al. 1998, Schulz & Zabel 2006). Porosity values were determined according to Flemming & Delafontaine (2000), applying the mean moisture content and dry bulk density of the aforementioned 8 peat sub-samples (Section 2.2.1).

Table 3. The concentration of PO_4^{3-} at 2 peat depths and resultant diffusive fluxes from the peat into the overlying bottom water in Day 0 cores as well as on Day 10 of the 3 winter treatments

	PO_4^{3-} (µmol L^{-1})		**$\frac{dC}{dX}$**	**Flux**
	Bottom water	**Peat depth 1.5 cm**	**(µmol L^{-1} cm^{-1})**	**(µmol cm^{-2} s^{-1})**
Day 0	0.24	7.49	5.18	17×10^{-6}
WinterOX5, Day 10	0.077	1.77	1.21	3.5×10^{-6}
WinterOD5, Day 10	1.25	4.47	2.30	6.7×10^{-6}
WinterOX15, Day 10	1.55	24.4	16.3	68×10^{-6}

2.5.3 Dissolved Fe measurement

The dissolved Fe (Fe_{diss}) concentration in bottom water and porewater samples was determined through inductively coupled plasma–optical emission spectrometry (ICP-OES; iCAP 7400 Duo, Thermo Fisher Scientific) with a salinity-matched calibration using diluted Atlantic Seawater from OSIL. Any remaining matrix effects were removed by using scandium (Sc) as the internal standard. Precision and trueness of the international reference material SLEW-3 (NRCC) spiked with 0.9 and 3.6 µmol L^{-1} Fe_{diss} were 3.7% and 0.5%, respectively. Baltic seawater was used as procedure blanks, to correct the Fe_{diss} concentration in the water column for contamination (0.2 µmol L^{-1}) by the microfiber filters.

2.5.4 Total Fe and P in peat layer samples

The contents of total P, Fe, and Al in the Day 0 peat sub-samples were acid-digested using a HNO_3-HF-$HClO_4$ mixture and analyzed by the same ICP-OES, using external calibration and Sc as the internal standard (Dellwig et al. 2019). Precision and trueness for the international reference material SGR-1b (USGS) were better than 5.7% and -5.4%, respectively.

Since the refractory Fe and P bound to alumosilicates (represented here by Al) are also included in total Fe and P, only a portion of total Fe and P in the samples was potentially available for redox reactions. This portion was deemed the excess Fe (Fe_{xs}) and P (P_{xs}) fractions, which were estimated according to the following formula (Dellwig et al. 2007) using Al (8.84%), Fe (4.83%) and P (0.07%) contents of glacial sediments from the Baltic Sea as the lithogenic background:

$$element_{xs} = element_{sample} - element_{glacial\ Baltic} \times Al_{sample} / Al_{glacial\ Baltic}$$

2.5.5 Automated particle analysis

Fractions were taken from peat sub-samples (depth: 0 – 0.7 cm) that were associated with Day 0 of the winter treatments. The fractions were resuspended and filtered onto Sartorius Stedim white polycarbonate 25 mm membrane filters (pore size: 0.8 µm), which were then dried (21 °C, 24 h) and carbon-coated. Automated particle analysis (SEM-EDX; scanning electron microscopy with energy dispersive X-ray fluorescence) was then performed on the carbon-coated filters (Cardell & Guerra 2016).

2.6 PolyP measurement and visualization

2.6.1 PolyP quantification

The polyP content in the upper 1 cm peat layer of each peat sub-sample from the winter treatment (Day 0 and the last day) was extracted and measured using an optimized version of the DAPI-based fluorescence spectroscopy method by Martin & van Mooy (2013). Due to the rigidity of cyanobacterial cell walls, 7 freeze-thaw cycles (-20, 24 °C) were consecutively carried out on the sub-samples to induce cell lysis. A 10-min bead beating step (glass bead diameter: 0.1 mm; BioSpec Products) was also performed to further disrupt the cellular material in each sub-sample. The sub-samples were then homogenized using a vortex mixer, and 200 µg of material was aliquoted from each sub-sample to measure polyP-P content. PolyP standards (0, 0.11, 0.22, 0.44, 0.88, 1.75, 3.5, and 7 µmol L^{-1}) were prepared using sodium phosphate glass (mean chain length 45 ± 5 P) from Sigma-Aldrich (S4379). DNase (SKU: 4716728001; Roche) and RNase (catalog number: AM2288; Invitrogen™) treatments (37 °C, 10 min) were then performed on both the sub-sample aliquots and the polyP standards to reduce matrix effects caused by the binding of DNA and RNA to DAPI. Proteinase K (catalog number: EO0491; Thermo Scientific™) treatment was then carried out (37 °C, 10 min) on both the aliquots and the standards to degrade proteins that might hinder the DAPI signal. The fluorescence intensity of each DAPI-treated sub-sample and standard was then quantified using the TECAN Infinite 200 PRO (fluorescence top precision <2% CV).

2.6.2 Microscopy of microbial mat

Both light and fluorescence microscopy were performed on surface peat layer sub-samples, to detect the presence of polyP, as well as to examine the morphology of the associated polyP-accumulating microorganisms forming the microbial mat. The microscopy was performed before the commencement of the winter, summer, and fall incubations. In preparation for fluorescence microscopy, samples were filtered onto a Sartorius Stedim black polycarbonate 25 mm membrane filter (pore size: 0.8 µm), and stained with DAPI (concentration: 10 mg L^{-1}) for 3 min. Milli-Q water was then used to flush out residual DAPI on the filter. The underlying mechanism is that polyP molecules form a polyP-DAPI complex which has a maximum fluorescence emission of 525 – 550 nm, displaying a greenish-yellow hue (Gomes et al. 2013). The stained samples were then viewed with a Zeiss Axioskop 2 Mot Plus microscope (360/40 nm excitation). To prepare for light microscopy, a drop of the sample (~100 µL) was pipetted onto a glass slide, and enclosed with a 24 × 60 mm coverslip. Light

microscopy was then performed using the same microscope. Images from both light and fluorescence microscopy were generated and processed using the Zeiss ZEN (blue edition) software.

2.7 Amplicon sequencing of microbial mat

2.7.1 DNA extraction and 16S rRNA sequencing

Two surface peat layer replicates (K1 and K2; 2 mL each) were obtained from the same peat fen (approximately 10 cm distance between the sample collection points), together with the summer incubation cores on Day 0. The replicates underwent RNA extraction using the RNeasy PowerSoil Total RNA Kit (Qiagen), following the manufacturer's instructions. Reverse transcription was then performed on the RNA extracts using the QuantiNova Reverse Transcription Kit (Qiagen) to generate the final cDNA product. Finally, 16S amplicon sequencing of the cDNA was performed on an Illumina MiSeq (2 × 300 bp) by LGC Genomics GmbH (Berlin). The primers used were the modified 341F (CCTAYGGG-RBGCASCAG) and 806R (GGACTACNNGGGTATCTAAT), targeting the V3-V4 regions of the 16S ribosomal DNA (Sundberg et al. 2013).

2.7.2 16S rRNA analysis

The obtained primer-clipped forward and reverse reads were joined using QIIME version 1.9.1 (Caporaso et al. 2010) with minimal overlap of 20 bp, resulting in sequence Multi-Fasta files that were processed by the SILVAngs pipeline (SILVAngs 1.4; Quast et al. 2012), with the pipeline's default settings. Each read was aligned using the SILVA Incremental Aligner (SINA v1.2.10 for ARB SVN, revision 21008; Pruesse et al. 2012) against the SILVA SSU rRNA SEED. Reads shorter than 50 aligned bases and reads with >2% ambiguities or homopolymers were excluded, as these were likely contaminants and artifacts. Chloroplasts, mitochondria, and unknown sequences (0.14 and 0.62% for K1 and K2, respectively) were eliminated from the 16S analyses. The percentage composition of each taxon was calculated. All obtained sequences have been submitted to the National Center for Biotechnology Sequences Read Archive under Bio Project accession number PRJNA713987.

2.8 Lab cultivation of microbial mat

A series of cultivation tests were implemented to determine the optimal conditions for a filamentous cyanobacteria-enriched mat (Fig. 5). The effects of germanium dioxide (GeO_2), temperature, salinity, growth medium, NH_4Cl, and agar on the survival and growth of

filaments were examined. The compound GeO_2 specifically disrupts silicate metabolism, thus inhibiting diatom growth (Lewin 1966). Although diatoms were present in negligible quantities in the microbial mat samples on the day of collection from the study site, they were involuntarily enriched and overran the mat during the initial 10-day lab acclimatization. Hence, the addition of GeO_2 was necessary to suppress diatom growth.

In cultivation test 1, we determined if the presence of GeO_2 had a detrimental effect on filament growth. The liquid growth medium BG-11 was the medium of choice for test 1 since it is commonly used for growing cyanobacteria (Berry et al. 2004). The amount of $KH_2PO_4 \times 3\ H_2O$ (generally used as the PO_4^{3-} source for BG-11), was adjusted to attain a default PO_4^{3-} concentration of 3.5 μmol L^{-1} for the cultivation tests. Approximately 0.1 mL of the microbial mat from the source culture was used as the inoculated material for each replicate in test 1. The mat pieces were grown in 100 mL of BG-11 at lab temperature (18 – 21 °C) and salinity of 9 psu. The final GeO_2 concentration in the culture media was 12 mg L^{-1}.

In cultivation tests 2 – 5, we determined the optimal temperature, salinity, growth medium, and NH_4Cl concentration, respectively, for the growth of large filaments, preferably those of the genus *Lyngbya*. In test 4, the medium "BG-11+ASN-III" consisted of both media BG-11 and ASN-III mixed in a 1:1 volume ratio.

In cultivation test 6, agar pieces were suspended in the culture to examine the effect of a solid attachment substrate on filament growth. Additionally, it was crucial to establish a microbial mat that could be easily extracted for downstream analysis; therefore, in test 7, the growth of the microbial mat was assessed on an agar substrate that formed a single, smooth layer at the bottom of the Greiner flask. The agar was prepared using BD Bacto™ Agar (ref no: 214010), and the agar concentration in both tests 6 and 7 was 20 g L^{-1}.

The aforementioned 7 cultivation tests were carried out in succession, with a single parameter being adjusted before the initiation of the next test. If a tested level (e.g., salinity, NH_4Cl) or the presence/absence (e.g., agar, GeO_2) of a parameter showed favorable filament growth in the microbial mat, it was set as the default condition for subsequent cultivation tests. In every cultivation test, triplicate cultures were set up for each culturing condition, and incubated for 20 days. For every new cultivation test, microbial mat pieces derived from the optimal culture in the preceding cultivation test were used as the inoculant. The microbial mats were cultured in sterile 250 mL Greiner cell culture flasks.

At the end of each cultivation test, the replicates were gently homogenized for 1 min via manual stirring of the medium with a glass rod. A total of 1800 µL of the homogenized medium was pipetted into a 2 mL Eppendorf tube, and the sample was fixed with 200 µL of 37% formaldehyde. Subsequent fluorescence microscopy was carried out with a procedure like that described in Section 2.6.2.

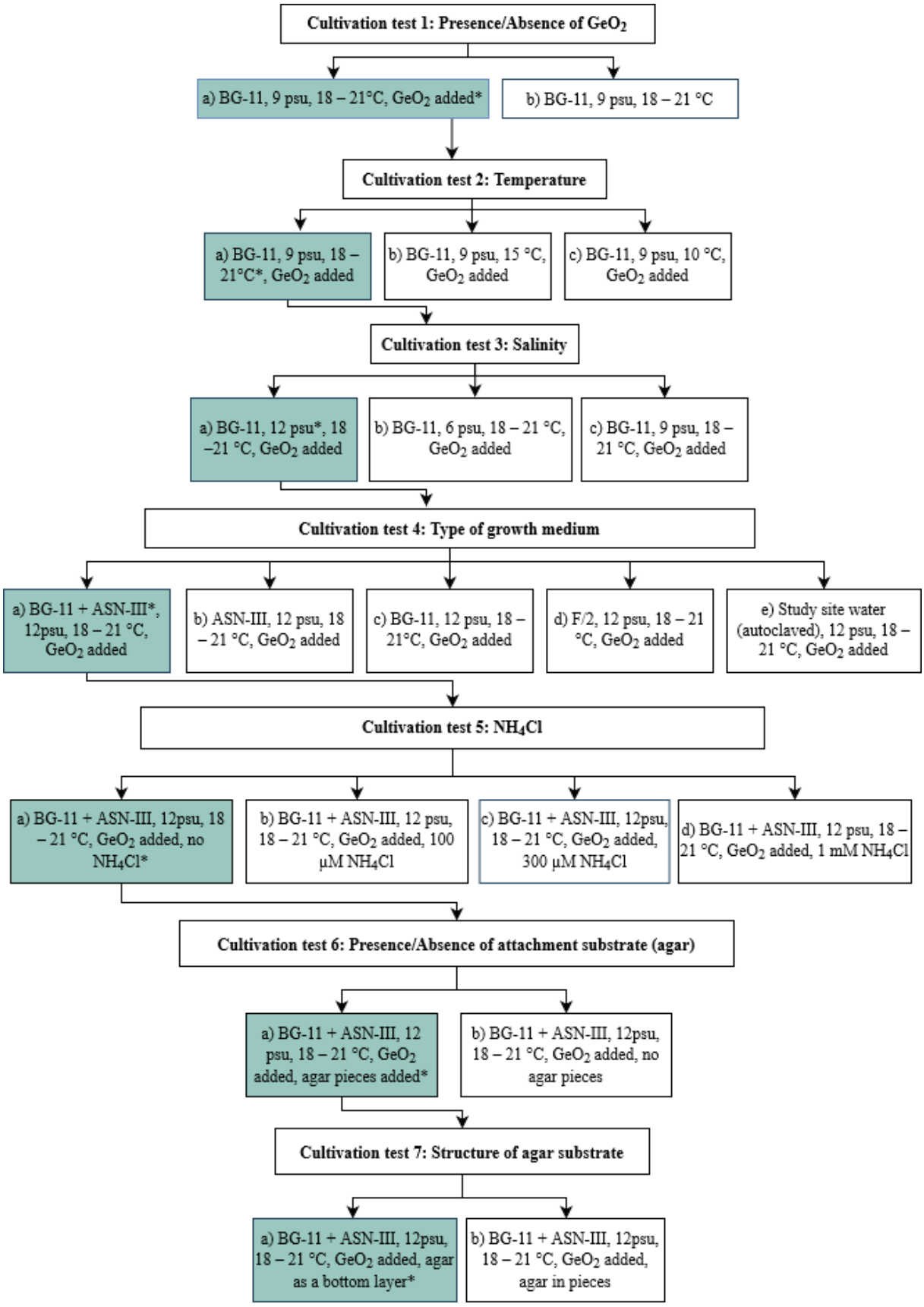

Fig. 5. A total of 7 consecutive cultivation tests were performed, to determine optimal conditions for the growth of filamentous cyanobacteria. In each cultivation test, parameters marked with a '*' in the blue-shaded boxes showed the greatest filament survival/growth and were set as the default for subsequent tests

2.9. Experiment on microbial response to PO_4^{3-} addition under varying conditions

2.9.1 Preparing microbial mat replicates

In relation to our first study (WP 1) where we examined the microbial-controlled P flux in environmental samples, the effect of a lab-cultured microbial mat on the P flux in the culture medium was investigated, and incubation was performed under 3 treatment conditions: *in-situ*, elevated temperature and reduced salinity. The *in-situ* treatment was set as the positive control, since growth conditions for the microbial mat were optimal in this treatment, as concluded from WP 2. In each treatment, the PO_4^{3-} response was tested at 11 time points: 0, 2, 8, 16, 24, 32, 40, 48, 56, 64, and 72 h. At each time point, 4 replicates were established. Therefore, 44 replicate cultures containing fully-grown cyanobacterial mats were prepared for each treatment.

Before starting the incubation experiment in WP 3, the 44 replicates were grown with the optimal conditions determined in WP 2. For each replicate, ~0.1 mL of mat material was affixed to a bottom agar layer in a sterile 250 mL Greiner flask. To obtain a sufficiently-grown mat, each inoculated replicate was then incubated for 20 days in BG-11+ASN-III medium with 12 mg L^{-1} GeO_2 at lab temperature (18 – 21 °C), a salinity of 12 psu, and no added NH_4Cl (Fig. 6). The starting KH_2PO_4 concentration in the growth medium was 14 µmol L^{-1}. By Day 10 and on the last day of incubation, no dissolved PO_4^{3-} was detected in the growth medium of all replicates, resulting in a P-deficient medium.

2.9.2 Start of incubation of lab-grown microbial mats

The microbial mat replicates were incubated in INFORS HT Multitron Pro incubators during the experiment, with parameters for each treatment summarized in Table 4. Before commencing the incubation, the current growth medium of each replicate was discarded and replenished with fresh medium (similar chemical composition). Just before the fresh medium was added, the interior of the Greiner flask was washed twice with Milli-Q water to remove residual salts. At the beginning of the incubation, KH_2PO_4 was added to all replicates (except time point '0' replicates) to give a final dissolved PO_4^{3-} concentration of 7.07 µmol L^{-1}. In all treatments, sub-sampling started at time point '0' and ended at time point '72 h'. Unfortunately, technical delays at the beginning of the *in-situ* incubation resulted in failure to collect sub-samples that were truly representative of the microbial mat's physiology at time point '0'.

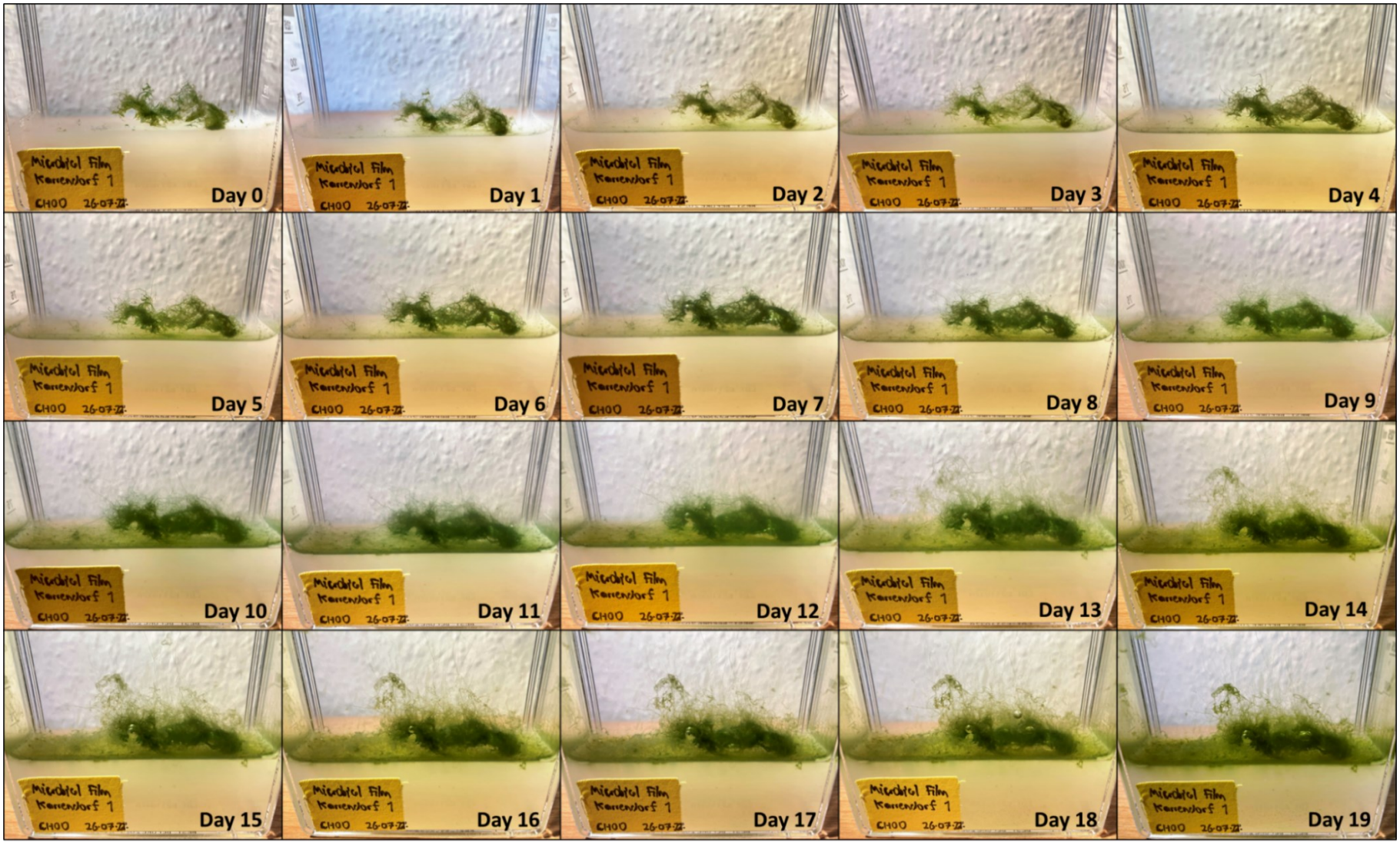

Fig. 6. Growth progression of the cyanobacterial-dominant mat on a bottom agar layer was documented over 20 days. Mat growth was gradually distributed across the agar layer during this period

Table 4. Experimental conditions implemented during each treatment. Conditions marked with a '*' were set using the INFORS HT Multitron Pro incubator

Experimental Conditions	Treatments		
	In-situ	**Elevated Temperature**	**Reduced Salinity**
Temperature (°C)*	20	30	20
Salinity (psu)	12	12	2
Light (lux)*	608	608	608
Light/Dark Cycle (h)*	12/12	12/12	12/12
Shaking (rpm)*	30	30	30

At each time point, sub-samples were obtained from replicates for various downstream analyses. From each replicate, 2 mL of growth medium was filtered through a Whatman® Spartan® syringe filter (pore size: 0.2 µm, diameter: 13 mm) and stored at -20 °C, to be used for measurement of the dissolved PO_4^{3-} concentration. Additionally, the entire microbial mat was dislodged from both the agar layer surface and the sides of the flask by using a cell culture scraper. The growth medium was filtered through a Whatman® nucleopore polycarbonate (PC) membrane filter (pore size: 0.8 µm, diameter: 47 mm) to retain the dislodged mat pieces. Before usage, each PC filter was weighed to obtain its dry weight. Approximately one-quarter of each filtered mat sample was sub-sampled for subsequent DNA and RNA extraction, as well as for light and fluorescence microscopy. The DNA and RNA sub-samples were flash-frozen in liquid nitrogen immediately after collection, and subsequently stored at -80 °C. The sub-samples allotted for microscopy were first preserved in a 4% formaldehyde solution, and then stored at 4 °C. Subsequent light and fluorescence microscopy were carried out with a procedure like that described in Section 2.6.2.

After collection of the aforementioned sub-samples, each PC filter sample with the remaining microbial mat was washed twice with Milli-Q water to remove salts and then oven-dried at 40 °C for 24 h. The dried filter samples were then weighed, and the dry weight of the unused filter was subtracted from the former to obtain the biomass of the microbial mat. Each dried filter sample was then rehydrated in 5 mL of HEPES-based buffer in an Eppendorf tube (5 mL), to dislodge the microbial mat from the filter. The filter was discarded, and the rehydrated microbial mat was stored at -20 °C for subsequent polyP-P quantification. The polyP-P quantification was carried out with a procedure like that described in Section 2.6.1.

2.9.3 Dissolved PO_4^{3-} measurement

The PO_4^{3-} concentration in the filtered sub-samples was measured according to the method used by Strickland & Parsons (1968) to determine reactive phosphorus in seawater. A total of 30 µL of 70 g L^{-1} of ascorbic acid and 30 µL of mixed reagent were added to 1 mL of sub-sample, and incubated in the dark at room temperature for 30 min. The mixed reagent consisted of 14.7 mmol L^{-1} ammonium paramolybdate, 1.4 mmol L^{-1} potassium antimonyl-tartrate, and 3.6 mol L^{-1} H_2SO_4. Following incubation, PO_4^{3-} absorbance in each sub-sample was determined spectrophotometrically at a wavelength of 882 nm, and the concentration was calculated using a blank (Milli-Q water) and a series of PO_4^{3-} standards ranging from 0 to 30 µmol L^{-1}.

2.9.4 Metagenomics and metatranscriptomics

Purification of DNA and RNA for sequencing

To determine the metagenomic and metatranscriptomic profile of the microbial mat throughout the period of active polyP accumulation, replicates of time points '0', 2 h, 24 h, and 48 h were selected for DNA/RNA extraction and sequencing. Both the DNA and RNA in each sub-sample were extracted and purified using the ZymoBIOMICS™ DNA/RNA Miniprep Kit (Catalog no.: R2002). A few modifications were made to the kit's protocol. Firstly, DNA/RNA Shield™-treated samples (in the section "Sample Preparation") were bead-beaten for only 4 min to reduce the fragmentation of nucleic acid strands. Secondly, in the section "DNA and RNA Purification", the step comprising the elution of DNase/RNase-free water (containing either DNA or RNA) from the column matrix was repeated twice using the same water (50 µL), to extract as much nucleic acid from the column matrix as possible. In addition, the RNA samples were treated with 3 rounds of DNase 1 (Fig. 7 & Fig. 8), until no contaminant DNA bands were detected via PCR. The concentration of extracted DNA from each sample was measured using the Qubit 4 Fluorometer (Invitrogen), set to the dsDNA Broad Range function (detection limit: 2 – 1000 ng μL^{-1}). The total RNA concentration in the RNA samples was also measured using the same fluorometer, set to the RNA Broad Range function (detection limit: 2 – 1000 ng μL^{-1}), and the resulting concentrations ranged from 30 – 283 ng μL^{-1}.

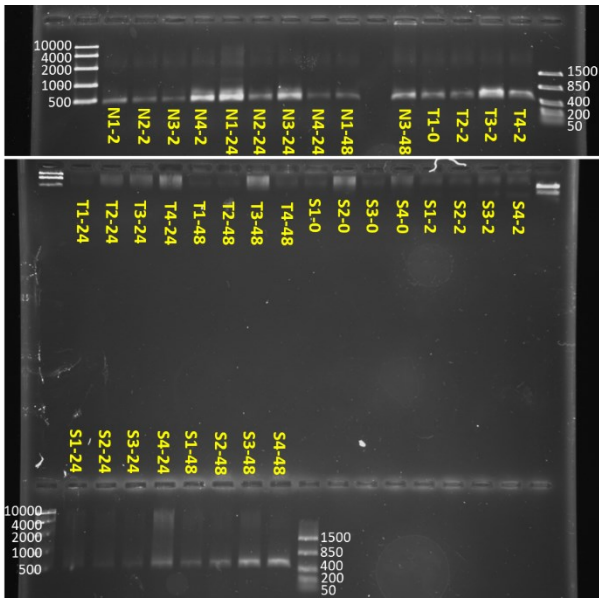

Fig. 7. Gel documentation imaging of RNA samples that had undergone the first round of DNase 1 treatment. The DNA bands for samples T1-24 to S4-2 (2nd row of wells), together with the DNA ladders flanking both ends of this row, failed to migrate successfully through the agarose gel, possibly due to an excessive addition of DNA loading dye which slowed the migration rate of the DNA, in contrast to the other ladders and samples in the same gel (3rd row of wells) which migrated successfully (30 min, 90 V)

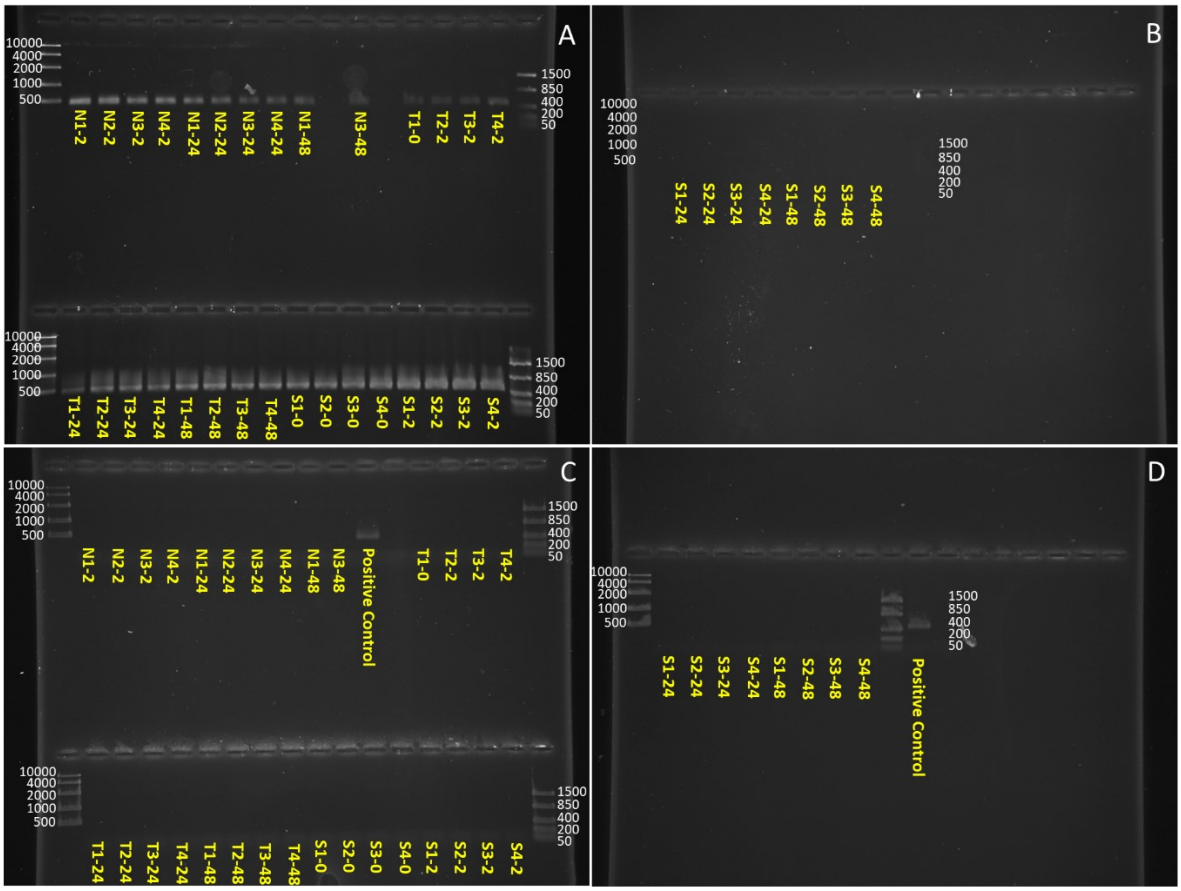

Fig. 8. Gel documentation imaging after the second (A and B) and third rounds (C and D) of DNase 1 treatment. (A) DNA bands (contaminants) on the gel were still present in the RNA samples. (B) No DNA bands (including the DNA ladder) were observed for the samples, possibly due to the gel being stained in expired ethidium bromide solution. (C and D) DNA bands were no longer visible for all samples, indicating a sufficient depletion of contaminant DNA. The positive control was an RNA sample (N1-32) that had not undergone prior DNase 1 treatment

Following the DNase 1 treatments, a removal protocol was performed on the RNA samples to eliminate DNase 1 from the samples. To each sample, aqua-phenol/chloroform (1:1) was added in a volume equal to that of the RNA mix in the sample and swirled gently. The sample was then centrifuged (13 000 × g) for 5 min. The aqueous phase was carefully extracted (avoiding the interface) and pipetted into a DNase-free Eppendorf tube (2 mL). Next, RNA was precipitated by adding sodium acetate (3 mol L^{-1}, pH 5.2, 0.1× of sample volume) and absolute ethanol (2.5× of sample volume) to the sample, and then incubated at -20 °C for 2 h. Subsequently, the sample was centrifuged (13 000 × g) for 30 min at 4 °C. The liquid was removed from the sample, and the remaining pellet was washed with 70% ethanol. The washed sample was centrifuged (13 000 × g) for 30 min at 4 °C, and the ethanol was removed from the sample via pipetting. The sample (containing the cleaned pellet) was then air-dried for at least 4 h, suspended in 50 µL of DEPC water, and incubated for 10 min at 60 °C.

Metagenomic and metatranscriptomic sequencing

DNA sequencing was performed on an Illumina NovaSeq (2×250 bp) by LGC Genomics GmbH, while RNA sequencing was performed on the Illumina NextSeq 500 (single reads, 1×75 bp) by Fasteris, Life Science Genesupport SA.

Metagenomic analysis

The sequenced DNA reads were then curated via an automated workflow (Fig. 9). The workflow was divided into 5 main components: quality control (trimming), co-assembly of multiple metagenomes and bin refinement (co_assembly), individual sample assembly and bin refinement (sample_assembly), dereplication and reassembly of both co-assembled and individual sample assembled bins (final_bins), and taxonomic classification and estimating the read coverage of each bin (bin_annotation). Additionally, manual refinement of the bins was carried out, using a combination of software tools (Anvi'o, BBMap, BUSCO, CheckM2, MIRA). During the curation of each bin in Anvi'o (v7.1), contigs not belonging to the bin were removed. The assembler software MIRA was then used to reassemble those bins which had been modified. Subsampling of high-coverage bins was performed with BBMap-38.90. The programs BUSCO (v5.2.2) and CheckM2 (v0.1.3) were run to determine the completeness of each bin. Finally, bin annotation, classification, and quantification were repeated on the manually refined bins (or MAGs: metagenome-assembled genomes). The genes were annotated using the PCycDB database as a reference. While calculating read coverage using coverM (v0.6.1), a minimum read percentage identity threshold of 95% was

used. Completion of the workflow resulted in normalized composition percentages of individual bacteria species in the microbial mat.

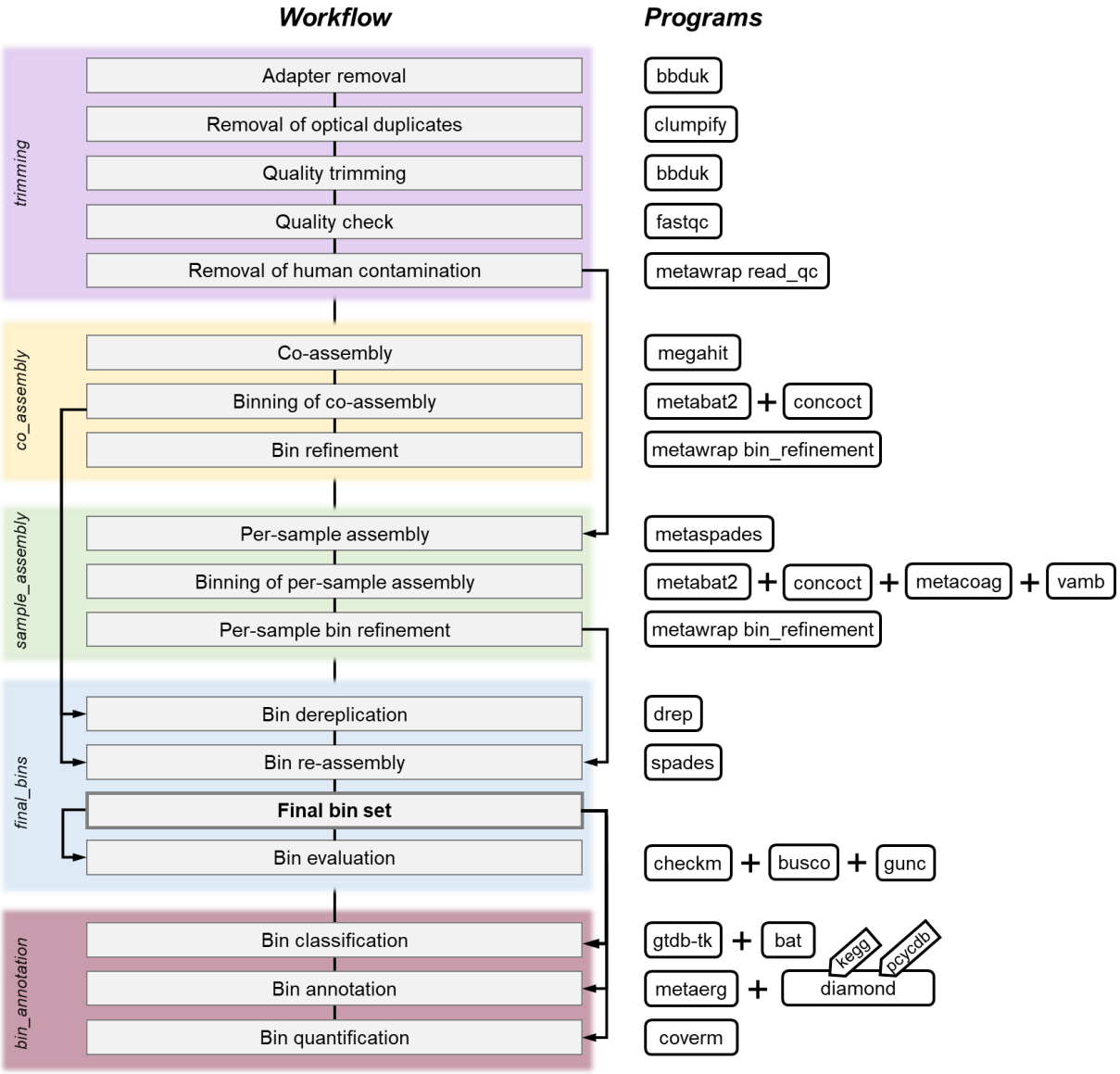

Fig. 9. Workflow to analyze paired-end metagenomic sequences generated on the Illumina platform. A majority of the workflow was carried out at the HLRN (North German Supercomputing Alliance). The software tools implemented at each step are indicated on the right. Workflow and image credit: Christiane Hassenrück

Metatranscriptomic analysis

The sequenced total RNA reads were analyzed through an independent approach (Fig. 10). The workflow was divided into 3 main components: read quality control (trimming), a taxonomic study of both rRNA and non-rRNA reads (taxonomic_analysis), and functional assignment of the assembled transcripts to known proteins as well as differential expression profiling (functional_analysis). During the mapping of RNA reads to MAGs, mappings with less than 95% similarity to the reference genome were removed. For the last step of the workflow, the output from featureCounts was read and reformatted using RStudio to be analyzed with the DESeq2 package (Bioconductor v3.14). Using DESeq2, the differential expressions of selected P metabolism-associated and stress-related genes were then compared between treatments as well as between time points. Since not all genes in each MAG had been fully identified (KEGG-annotated) at the time of writing this dissertation, already KEGG-annotated P metabolism-associated (Marzan & Shimizu 2011, Santos-Beneit 2015, Santoro et al. 2023) and stress-related genes (Ito et al. 2014, Klähn et al. 2021) (Table S2 & Table S3) were selected for the DESeq2 analysis, based also on the premise that these genes constitute either major or well-studied operons, as well as the role that the P metabolism-associated genes play in polyP synthesis and degradation.

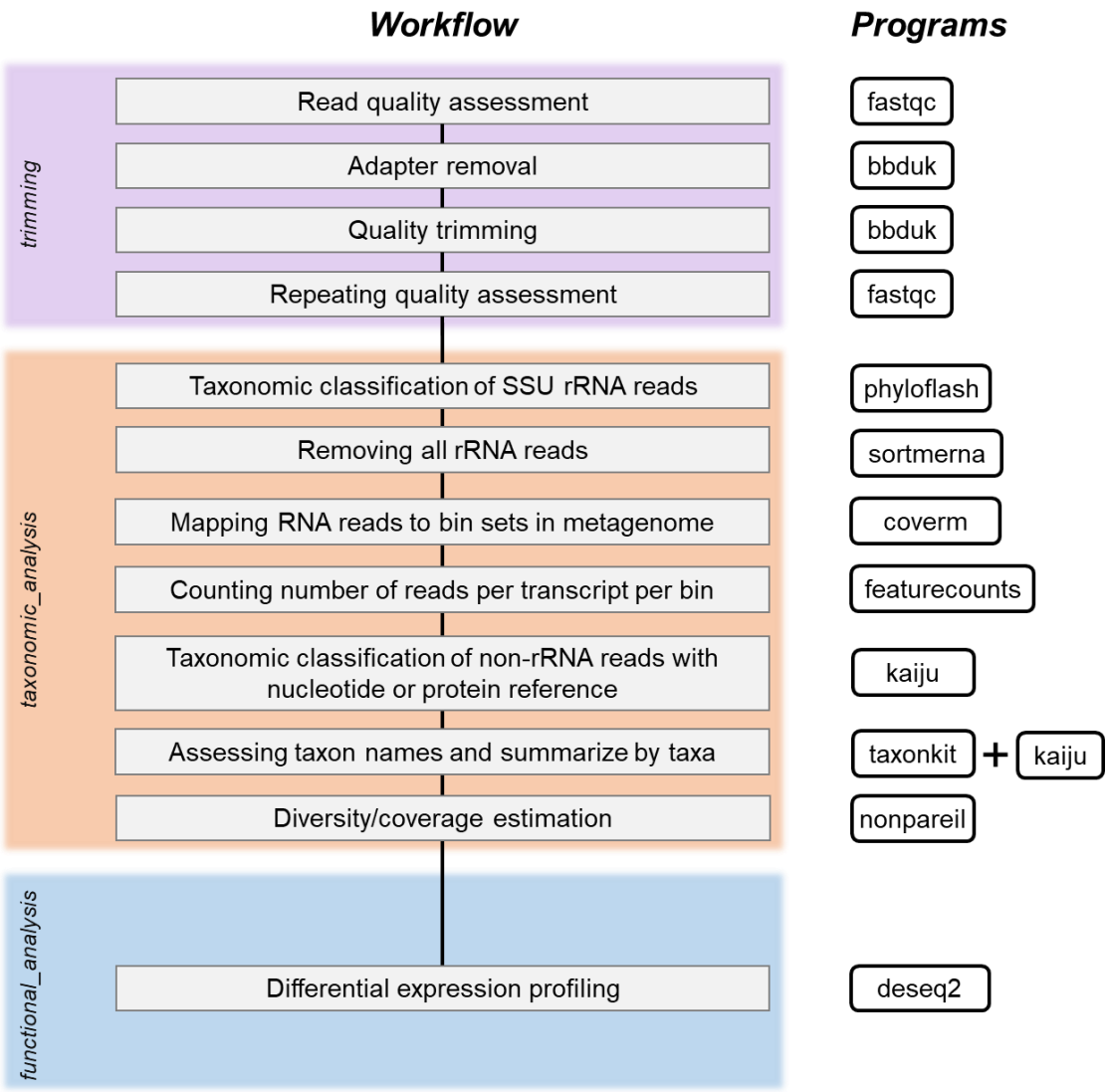

Fig. 10. Workflow to analyze sequenced metatranscriptomes (Illumina-generated) of the microbial mat samples, carried out on the IOW's server. Workflow and image credit: Christiane Hassenrück

3 Results

3.1 Nutrient dynamics in the benthic layer of a coastal peatland (WP 1)

3.1.1 Microbial PolyP accumulation in the peat surface

The average polyP-P content in the upper 1 cm layer of peat in the winter treatment cores on Day 0 was 2.23 µmol g^{-1} (Fig. 11), corresponding to 5% of the total P content (49 µmol g^{-1}) in the surface peat layer (Table 5). On the last day of the winter incubation (Day 10), the average polyP-P content in treatments WinterOX5, WinterOD5, and WinterOX15 was 2.08 µmol g^{-1}, 3.20 µmol g^{-1} and 3.25 µmol g^{-1}, respectively (Fig. 11). This indicated a 0.9× decrease, 1.4× increase and 1.5× increase in polyP-P, respectively as compared to Day 0. To determine if there were significant differences in the polyP-P content between the treatments on Day 0 and Day 10, a Wilcoxon rank-sum test was run. The resulting p-values were 0.66 (WinterOX5), 0.19 (WinterOD5), and 0.38 (WinterOX15), indicating no significant difference ($p \geq 0.05$) in all winter treatments.

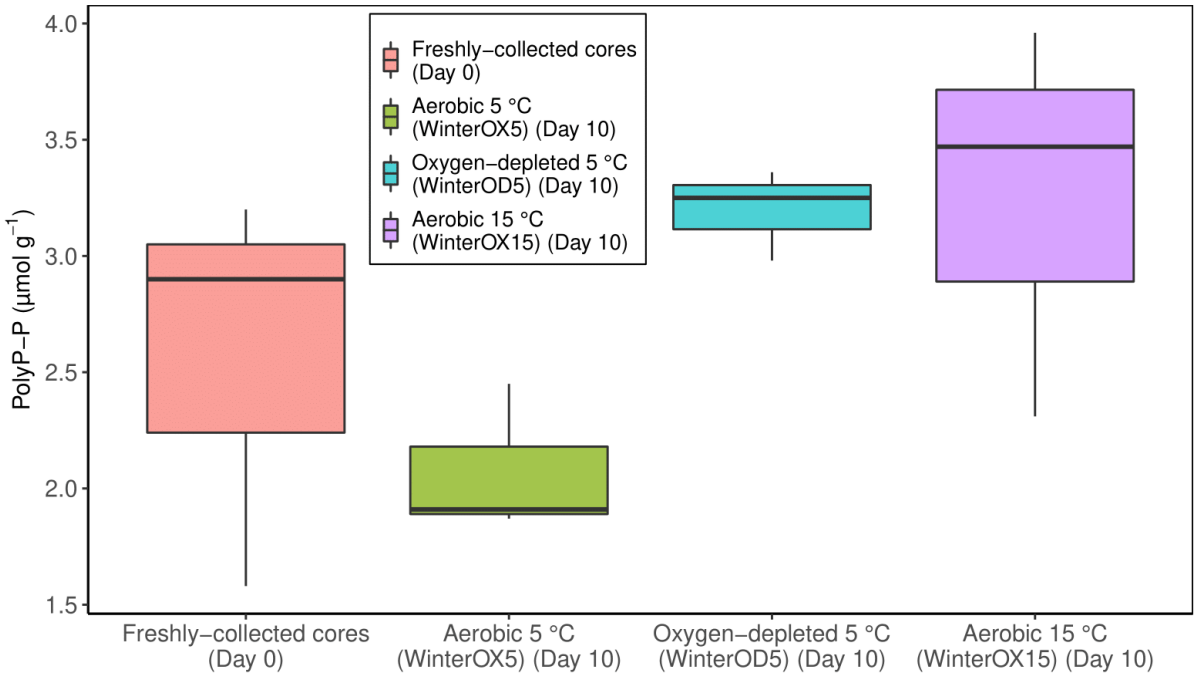

Fig. 11. Boxplot showing the polyP-P content in the upper 1 cm layer of peat in freshly-collected cores on Day 0, and in the 3 winter treatments on Day 10. Boxes show upper and lower quartiles; horizontal line: median; whiskers: max./min.

Table 5. Contents of Fe (total and excess [Fe_{xs}]), P (total and excess [P_{xs}]), and Fe:P and Fe_{xs}:P_{xs} molar ratios in 8 surface peat layer replicates during the winter. Fe_{xs} and P_{xs} are the Fe and P fractions potentially available for redox reactions

Replicate	Total Fe (µmol g^{-1})	Fe_{xs} (µmol g^{-1})	Total P (µmol g^{-1})	P_{xs} (µmol g^{-1})	Total Fe:P (molar ratio)	Fe_{xs}:P_{xs} (molar ratio)
1	268	108	44	39	6.0	2.7
2	239	92	38	34	6.3	2.7
3	311	144	53	48	5.9	3.0
4	300	111	49	43	6.1	2.6
5	265	106	43	38	6.1	2.8
6	243	73	43	38	5.6	1.9
7	312	131	57	52	5.4	2.5
8	334	157	61	56	5.5	2.8
Mean	**285**	**115**	**49**	**43**	**5.9**	**2.6**

DAPI-stained imaging of Day 0 samples of the surface peat layer showed polyP incorporated in filamentous cells which formed a dense network (Fig. 12A). Accumulation of polyP was also found in diatoms; nevertheless, they were highly scarce as compared to the polyP-accumulating filaments (Fig. S2). Compared to treatments WinterOD5 and WinterOX15 on Day 10, the greenish-yellow fluorescence (as a result of the DAPI-polyP complex) in WinterOX5 was reduced, suggesting that polyP content was lower (Fig. 12B). Filaments which were morphologically similar to members of the genus *Lyngbya* on Day 0 were also dominant on the last day of the WinterOX5 and WinterOX15 incubations (Fig. 12B & D). In WinterOD5, aside from the sizeable presence of *Lyngbya*-like filaments, thinner polyP-accumulating filaments (mean ± SD diameter: 4.3 ± 0.3 µm) were also noticeable (Fig. 12C) (Olenina et al. 2006).

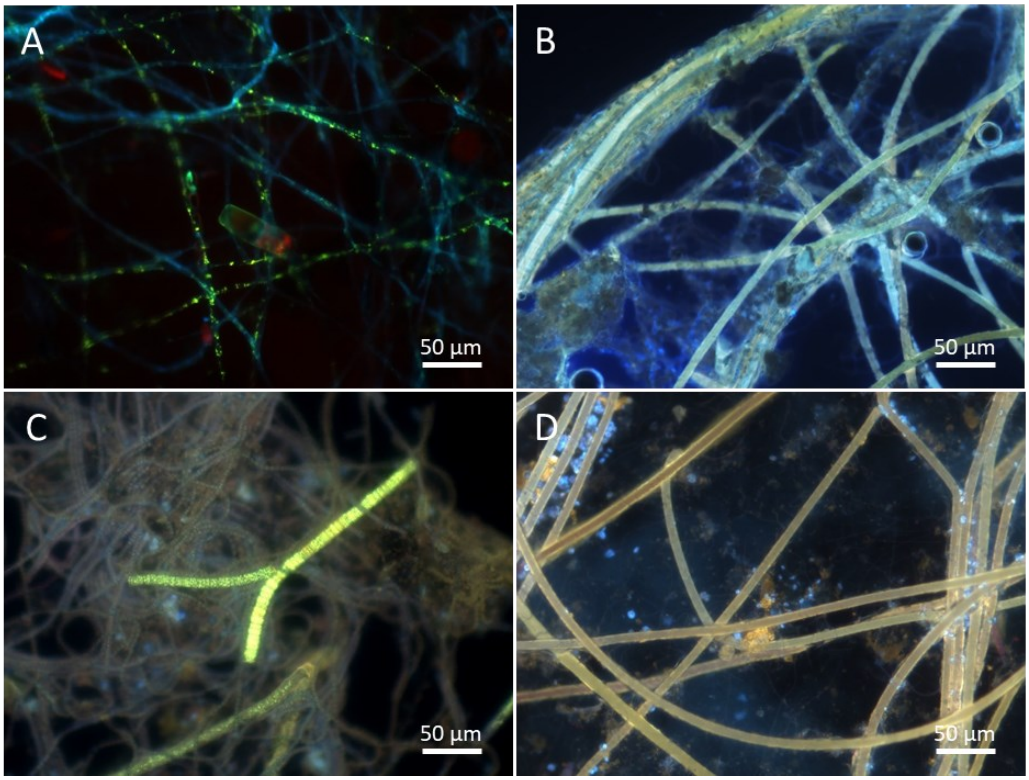

Fig. 12. DAPI-stained fluorescence imaging of the surface peat layer of winter treatment cores on (A) Day 0 and Day 10 in (B) WinterOX5, (C) WinterOD5, and (D) WinterOX15. A polyP-containing filamentous mat was present in all winter cores as visualized by the greenish-yellow fluorescence of polyP at a wavelength of 550 nm. The filaments in WinterOX5 displayed reduced greenish-yellow fluorescence than the other 2 winter treatments on Day 10, indicating comparatively lower polyP content in the mat

In contrast, the surface peat layer of the fall treatment FallOD5 was devoid of polyP-accumulating filaments on both Days 0 and 10; however, some polyP was present in a few smaller, non-filamentous single cells which ranged from 1 – 3 µm in diameter, corresponding to that of typical prokaryotes (Fig. 13).

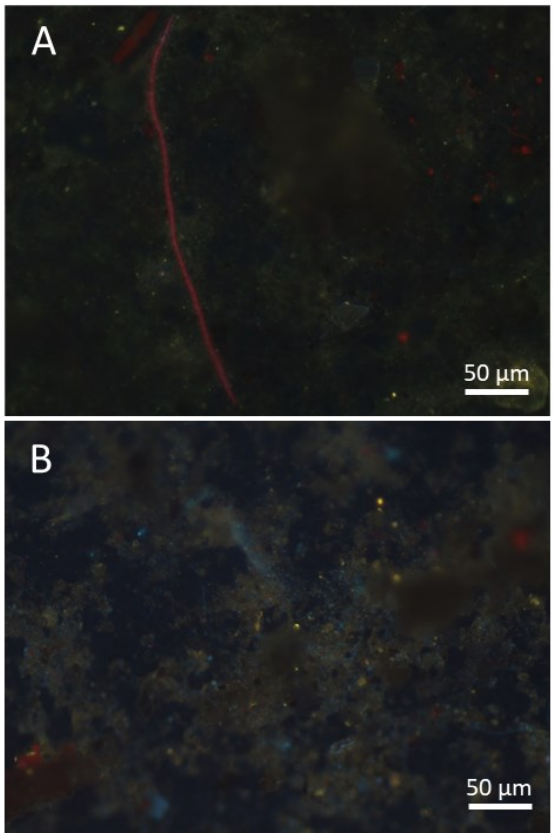

Fig. 13. DAPI-stained fluorescence imaging of the surface peat layer in the FallOD5 treatment on (A) Day 0 and (B) Day 10. While a few smaller cells could be identified, filamentous mats were nearly absent in the fall core

Aside from some small polyP-accumulating microorganisms, polyP-filled filaments were also evident in the surface peat layer on Day 0 of the SummerOX25 treatment (Fig. 14A). As previously mentioned in Section 2.3, the upper 1 cm layer of peat (including the microbial mat) had been removed from all summer treatment cores at the end of Day 2. On the last day of the SummerOX25 treatment, only the smaller single cells were present (Fig. 14B). In comparison, despite the prior removal of the surface peat layer, clumps of mat-forming, polyP-filled filaments resembling those on Day 0 were present in samples from the SummerOD15 (Fig. 14C) and SummerOX15 (Fig. 14D) treatments, revealing a resurgence of the mat. Accompanying light microscopy on the same samples also indicated that the filaments in SummerOD15 (Fig. 14E) and SummerOX15 (Fig. 14F) were unbranched photosynthetic microbes (av. diameter of 8.9 ± 0.7 µm).

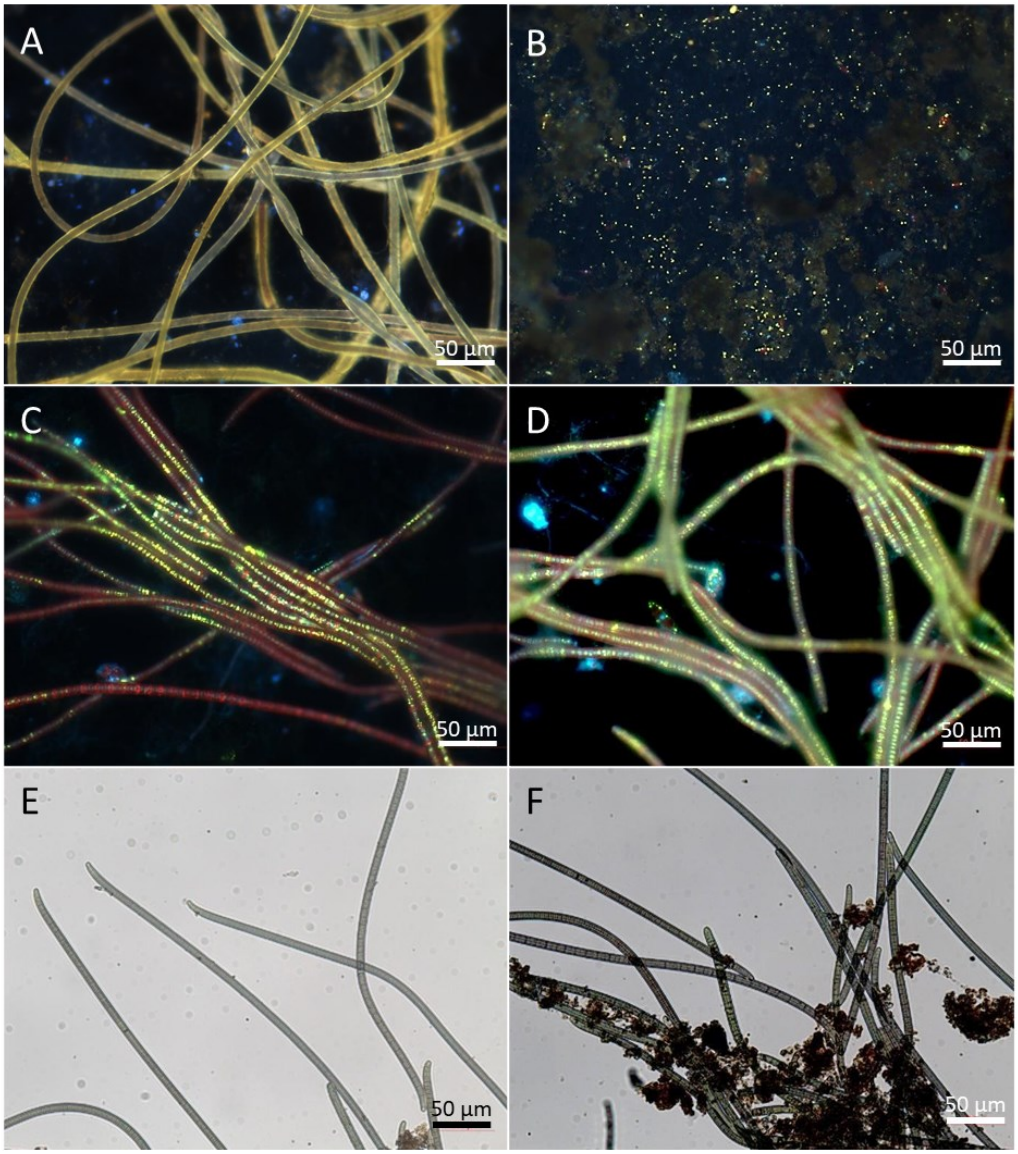

Fig. 14. Microscopic imaging of the surface peat layers from the summer treatment cores. Fluorescence microscopy showed (A) polyP-filled filaments on Day 0 of the SummerOX25 treatment, (B) the absence of filaments but the presence of small polyP-accumulating microorganisms in the same treatment at the end of the incubation, and polyP-rich filamentous bacteria in the (C) SummerOD15 and (D) SummerOX15 treatment cores at the end of the incubation. Light microscopy showing photosynthetic filaments from the (E) SummerOD15 and (F) SummerOX15 treatments

Their morphology, length, and diameter corresponded to members of the filamentous cyanobacterial order *Oscillatoriales*, which encompasses polyP-accumulating genera such as *Arthrospira*, *Lyngbya,* and *Phormidium* (Sanz-Luque et al. 2020). From 16S rRNA gene sequencing, filaments of the genus *Lyngbya* were the dominant bacteria in the surface peat layer in summer on Day 0, comprising 27% and 9% of the replicates K1 and K2, respectively (Table 6). The cyanobacteria with the second-highest proportion in K1 and K2 were from the genera *Nodularia* (0.89%) and *Limnothrix* (0.41%), respectively.

Table 6. The 20 genera of cyanobacteria showing the highest compositions, from two replicates (K1 and K2) derived from the surface peat layer in Karrendorfer Wiesen, during core collection for the summer incubation on Day 0. The genus with the highest composition in both replicates, *Lyngbya* was also compositionally highest among all bacteria. RC, relative composition

Genus (K1)	**RC - K1 (%)**	**Genus (K2)**	**RC - K2 (%)**
Lyngbya	27.04	*Lyngbya*	9.02
Nodularia	0.89	*Limnothrix*	0.41
Limnothrix	0.75	*Anabaena*	0.23
Symphothece	0.43	*Nodularia*	0.20
Synechocystis	0.34	*Synechocystis*	0.16
Leptolyngbya	0.33	*Symphothece*	0.15
Snowella	0.29	*Nodosilinea*	0.09
Trichodesmium	0.21	*Leptolyngbya*	0.06
Coleofasciculus	0.20	*Snowella*	0.06
Nodosilinea	0.20	*Coleofasciculus*	0.04
Anabaena	0.16	*Pseudanabaena*	0.03
Symploca	0.16	*Cyanobium*	0.02
Anabaena	0.13	*Trichodesmium*	0.02
Phormidesmis	0.07	*Phormidesmis*	0.02
Pseudanabaena	0.06	*Symploca*	0.02
Cyanobium	0.06	*Xenococcus*	0.01
Rivularia	0.05	*Schizothrix*	0.01
Schizothrix	0.05	*Tychonema*	0.01
Halomicronema	0.03	*Dolichospermum*	0.01
Sphaerospermopsis	0.03	*Arthrospira*	0.01

3.1.2 Bulk Fe and P in the surface peat

The average total Fe and P contents in the surface peat layer in winter were 285 and 49 µmol g^{-1}, respectively. The excess contents of both elements added to the less reactive geogenic background (referring to contents that were available for redox reactions) had a mean of 115 µmol g^{-1} (Fe_{xs}) and 43 µmol g^{-1} (P_{xs}). Among the replicates, the range of the molar Fe_{xs}:P_{xs} ratio was 1.9 – 3.0, with an average value of 2.6 (Table 5). A good correlation (R^2 = 0.80) between Fe_{xs} and P_{xs} points to Fe oxyhydroxides as a potential source of inorganic P in the surface peat layer (Fig. 15), although a non-Fe-bound P component was also present (indicated by positive *y*-axis intercept). According to SEM-EDX of particles in the surface peat layer, P content was present in Fe oxyhydroxides, plagioclase, illite, and unidentified organic matter (Table S1).

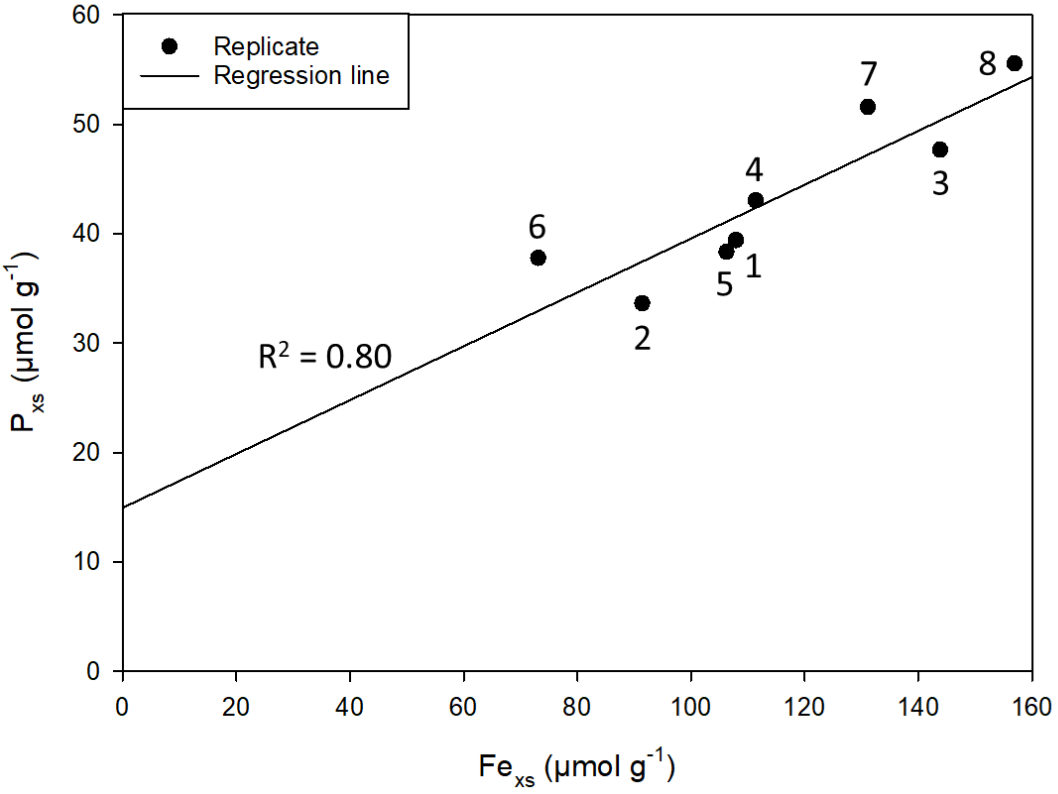

Fig. 15. Correlation between Fe_{xs} and P_{xs} content in each of the 8 replicate sub-samples listed in Table 5. A linear regression line (R^2 = 0.80) illustrates the role of peat Fe compounds as a potential source of P

3.1.3 Bottom water nutrient and Fe trends during incubation

During the winter experiment, the bottom water PO_4^{3-} concentration in the aerobic, *in-situ* temperature treatment WinterOX5 remained low throughout the incubation (0.08 – 0.23 µmol L^{-1}), even declining 3× between Days 0 and 10 (Fig. 16A); however, polyP-P also decreased (0.9×) in the same period (Fig. 11, Table 8). In contrast, bottom water PO_4^{3-} concentrations in the temperature-elevated WinterOX15 and oxygen-depleted WinterOD5 treatments increased 6× and 5×, respectively, within the first 2 days of incubation, and remained at a heightened level until the last day of the incubation.

While the oxygen-depleted FallOD5 treatment was exposed to the same conditions as in WinterOD5, mat-forming filaments in FallOD5 were substantially less abundant than in the latter treatment (Fig. 12C & Fig. 13B). At 2.3 µmol L^{-1} on Day 0, the bottom water PO_4^{3-} concentration in FallOD5 was >10× higher than in WinterOD5 (Fig. 17A). Moreover, the PO_4^{3-} concentration by Day 10 was much higher in the mat-deficient FallOD5, reaching a maximum of 87.4 µmol L^{-1}.

In the summer experiment, the bottom water PO_4^{3-} concentration across all treatments (SummerOX15, SummerOD15, and SummerOX25) was <0.5 µmol L^{-1} on Day 0 (Fig. 17C). After removing the surface peat layer (upper 1 cm) on Day 2, PO_4^{3-} concentrations greatly increased, especially in SummerOX25 and SummerOD15. The PO_4^{3-} concentrations reached a maximum on Day 4, thereafter declining rapidly, nearly reaching their initial level by Day 8. Contrastingly, the bottom water PO_4^{3-} level only increased 1.4× during Days 2 – 3, remaining constant from Days 3 – 8.

The level of Fe_{diss} in the bottom water of WinterOX5 remained low throughout the incubation and even exhibited a general decrease (1.9×) from Days 0 – 10 (Fig. 16B). Aside from minor fluctuations, there was a general increase (16×) in the bottom water Fe_{diss} concentration of WinterOD5 from Day 0 – 10. In WinterOX15, the bottom water Fe_{diss} concentration increased 6× by Day 7 and then decreased 2.5× by the end of the incubation.

While the NO_x^- concentration (NO_3^- + NO_2^-) remained low throughout WinterOD5, it displayed increasing concentrations in WinterOX5 and WinterOX15 (Fig. 16C). In particular, the NO_x^- concentration increased considerably in WinterOX15, as compared to the more uniform patterns observed in WinterOX5 and WinterOD5.

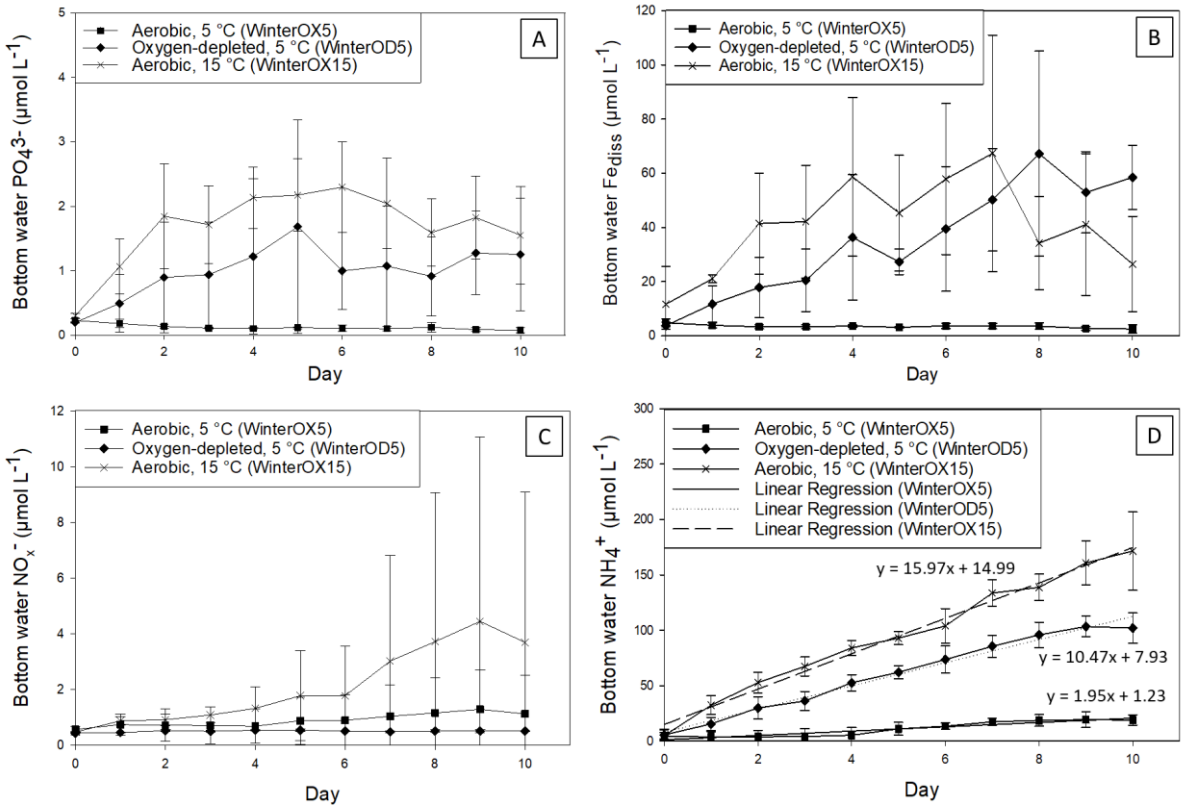

Fig. 16. Bottom water dissolved (A) PO_4^{3-}, (B) dissolved Fe_{diss}, (C) NO_x^- (NO_3^- + NO_2^-), and (D) NH_4^+ concentrations (mean ± SD, n = 3) in the 3 winter treatments from Day 0 – 10. Linear regression analyses were done on NH_4^+ concentration to estimate the rate of nutrient release from organic matter degradation in the 3 treatments

Although the NH_4^+ concentration increased in the bottom water of WinterOX5 (4 – 19 µmol L^{-1}) during the incubation, it remained distinctly lower as compared to the other winter treatments. A gradual increase in NH_4^+ concentration was seen in WinterOD5 (18×) and WinterOX15 (35×) from Day 0 – 10 (Fig. 16D). Differences in the NH_4^+:PO_4^{3-} increase between the Day 0 – 5 and Day 5 – 10 segments in the winter treatments were observed, including the steeper slope in the latter segment (Fig. 18).

In the mat-deficient fall treatment FallOD5, the bottom water NH_4^+ concentration increased 4× from Day 0 – 4, reaching 243 µmol L^{-1} by the end of the incubation (Fig. 17B). While the bottom water NH_4^+ concentration in FallOD5 was 8.4× higher than in WinterOD5 at the beginning, this factor declined to only 2.4× by Day 10.

In the summer experiment, the bottom water NH_4^+ concentration in both SummerOX15 and SummerOD15 rose sharply after the removal of the surface peat layer on Day 2 (Fig. 17D). In the SummerOX25 treatment, however, a pronounced increase in NH_4^+ concentration (170× from Day 0 – 3) had already occurred before removal of the layer, followed by a gentler increase (1.4×) until the end of the incubation. Contrastingly, the NH_4^+ concentration in SummerOD15 and SummerOX15 remained almost constant from Day 3 – 8.

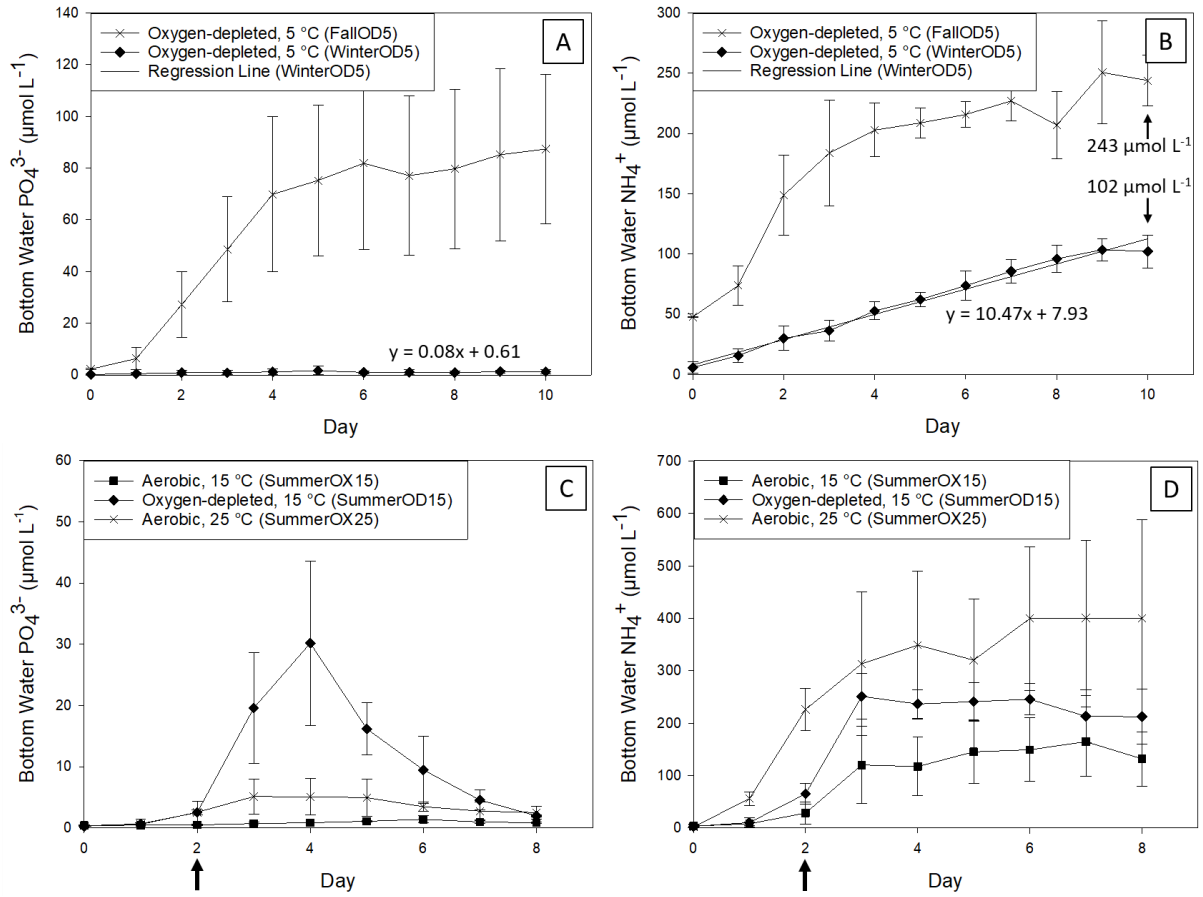

Fig. 17. Concentrations of (A) PO_4^{3-} and (B) NH_4^+ in winter (WinterOD5) and fall (FallOD5) treatments (mean ± SD, n = 3). The concentration of PO_4^{3-} was higher in FallOD5 when the mat was nearly absent, in comparison to WinterOD5 where a mat was present. The NH_4^+ concentrations were 102 µmol L^{-1} (WinterOD5) and 243 µmol L^{-1} (FallOD5) by Day 10, respectively. Also shown are the concentrations of (C) PO_4^{3-} and (D) NH_4^+ (mean ± SD, n = 3) in the summer treatments. The PO_4^{3-} concentration increased most significantly in SummerOD15, after removal of the surface peat layer on Day 2 (indicated by arrows); a sharp decrease in PO_4^{3-} concentration from Day 4 onwards indicated the effect of a PO_4^{3-} uptake mechanism

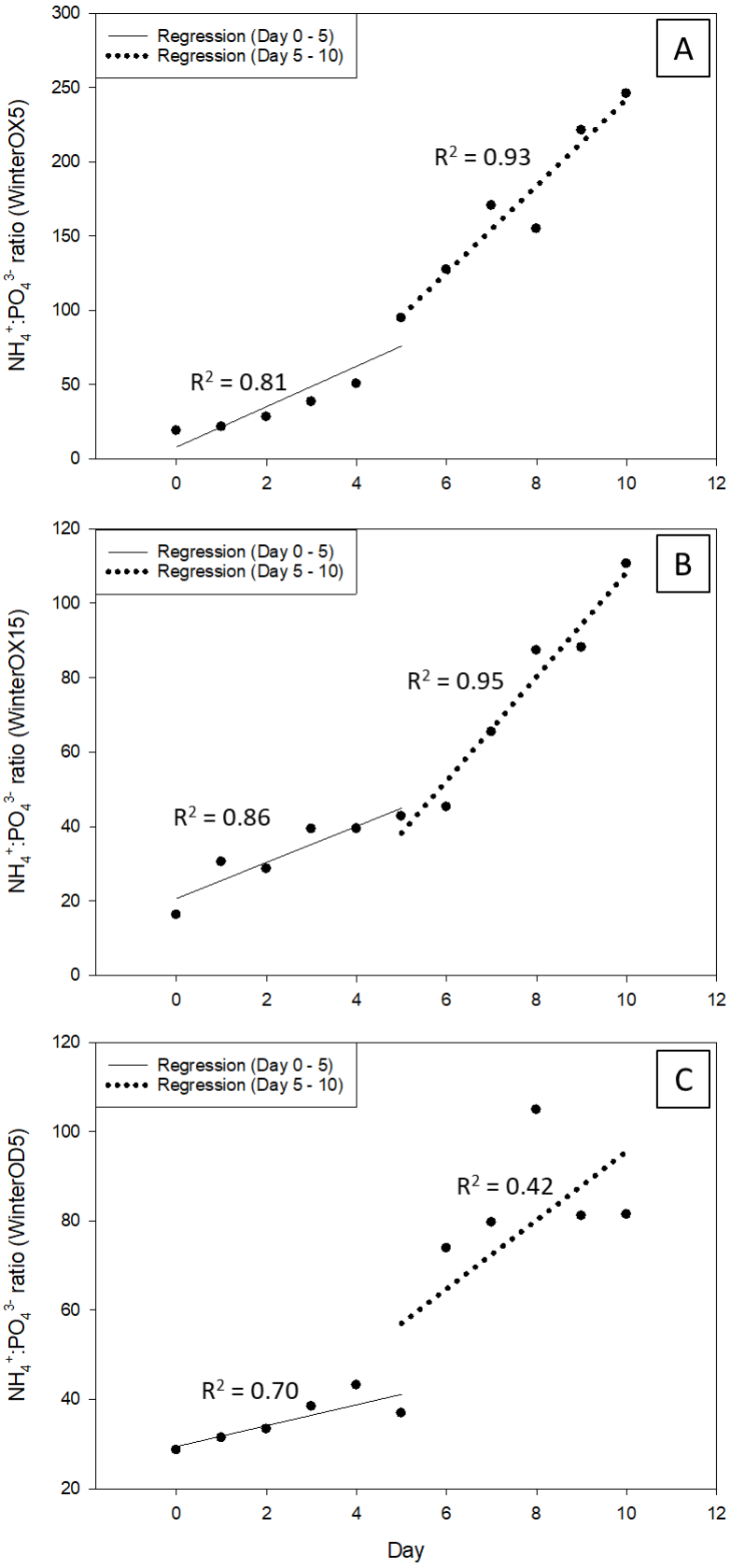

Fig. 18. Comparison of linear-fitted increase between Days 0 – 5 and 5 – 10 in the bottom water NH_4^+:PO_4^{3-} ratio of the (A) WinterOX5, (B) WinterOX15, and (C) WinterOD5 treatment

3.1.4 Dissolved PO_4^{3-} and Fe in bottom water and porewater in winter treatments

On Day 0, the porewater PO_4^{3-} concentration (peat depth = 1.5 cm) was approximately 30× higher than in the overlying bottom water (Fig. 19A & Table 3). On Day 10, at the same peat depth, the porewater PO_4^{3-} concentration was 23×, 4×, and 16× higher than in the bottom water of WinterOX5, WinterOD5, and WinterOX15, respectively. As a result, there was a net efflux from the peat to the water column in all treatments (Table 3). Among the winter treatments on Day 10, WinterOX15 exhibited the highest PO_4^{3-} flux (68×10^{-6} µmol cm^{-2} s^{-1}), while the flux was lowest in WinterOX5 (3.5×10^{-6} µmol cm^{-2} s^{-1}).

While a narrow concentration range was observed with bottom water and porewater Fe_{diss} on Day 0, porewater Fe_{diss} concentration at the same peat depth (1.5 cm) was 26×, 4× and 6× higher than in the bottom water in WinterOX5, WinterOD5, and WinterOX15, respectively, on Day 10.

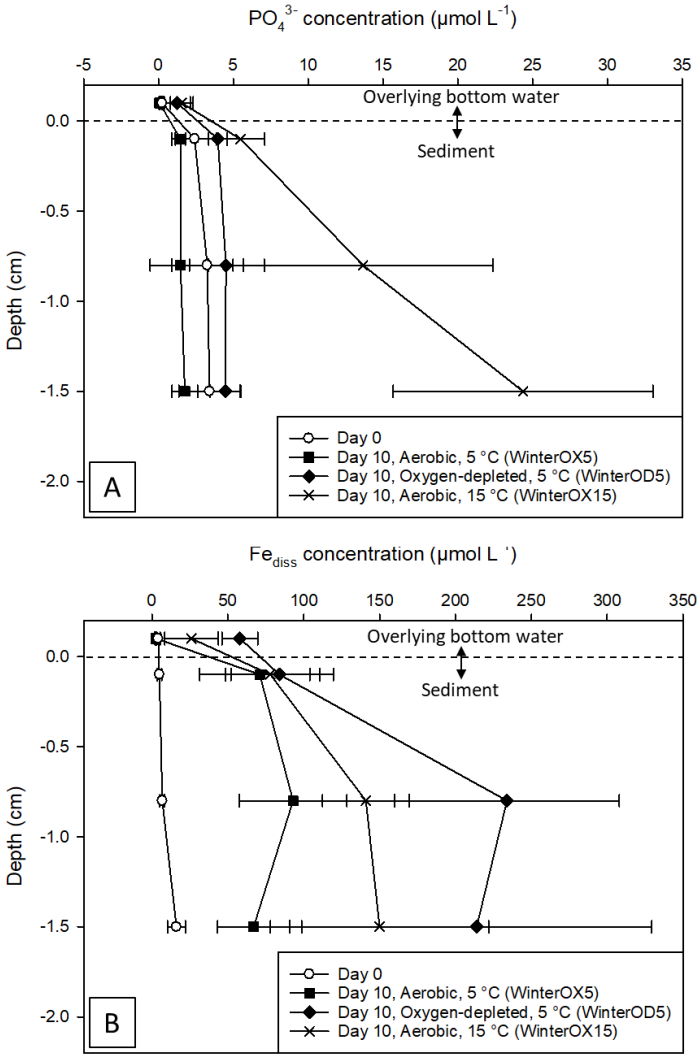

Fig. 19. Concentrations of (A) PO_4^{3-} and (B) Fe_{diss} in the bottom water and porewater (mean ± SD, n = 3) of winter cores on Day 0 and 10 in the WinterOX5, WinterOD5, and WinterOX15 treatments

3.2 Lab cultivation of microbial mat (WP 2)

3.2.1 Growth with GeO_2 (Cultivation test 1)

In the presence of 12 mg L^{-1} GeO_2, diatoms were visibly absent in the culture media (Fig. 20A). In addition to this, filaments which accumulated some polyP were still present in the culture. The average diameter of the filaments was 2.2 ± 0.3 µm (mean ± SD; Fig. 20A), which was 4× thinner than the range typical of members of the genus *Lyngbya*. In the absence of GeO_2, diatoms which were naviculoid-shaped were present in large quantities (Fig. 20B).

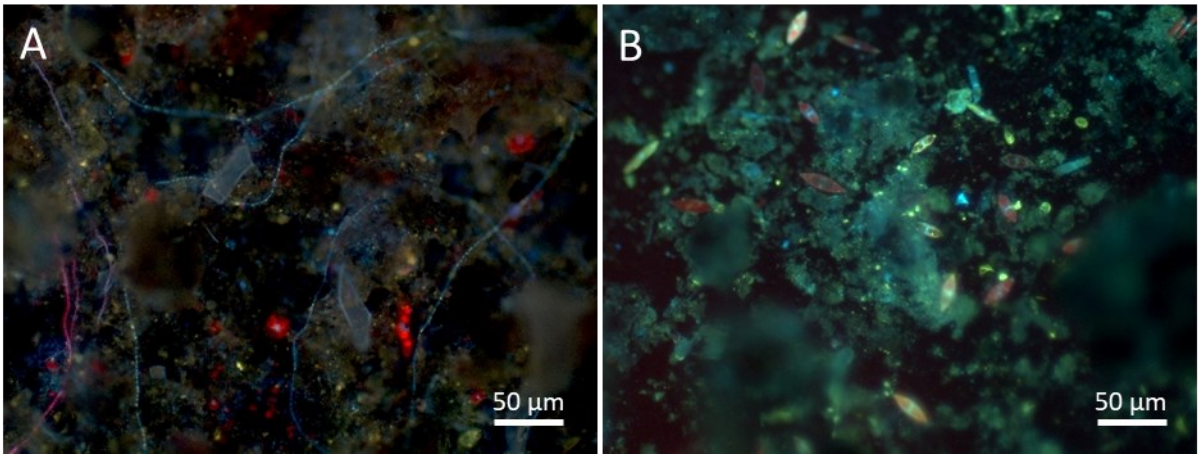

Fig. 20. DAPI-stained fluorescence imaging illustrated that (A) while diatoms were noticeably absent, polyP-accumulating filaments were still present in cultures with 12 mg L^{-1} GeO_2, while (B) diatoms (mostly naviculoid-shaped) were evident in cultures without any addition of GeO_2

3.2.2 Temperature dependency (Cultivation test 2)

At the end of this incubation, a microbial mat comprising a dense filament network was observed at 18 – 21 °C. A few *Lyngbya*-like filaments were present in the network; however, most filaments within did not morphologically resemble *Lyngbya* spp., and likely comprised a variety of species (Fig. 21A). At 15 °C (Fig. 21B) and 10 °C (Fig. 21C), no filament clusters were detected. Instead, filaments in these two temperature treatments were scarcely distributed in the sample, and the originally-inoculated microbial mat piece did not appear enriched.

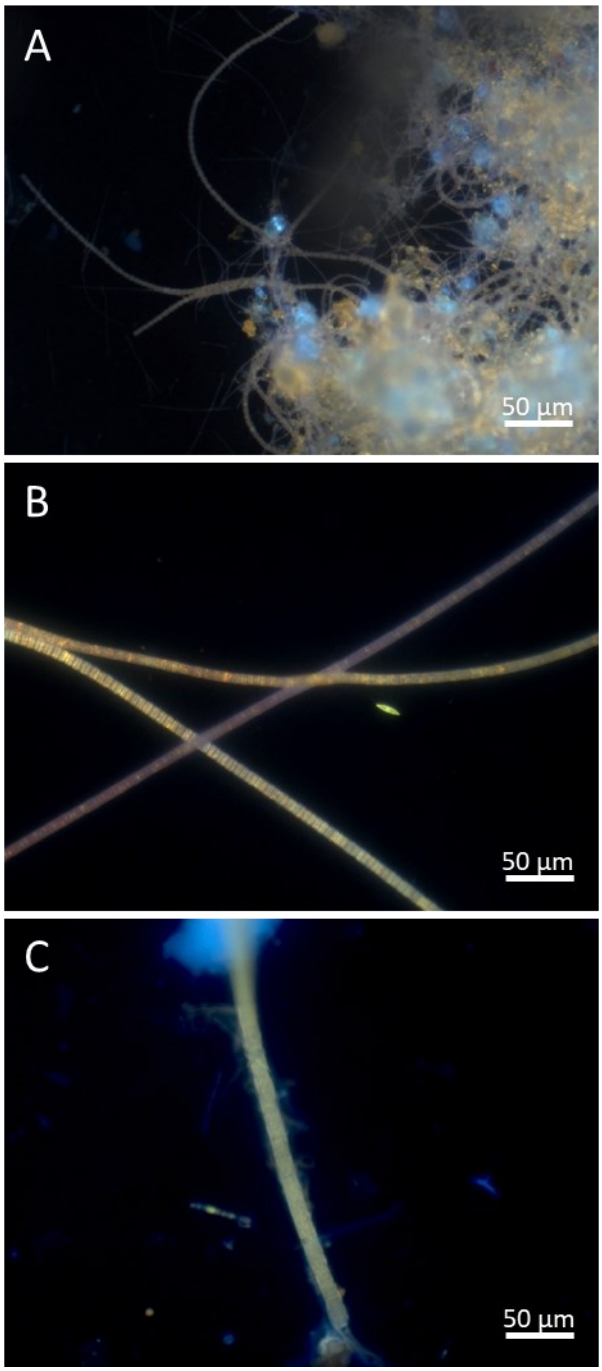

Fig. 21. DAPI-stained fluorescence imaging revealed a dense filament network in the (A) 18 – 21 °C treatment, but not in the (B) 15 °C and (C) 10 °C treatments where filaments were scarcely distributed

3.2.3 Salinity dependency (Cultivation test 3)

In the cultures grown at 6 (Fig. 22A) and 9 psu (Fig. 22B), the microbial mat was comprised mainly of thin photosynthetic filaments (mean ± SD diameter: 2.4 ± 0.5 µm). In the 12 psu treatment, filaments (mean ± SD diameter: 4.5 ± 0.4 µm) resembling *Nodularia* spp. made up a substantial portion of the microbial mat (Fig. 22C).

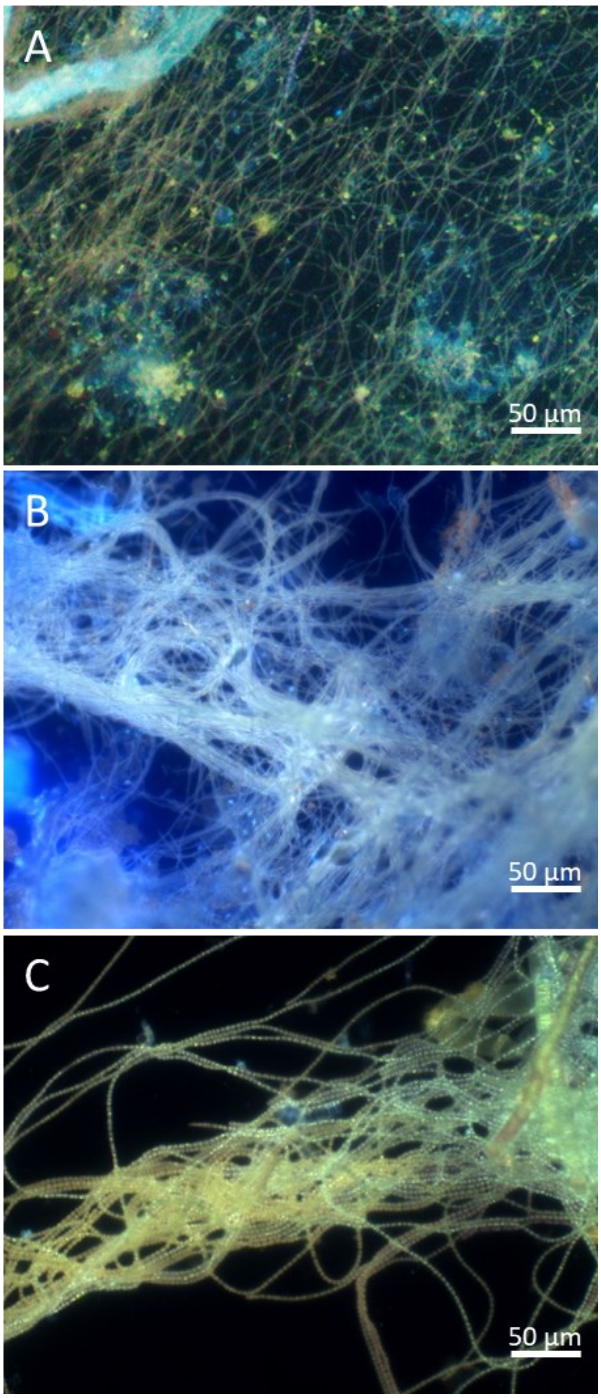

Fig. 22. DAPI-stained fluorescence imaging showed that thin polyP-accumulating photosynthetic filaments mainly comprised the microbial mat at salinities of (A) 6 psu and (B) 9 psu, while thicker filaments were much more evident at (C) 12 psu

3.2.4 Growth medium dependency (Cultivation test 4)

In 3 types of growth media (BG-11, ASN-III, and BG-11+ASN-III), an enrichment of the microbial mat was observed. In the BG-11 treatment, a mix of polyP-accumulating filamentous species was observed, although none of which morphologically resembled *Lyngbya* spp. (Fig. 23A). Among the 5 different growth media tested, the mat in the BG-11 treatment was most replete with polyP. In the BG-11+ASN-III (Fig. 23C) and ASN-III treatments (Fig. 23B), a distinct portion of filaments was thin. However, clusters of *Lyngbya*-like filaments were noticeable in these two treatments. PolyP accumulation in *Lyngbya*-like

clusters in the BG-11+ASN-III treatment appeared to be higher as compared to those in the ASN-III treatment. In contrast, the enrichment of the microbial mat was lower in the F/2 treatment (Fig. 23D). PolyP was mainly observed in non-filamentous entities, and the mat was almost devoid of filaments. In the treatment using autoclaved water from the study site as the growth medium, no enrichment of the mat was observed, and filaments appeared to be damaged (Fig. 23E).

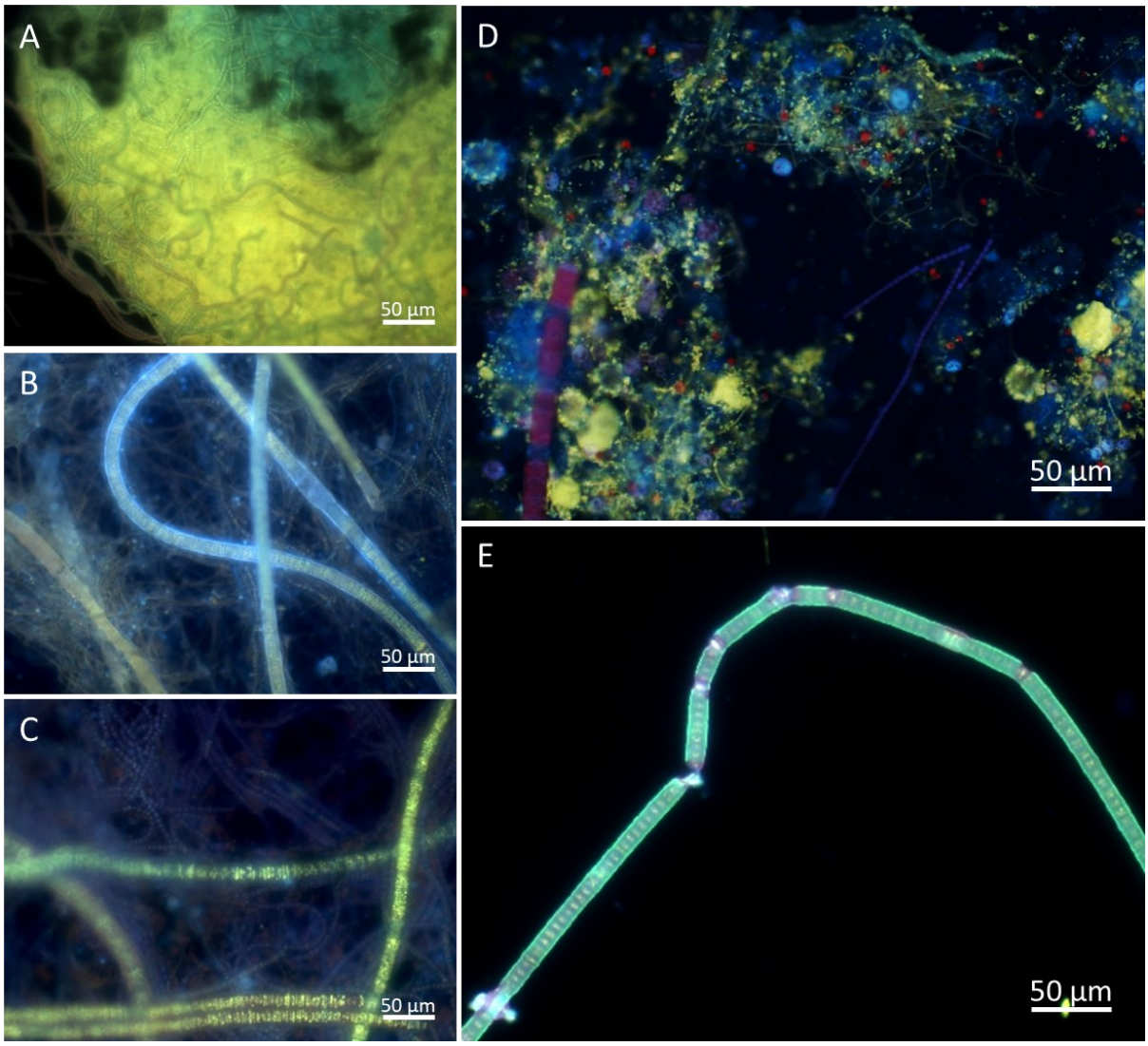

Fig. 23. DAPI-stained fluorescence imaging of cultures grown in (A) BG-11, (B) ASN-III, (C) BG-11+ASN-III, (D) F/2 media and (E) autoclaved study site-derived water. Filament enrichment was observed in A, B, and C; however, *Lyngbya*-like filaments were seen only in B and C. A scarcity of filaments was noted in D and E

3.2.5 Ammonia dependency (Cultivation test 5)

PolyP-accumulating filaments resembling *Lyngbya* spp. were observed only in the treatment without the addition of NH_4Cl (Fig. 24A). In the 100 µM (Fig. 24B) and 300 µM NH_4Cl (Fig. 24C) treatments, thin polyP-accumulating filaments were present. However, in the 1 mM NH_4Cl treatment, filaments were barely detected (Fig. 24D). Instead, polyP appeared to be trapped mostly in non-filamentous entities.

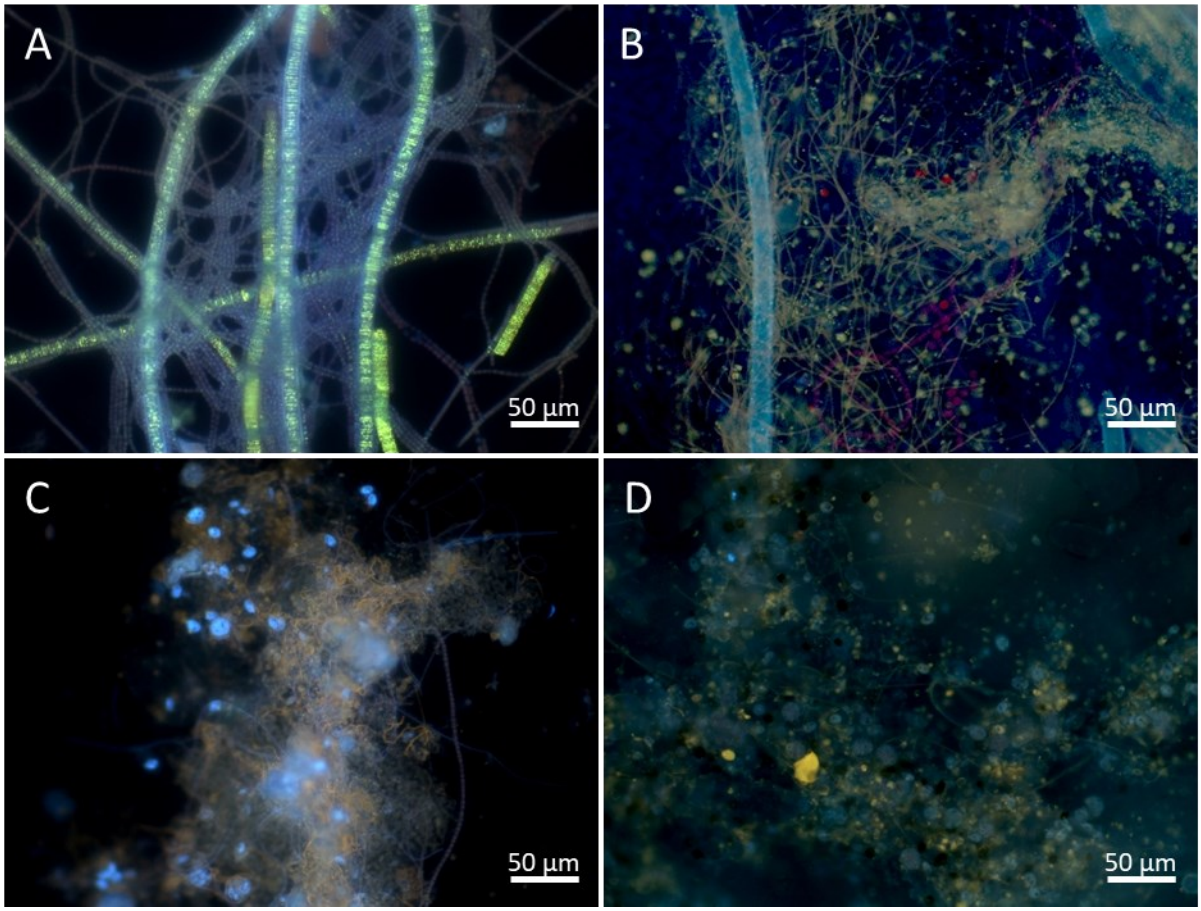

Fig. 24. DAPI-stained fluorescence imaging of treatments with (A) no added NH_4Cl, (B) 100 µmol L^{-1}, (C) 300 µmol $L^{-1,}$ and (D) 1 mmol L^{-1} NH_4Cl. PolyP-accumulating filaments resembling *Lyngbya* spp. were present only in A, while in B and C, thinner polyP-accumulating filaments were present. In D, filaments were barely detected; instead, polyP was observed in small non-filamentous entities

3.2.6 Growth on attachment substrate (Cultivation tests 6 and 7)

In both the absence and presence of agar substrate (test 6), clusters of *Lyngbya*-like filaments were the primary constituents of the microbial mat (Fig. 25A & B). In the presence of agar substrate, the filament clusters were mostly attached to the agar pieces, resulting in denser clusters (Fig. 25A). Therefore, the presence of agar was included as a default parameter in the following cultivation test.

In test 7, a similar level of enrichment of polyP-accumulating *Lyngbya*-like filaments in the microbial mat was observed, regardless of whether the agar attachment substrate was a single layer or in pieces (Fig. 25C & D). Therefore, agar prepared as a bottom layer in Greiner culture flasks was the ideal design for the incubation experiment in WP 3.

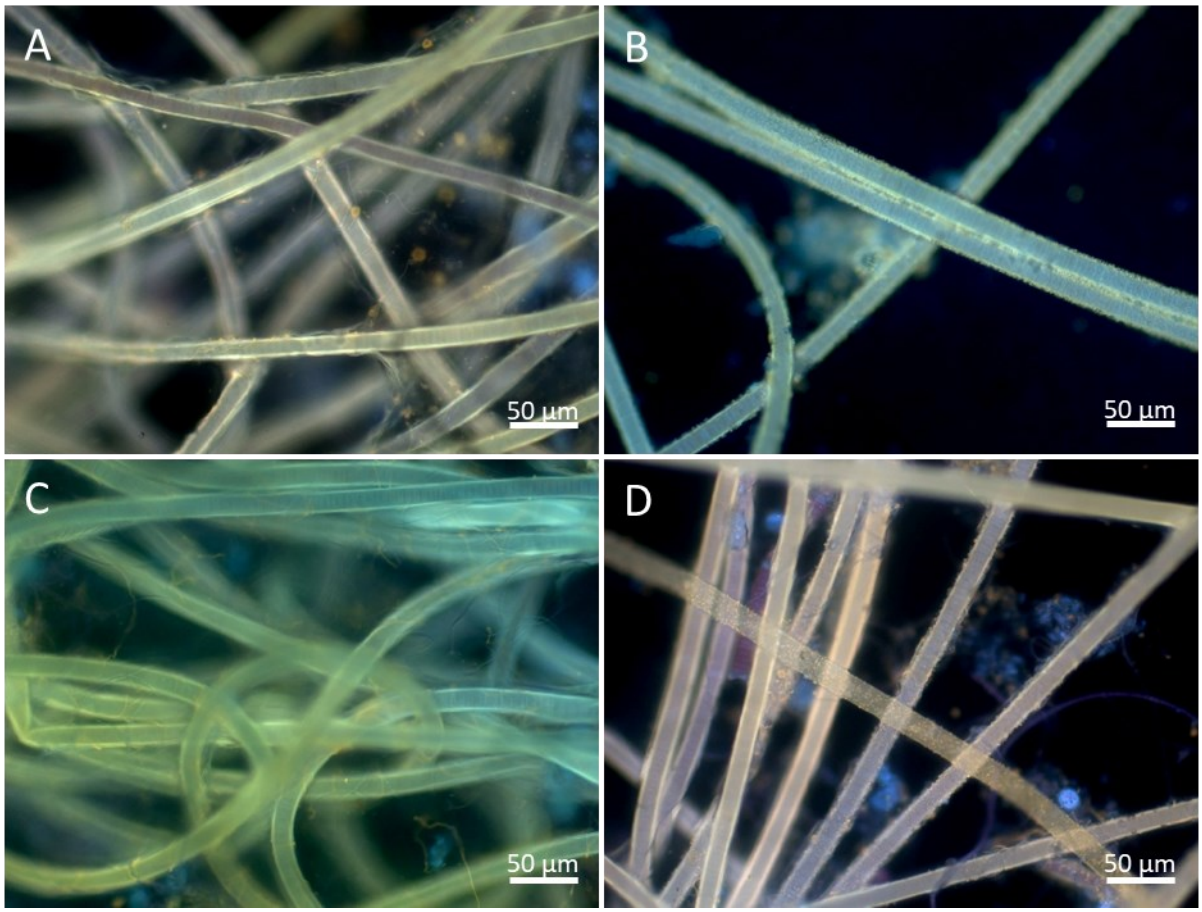

Fig. 25. DAPI-stained fluorescence imaging of treatments. In cultivation test 6, (A) the presence of agar pieces and (B) the absence of agar. In test 7, treatments with agar (C) as a bottom layer and (D) in pieces

3.3 Microbial mat's response to dissolved PO_4^{3-} addition (WP 3)

3.3.1 Microbial composition of mat

Light microscopy

From light microscopy, the microbial mat largely comprised photosynthetic filamentous cyanobacteria in all treatments (Fig. 26). The microbial composition of the mats across the treatments appeared largely similar, comprising a variety of photosynthetic filamentous species. The thickest filaments had an average diameter of 8.4 ± 0.8 µm (n = 20) and fit the morphological profile of members of the genus *Lyngbya*.

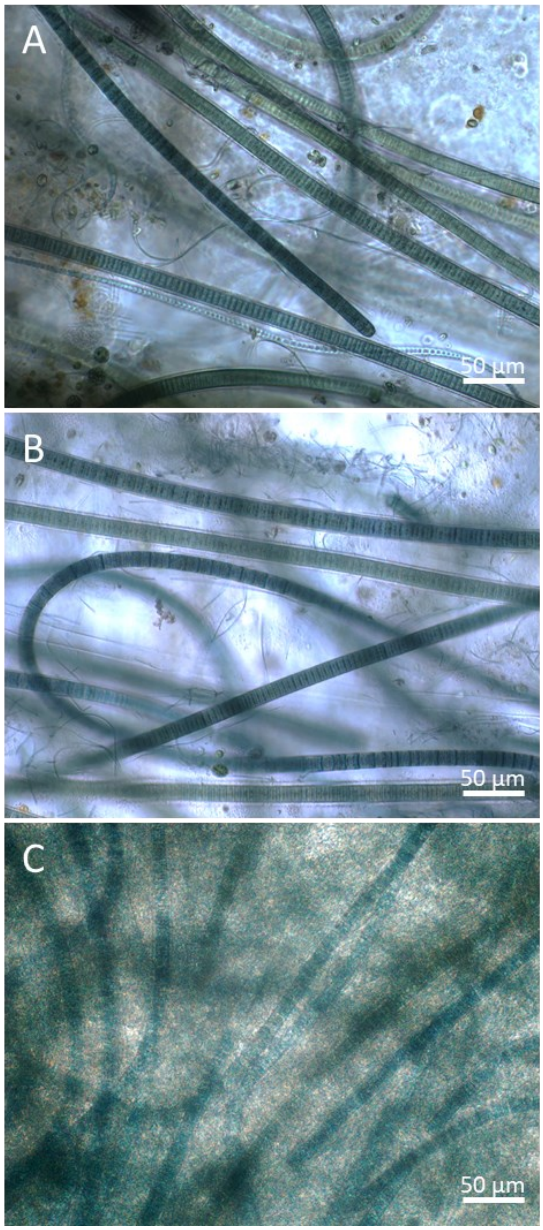

Fig. 26. Light microscopy of the microbial mat in time point '0' replicates of the (A) *in-situ*, (B) elevated temperature and (C) reduced salinity treatments

Bacterial composition during the incubation

Across the 3 treatments, 156 discrete bacterial MAGs were identified from the microbial mat, which covered >90% of genomic sequencing data generated from the microbial mat community. A total of 38 distinct bacterial orders were detected from time points '0', 2 h, 24 h, and 48 h of the incubation (Fig. 27). Four orders were associated with cyanobacteria, namely *Cyanobacteriales*, *Elainellales*, *Phormidesmiales,* and *PCC-6307*, of which the former 3 orders include filamentous member species. In addition, the order *Cyanobacteriales* also includes the genus *Lyngbya*. Between 5 – 56% of total bacterial genomic reads in the *in-situ* replicates, 2 – 12% in the elevated temperature replicates, and 0.1 – 2% in the reduced salinity replicates, were affiliated with the order *Cyanobacteriales*. With order *Elainellales*, the composition of affiliated reads in each treatment incubation ranged between 0.5 – 12% (*in-situ*), 0.2 – 5% (elevated temperature), and 6 – 35% (reduced salinity). Across all treatment replicates, the reads affiliated with both the orders *Phormidesmiales* and *PCC-6307* comprised ≤1% of total bacterial genomic reads. In addition, across all replicates, the percentage of bacterial genomic reads affiliated with selected bacterial orders was as follows: *Cytophagales* (2 – 17%), *Enterobacterales* (0.2 – 35%), *Pirellulales* (0.6 – 25%) and *Rhodobacterales* (11 – 52%).

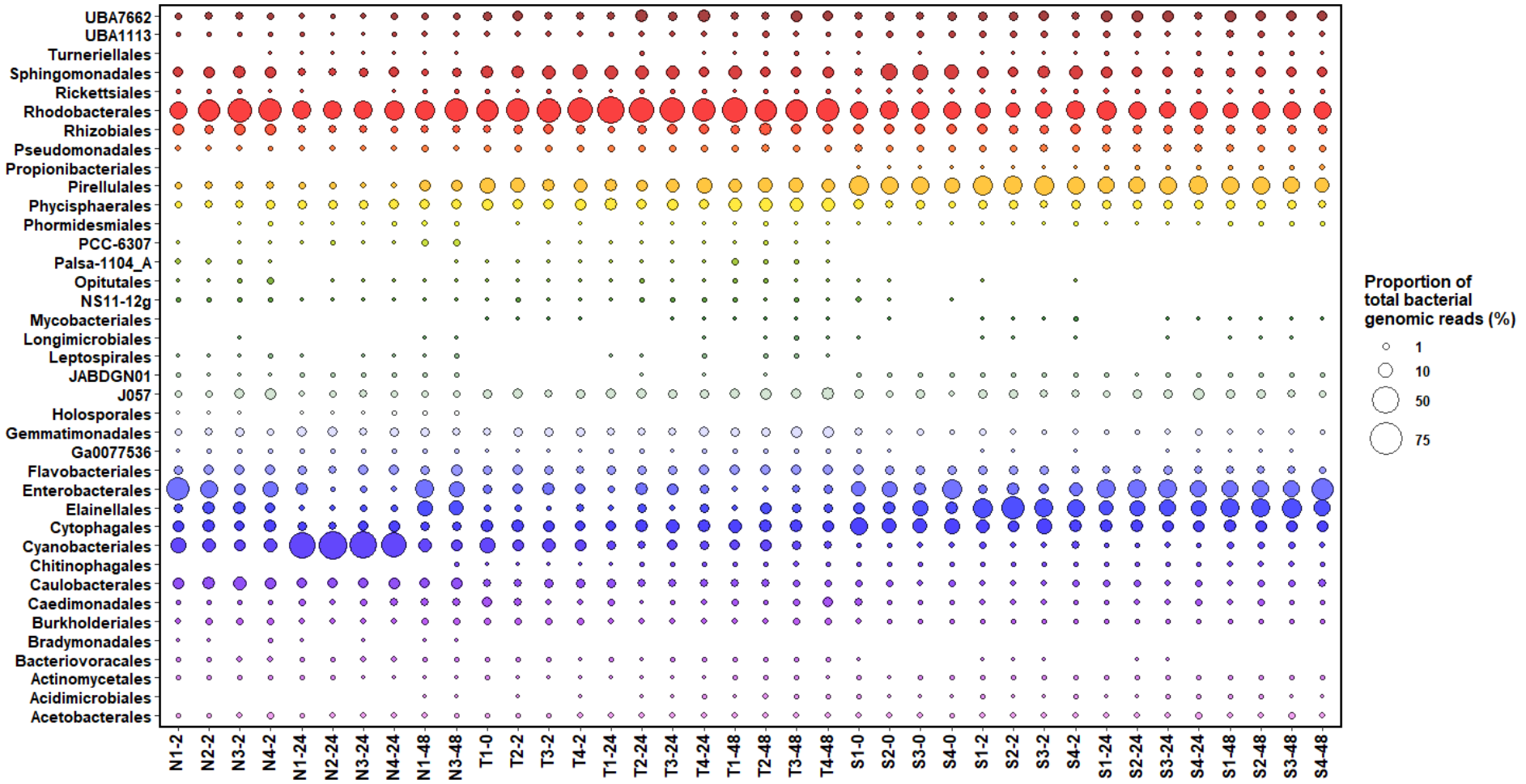

Fig. 27. Proportion of reads (out of total bacterial genomic reads in each replicate) affiliated to the 38 bacterial orders present in the microbial mat, across treatment replicates for time points '0', 2 h, 24 h, and 48 h. As mentioned in section 2.9.2, technical delays during the experiment resulted in a failure to collect time point '0' *in-situ* treatment replicates. Refer to Glossary for the description of each replicate

3.3.2 Microbial PO_4^{3-} uptake in various conditions

Within 2 h of KH_2PO_4 addition, the PO_4^{3-} content in the culture media decreased by 14×, 10× and 13× in the *in-situ*, elevated temperature, and reduced salinity treatments respectively (Fig. 28). Between 2 h and 8 h, PO_4^{3-} concentration further decreased 7× and 2× in the *in-situ* and elevated temperature treatments, respectively, while PO_4^{3-} was exhausted in the reduced salinity treatment after 8 h. Between 8 h and 72 h, the level of PO_4^{3-} across all treatments remained below 0.6 µmol L^{-1}. In this period, the PO_4^{3-} concentration was consistently higher in the elevated temperature treatment (0.20 – 0.56 µmol L^{-1}) than in the other treatments (*in-situ*: 0.06 – 0.17 µmol L^{-1}, reduced salinity: 0 µmol L^{-1}).

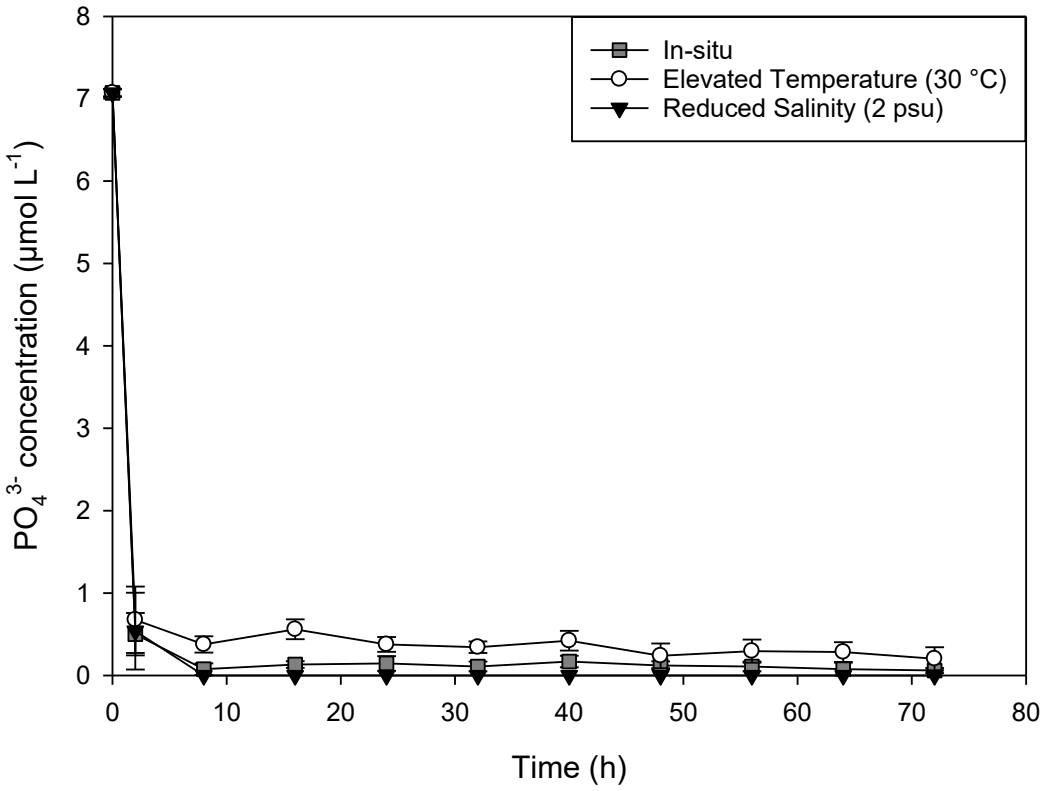

Fig. 28. Concentration of PO_4^{3-} (mean ± SD, n = 4) in the 3 treatments (*in-situ*, elevated temperature, reduced salinity) over the 72-h incubation period. The starting PO_4^{3-} concentration in all treatments was 7.07 µmol L^{-1}

3.3.3 Corresponding microbial polyP accumulation under various conditions

A near-consistent increase in microbial polyP-P content was observed in all treatments during a large part of the incubation starting from time point '0' (Fig. 29). The polyP-P content in the *in-situ* and reduced salinity treatments peaked at approximately 64 h and 48 h, respectively. In contrast, no polyP-P peak was observed under elevated temperature; instead, an increase in polyP-P content was observed right up to time point 72 h. From time point '0' to the time point showing the highest polyP-P content, all treatments displayed an approximately 3× increase in the amount of polyP-P. Under reduced salinity, the polyP-P content decreased after the peak, continuing to do so until the end of the incubation period (Fig. 29).

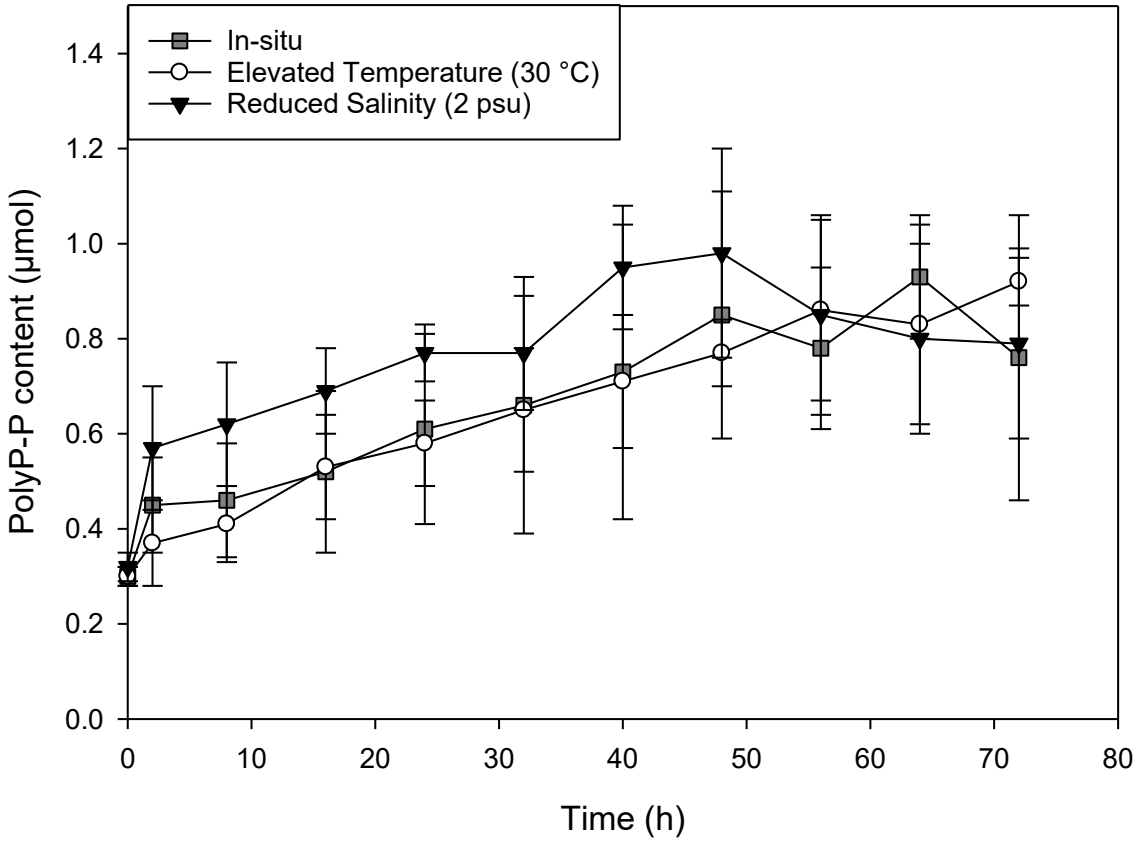

Fig. 29. PolyP-P content (mean ± SD, n = 4) in the 3 treatments during the 72-h incubation period

A mass balance polyP-P/PO_4^{3-} budget constructed for the *in-situ* treatment showed that the increase in average microbial polyP-P content could account for a maximum of 89% of the total microbial PO_4^{3-} uptake (polyP-P/PO_4^{3-}), which occurred at 64 h (Fig. 30). Within 2 h from the start of the incubation, polyP-P/PO_4^{3-} had reached 23%, and this was followed by a 4× increase between 2 h and 64 h. Between 64 h and 72 h, however, polyP-P/PO_4^{3-} had declined 1.4× to 66%.

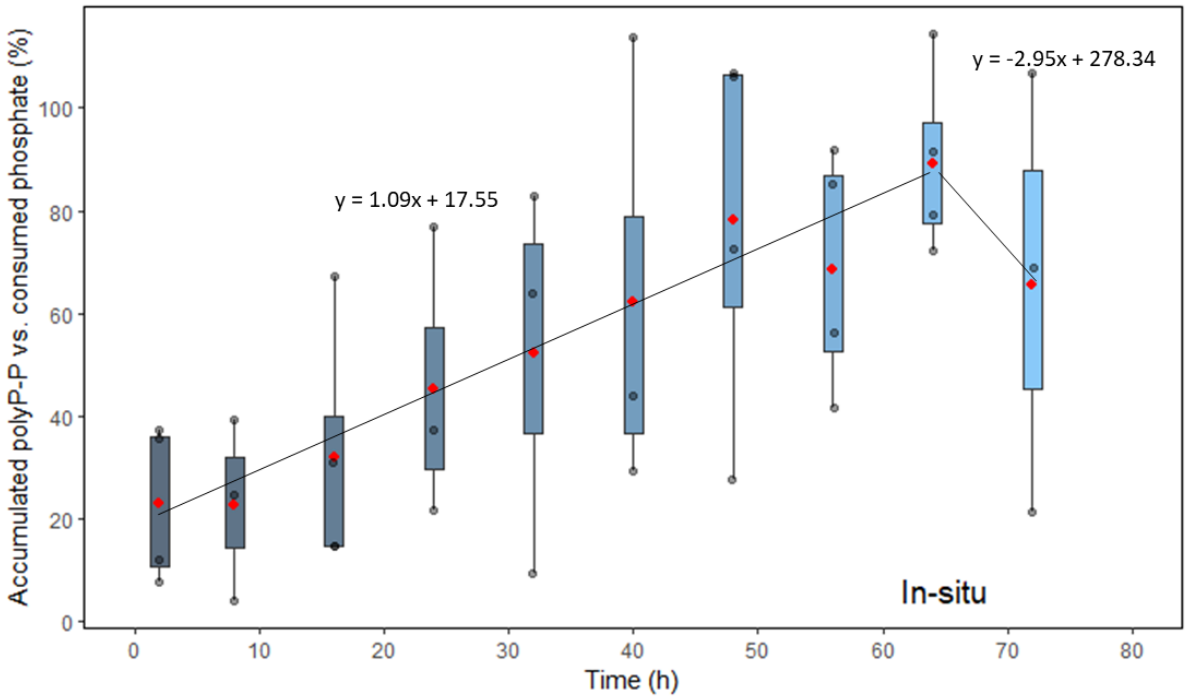

Fig. 30. The mass balance polyP-P/PO_4^{3-} budget for the *in-situ* incubation over 72 h. Boxes show upper and lower quartiles; red circle: mean; grey dots: replicate values; whiskers: max./min.

From DAPI-stained imaging of the *in-situ* samples, polyP content in the filamentous microbial mat was lowest at time point '0' (Fig. 31A). Increased accumulation of polyP (greenish-yellow fluorescence) was observed after 2 h (Fig. 31B), and a significantly higher level of accumulation at 64 h (Fig. 31C), which corresponded to the polyP-P/PO_4^{3-} peak (Fig. 30). At the end of the incubation, polyP was still retained in the filaments (Fig. 31D).

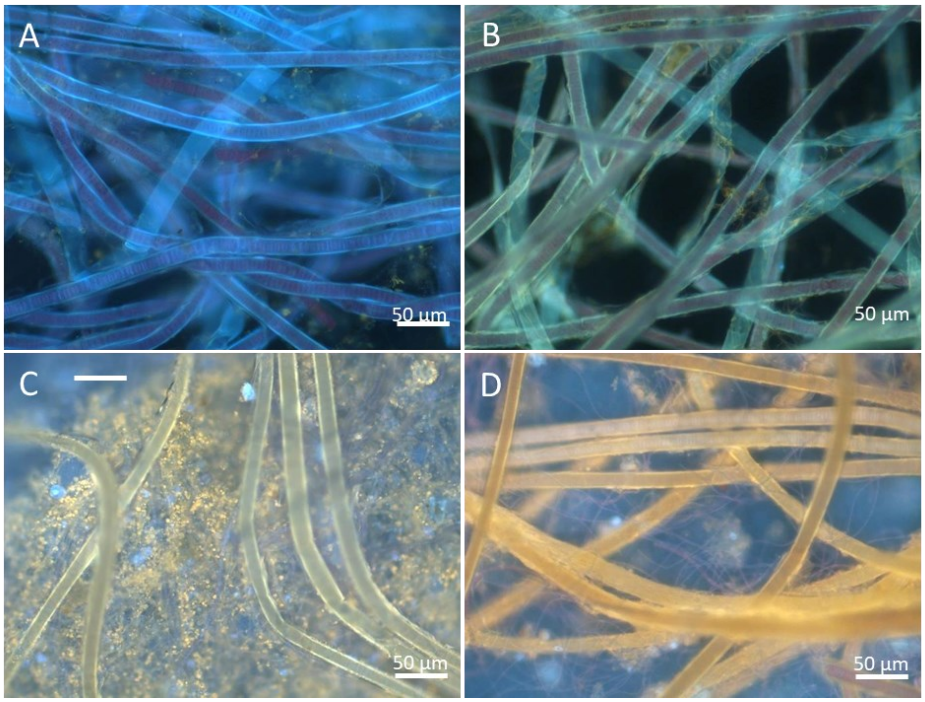

Fig. 31. DAPI-stained fluorescence imaging of the microbial mat in the *in-situ* treatment at time points (A) '0', (B) 2 h, (C) 64 h, and (D) 72 h. Between '0' and 2 h, a slight increase in polyP content (greenish-yellow fluorescence) in the filament-dominant mat was observed. At 64 h and 72 h, the polyP content was relatively higher

Under elevated temperature conditions, polyP-P/PO_4^{3-} reached a maximum of 90% by 72 h (Fig. 32). An almost constant increase in polyP-P/PO_4^{3-} was observed throughout the incubation, except for a slight decline between 56 h and 64 h.

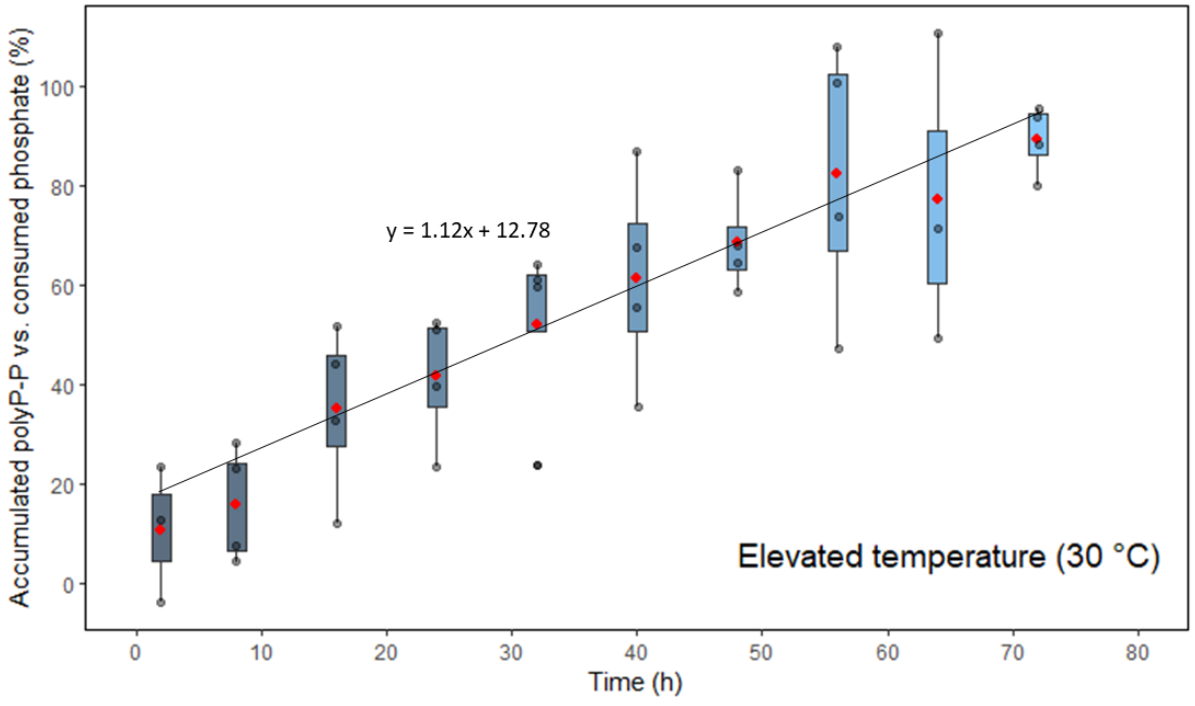

Fig. 32. The mass balance polyP-P/PO_4^{3-} budget for the elevated temperature incubation over 72 h. Boxes show upper and lower quartiles; red circle: mean; grey dots: replicate values; whiskers: max./min.

Likewise, DAPI-stained images reflected a gradual accumulation of polyP at elevated temperature (Fig. 33). At 2 h, polyP accumulation was visible in filaments (Fig. 33B). However, by the end of the incubation, the polyP signal (greenish-yellow fluorescence) was noticeably stronger in thinner filaments (Fig. 33C).

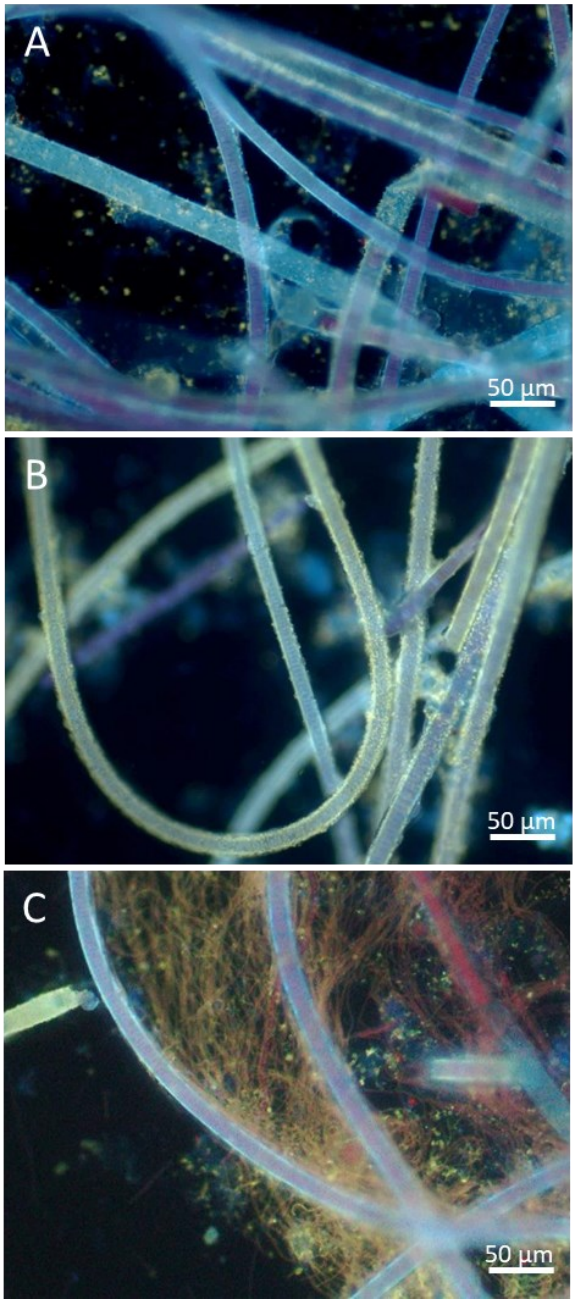

Fig. 33. DAPI-stained fluorescence imaging of the microbial mat in the elevated temperature treatment at the time points (A) '0', (B) 2 h, and (C) 72 h. Compared to '0', there was a slight increase in polyP accumulation in the filaments at 2 h. At 72 h, polyP accumulation was noticeably greater in thinner filaments

Under reduced salinity, the polyP-P/PO_4^{3-} maximum (93%) was observed at 48 h (Fig. 34). At 2 h into the incubation, polyP-P/PO_4^{3-} was already at 39%. A continual increase in polyP-P/PO_4^{3-} was recorded from time point 2 h to 48 h, followed by an immediate decline until the end of the incubation.

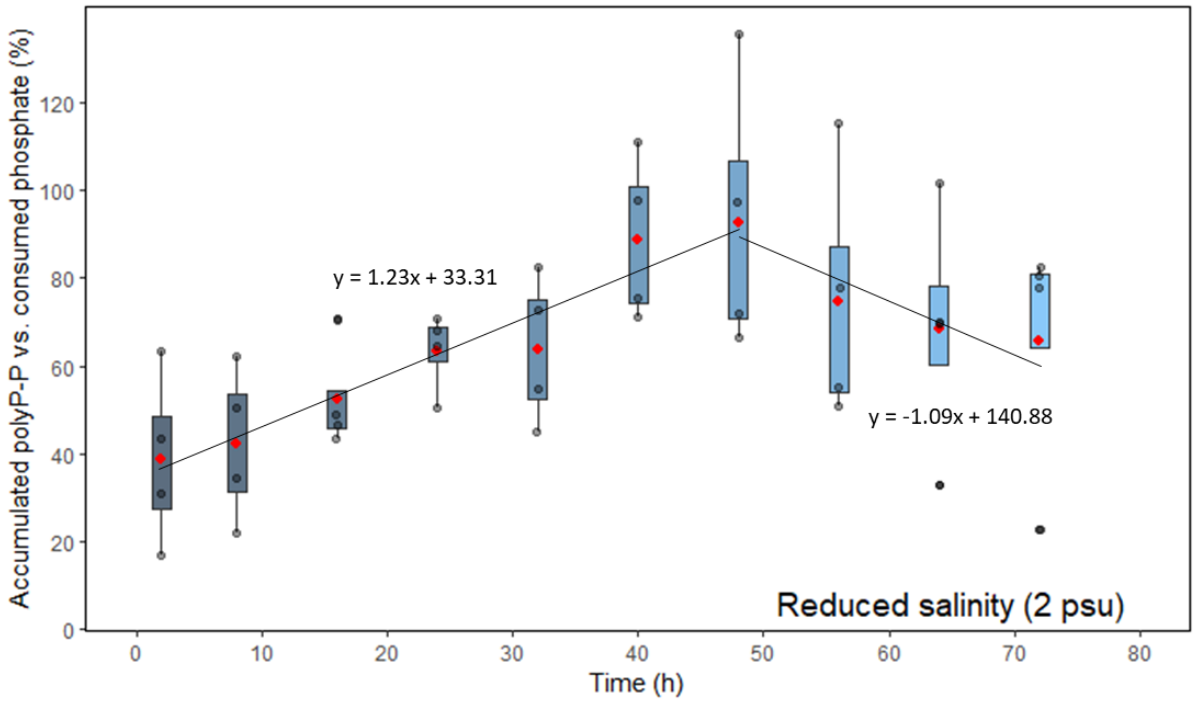

Fig. 34. The mass balance polyP-P/PO_4^{3-} budget for the reduced salinity incubation over 72 h. Boxes show upper and lower quartiles; red circle: mean; grey dots: replicate values; whiskers: max./min.

Corresponding DAPI imaging from the reduced salinity treatment reflected a slight increase in polyP content in the mat after 2 h (Fig. 35B), and visibly greater polyP accumulation at 48 h (Fig. 35C), which was observed mainly in thin filaments. At 72 h, the greenish-yellow fluorescence signal was slightly lower than at 48 h, indicating a slight decrease in polyP content at 72 h (Fig. 35D).

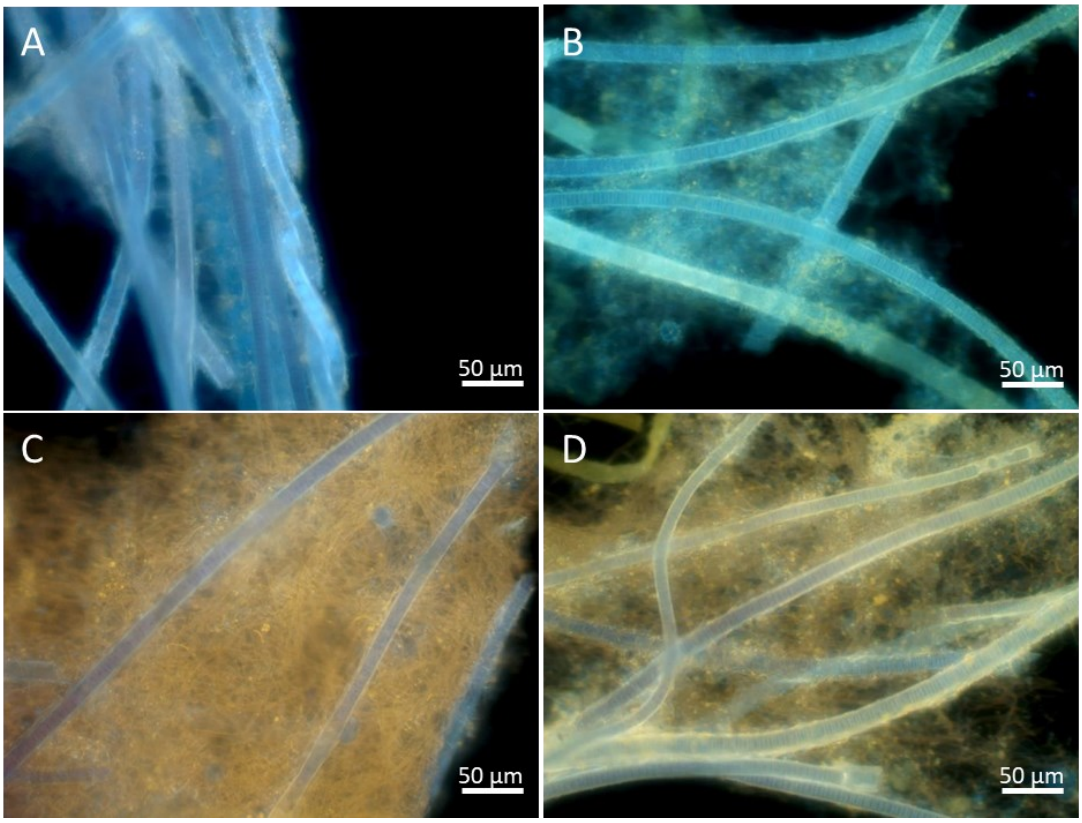

Fig. 35. DAPI-stained images of the microbial mat during the reduced salinity incubation at the time points (A) '0', (B) 2 h, (C) 48 h, and (D) 72 h. Compared to '0', there was a slight increase in polyP accumulation in the filaments at 2 h, followed by a visibly higher accumulation at 48 h, mainly in thin filaments. At 72 h, polyP accumulation appeared to be slightly lower than at 48 h

3.3.4 Differential expression of P-metabolising genes

General transcript levels within the microbial mat community

In all replicates, genes associated with phosphate-specific uptake and transport (*pstSCAB*) and phosphate-scavenging (*phoABDRU*) displayed high transcript levels within the microbial mat community; the highest level was observed with *pstS* (Fig. 36). In comparison, transcripts assigned to phosphonate/phosphate transport-associated genes (*phnCDEFGHJKLM*) had a noticeably lower level among the replicates.

From time point '0' to 2 h (reduced salinity)

Under reduced salinity, the genes *pstSCAB*, *phoABDRU,* and *phnCDE* were downregulated (log2-fold change < 0), while the genes *phnFGJKLM* were upregulated (log2-fold change > 0) (Fig. 36). On the other hand, genes involved in polyP synthesis (*ppk1*, *ppk2*) and polyP degradation (*ppx-gppA*) were downregulated, while the polyP degradation-associated gene *pap* was significantly upregulated (log2-fold change ≥ 1).

From 2 h to 24 h

Across all treatments, genes *pstSCAB* were mostly upregulated (Fig. 36). The *pho* genes were also mostly upregulated, except for *phoA* which was upregulated only under reduced salinity. Interestingly, genes *phnCDE* were significantly upregulated under reduced salinity but showed mixed regulatory signals under *in-situ* and elevated temperature conditions. In addition, genes *phnFGJKLM* were mostly downregulated under all treatment conditions. In all treatments, *ppk1* and *ppk2* were upregulated, with significant upregulation observed under *in-situ* and elevated temperature conditions. However, mixed results were observed with genes linked to polyP degradation: both the *pap* and *ppgK* genes were downregulated, while *ppx-gppA* and *ppa* were upregulated under all conditions.

In general, the 24 h vs. 2 h expression profile of P metabolism-associated genes was fairly similar among the 3 treatments (Fig. 36). However, while 60% of the genes were significantly up-/downregulated under *in-situ* conditions, only 7% and 23% were significantly up-/downregulated under elevated temperature and reduced salinity conditions, respectively.

When compared with the *in-situ* treatment, the type of expression (up-/downregulation) of the selected P metabolism-associated genes (Fig. 36) was 90% similar in the elevated temperature and 77% similar in the reduced salinity treatment.

From 24 h to 48 h

The *pstSCAB* genes were downregulated under *in-situ* and elevated temperature conditions, but upregulated under reduced salinity (Fig. 36). In all treatments, the *phoBRU* genes were mostly downregulated, in contrast to *phoA* and *phoD* which were largely upregulated. The genes *phnCDE* were mostly upregulated. The *phnFGJKLM* genes were also mainly upregulated, except under reduced salinity where *phnF* and *phnH* were downregulated. Downregulation of *ppk1* and *ppk2* was generally observed across all conditions, being most significantly expressed under *in-situ* conditions. The *pap* and *ppgK* genes were upregulated, while *ppx-gppA* and *ppa* were downregulated under all conditions.

When compared with the *in-situ* treatment, the type of expression (up-/downregulation) of the selected P metabolism-associated genes (Fig. 36) was 57% similar in the elevated temperature and 87% similar in the reduced salinity treatment.

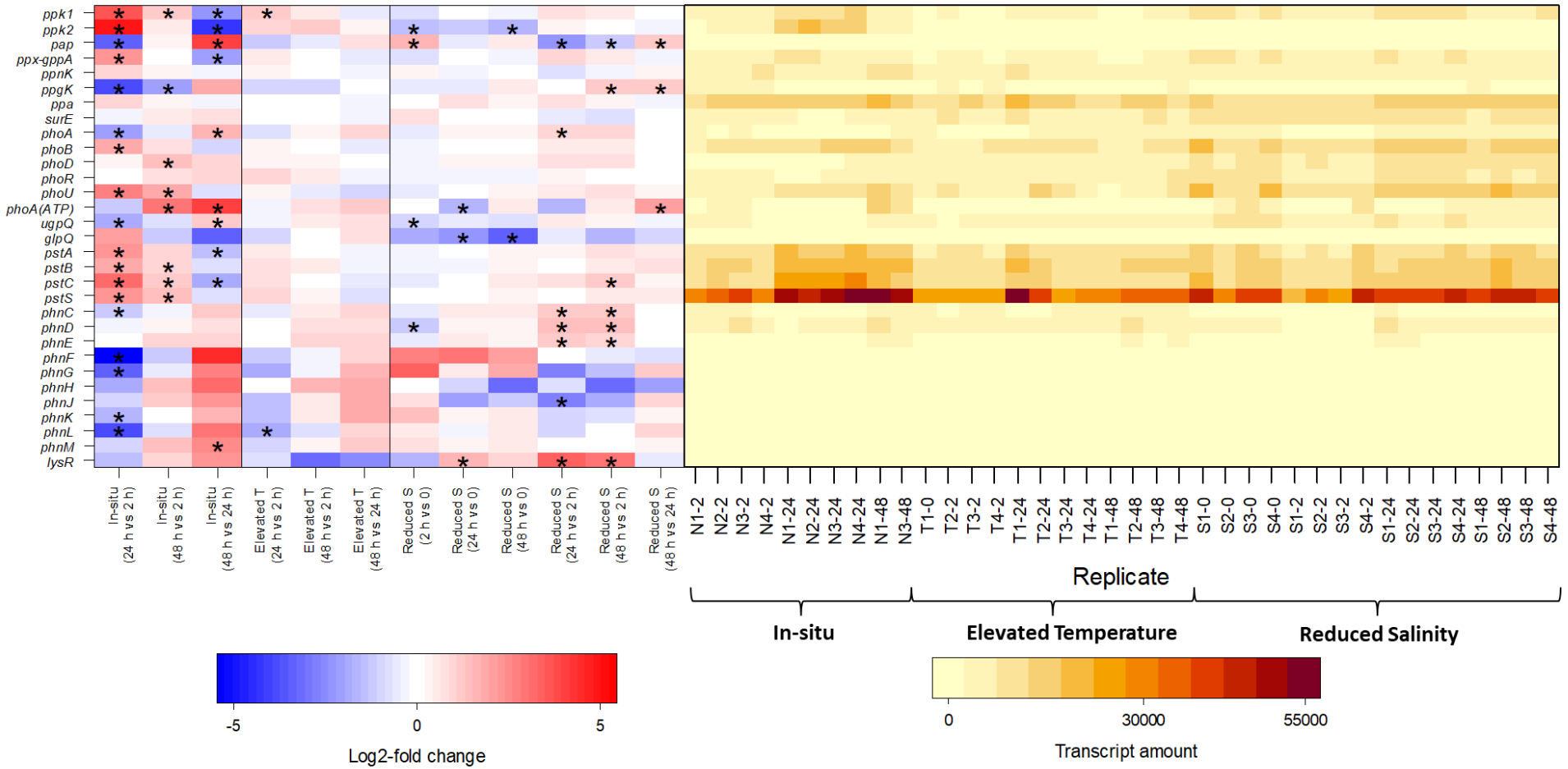

Fig. 36. Differential gene expression of P-metabolizing genes between time points in the 3 treatments (left), where blue-shaded boxes (log2-fold change < 0) indicate downregulation, and red-shaded boxes (log2-fold change > 0) indicate upregulation. In addition, a heat map (right) displays the corresponding gene transcript composition across all sequenced replicates from the 3 treatments. Significantly differentially expressed genes are marked with a '*'. Differential expression was considered significant when both the log2-fold change ≥ 1 and the adjusted *p*-value (padj) ≤ 0.1. Refer to Glossary for the description of each replicate

3.3.5 Differential expression of stress response genes

Heat stress response

The expression of the major heat/general stress-related genes was compared between the *in-situ* and the elevated temperature treatment, at time point 2 h, as well as at "24 h vs. 2 h" of the elevated temperature treatment (Fig. 37A). As mentioned previously, at time point '0', only one replicate of the elevated temperature treatment was collected, while no *in-situ* replicates could be obtained. Therefore, we established the *in-situ* (2 h) time point as a non-stressed scenario that other treatments could be compared to.

At 2 h (elevated temperature vs. *in-situ*), significant differential expression was only observed for *hsp17*, which was upregulated (Fig. 37A). Additionally, 5 heat/general stress-related genes (*clpB*, *dnaJ*, *dnaK*, *groEL*, *htpG*) were noticeably upregulated (log2-fold change ≥ 0.5), while the gene (*sigB*) was noticeably downregulated (log2-fold change ≤ -0.5).

At "24 h vs. 2 h" under elevated temperature, significant differential expression was only observed for *rpoS*, which was downregulated (Fig. 37B). Furthermore, 2 heat/general stress-related genes (*groEL*, *hscA*) were noticeably downregulated (log2-fold change ≤ -0.5). In contrast, noticeable upregulation was observed with *hsp17* (log2-fold change ≥ 0.5).

Salinity stress response

Expression of the major salinity/general stress-related genes was compared in 2 scenarios: reduced salinity (2 h vs. time point '0') and reduced salinity (24 h vs. 2 h) (Fig. 38). Under reduced salinity, 7 genes (*dnaK1*, *msrR*, *rpoS*, *sigB*, *slr0750*, *slr2019*, *stpA*) were significantly upregulated at 2 h, relative to time point '0' (Fig. 38A). In addition, 4 salinity/general stress-related genes (*sll0947*, *sll1988*, *slr1894*, *dnaJ*) were noticeably upregulated (log2-fold change ≥ 0.5). In contrast, *sll1037* and *sll1566* were significantly downregulated.

At "24 h vs. 2 h", 10 salinity/general stress-related genes (*dnaK1*, *ggpS*, *msrR*, *rpoS*, *sigB*, *sll0947*, *slr0750*, *slr1894*, *slr2019*, *stpA*) were significantly downregulated (Fig. 38B). Furthermore, 2 other genes (*sll1566*, *sod2*) were noticeably downregulated (log2-fold change ≤ -0.5). Only one gene (*sll0248*) was significantly upregulated.

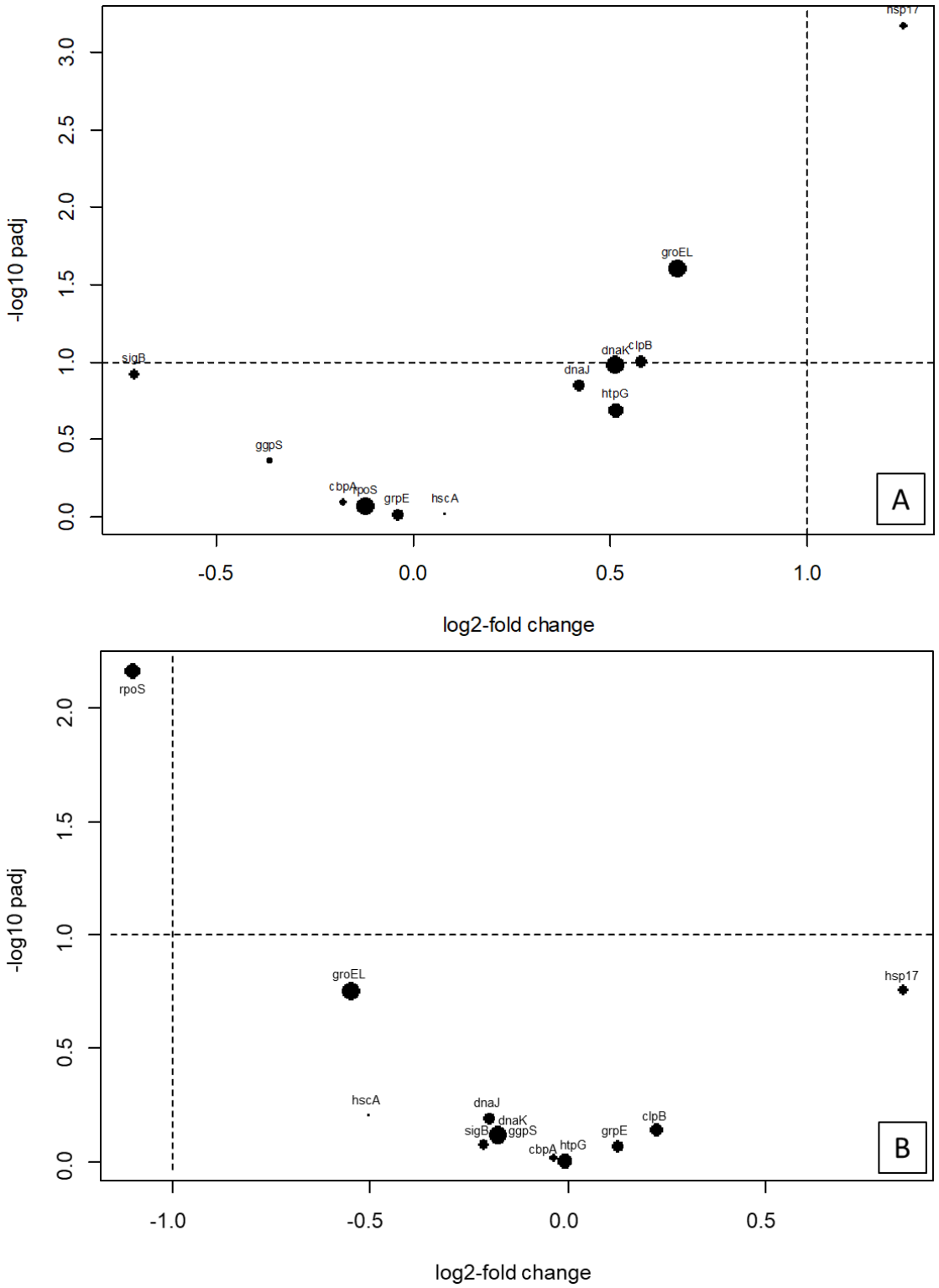

Fig. 37. (A) Differential expression of heat/general stress-associated genes in the elevated temperature treatment relative to the *in-situ* treatment at time point 2 h, since only a single time point '0' replicate was collected at the start of the elevated temperature incubation. (B) Differential expression of heat/general stress-associated genes in the elevated temperature treatment at 24 h, relative to 2 h. Differential expression was considered significant when both the absolute value of log2-fold change ≥ 1 (*x*-axis) and the -log10 adjusted *p*-value (padj) ≥ 1 (*y*-axis), with both thresholds indicated by dotted lines. The size of each data point corresponds to the mean of normalized counts of all samples

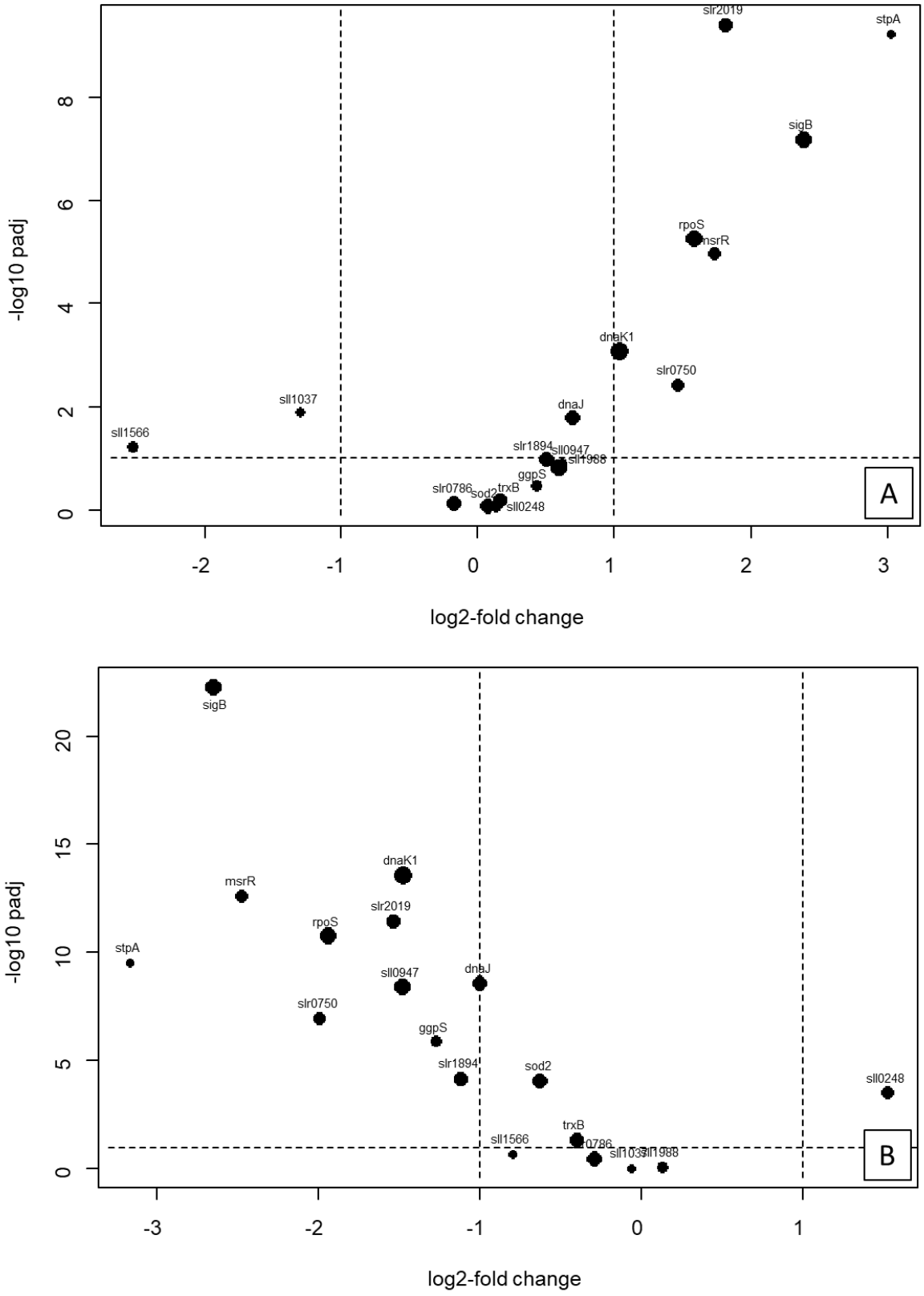

Fig. 38. Differential expression of salinity/general stress-associated genes in the reduced salinity treatment at (A) 2 h, relative to time point '0', and at (B) 24 h, relative to time point 2 h. Differential expression was considered significant when both the absolute value of log2-fold change ≥ 1 (*x*-axis) and the -log10 adjusted *p*-value (padj) ≤ 0.1 (*y*-axis), with both thresholds indicated by dotted lines. The size of each data point corresponds to the mean of normalized counts of all samples

3.3.6 Transcript levels of *ppk* and *pstS* genes across treatments

A heat map analysis of the 10 bacteria MAGs (family level) contributing the most to *ppk1* transcript levels showed differences in the dominant bacteria families expressing *ppk1* activity among the treatments (Fig. 39A). Moreover, *ppk1* activity was dominated by a single bacterial MAG (affiliated with the family *Geitlerinemaceae*, comprising various species of filamentous cyanobacteria, including the genus *Lyngbya*) at 24 h in the *in-situ* treatment. In the stressed treatments, however, the *ppk1* activity of this MAG was greatly reduced, while the activity of the other MAGs (e.g., families *Alteromonadaceae*, *Cyclobacteriaceae*, *Elainellaceae*) increased. The heat map analysis of *ppk2* also showed activity being dominated by the MAG *Geitlerinemaceae* under *in-situ* conditions; however, a lack of *ppk2* activity was observed under stressed conditions (Fig. 39B).

For *pstS*, a heat map analysis showed that most *pstS* activity in the *in-situ* treatment at 24 h originated from 2 bacterial MAGs (both affiliated with *Geitlerinemaceae*); at 48 h, however, *pstS* activity was dominated by MAGs belonging to the families *Alteromonadaceae* and *Elainellaceae* (Fig. 39C). In the stressed treatments, *pstS* activity was strong in MAGs affiliated with the families *Alteromonadaceae* and *Elainellaceae*; in addition, other MAGs affiliated with *Microcoleaceae* and *Nostocaceae* also exhibited noticeable but comparatively moderate *pstS* activity under elevated temperature.

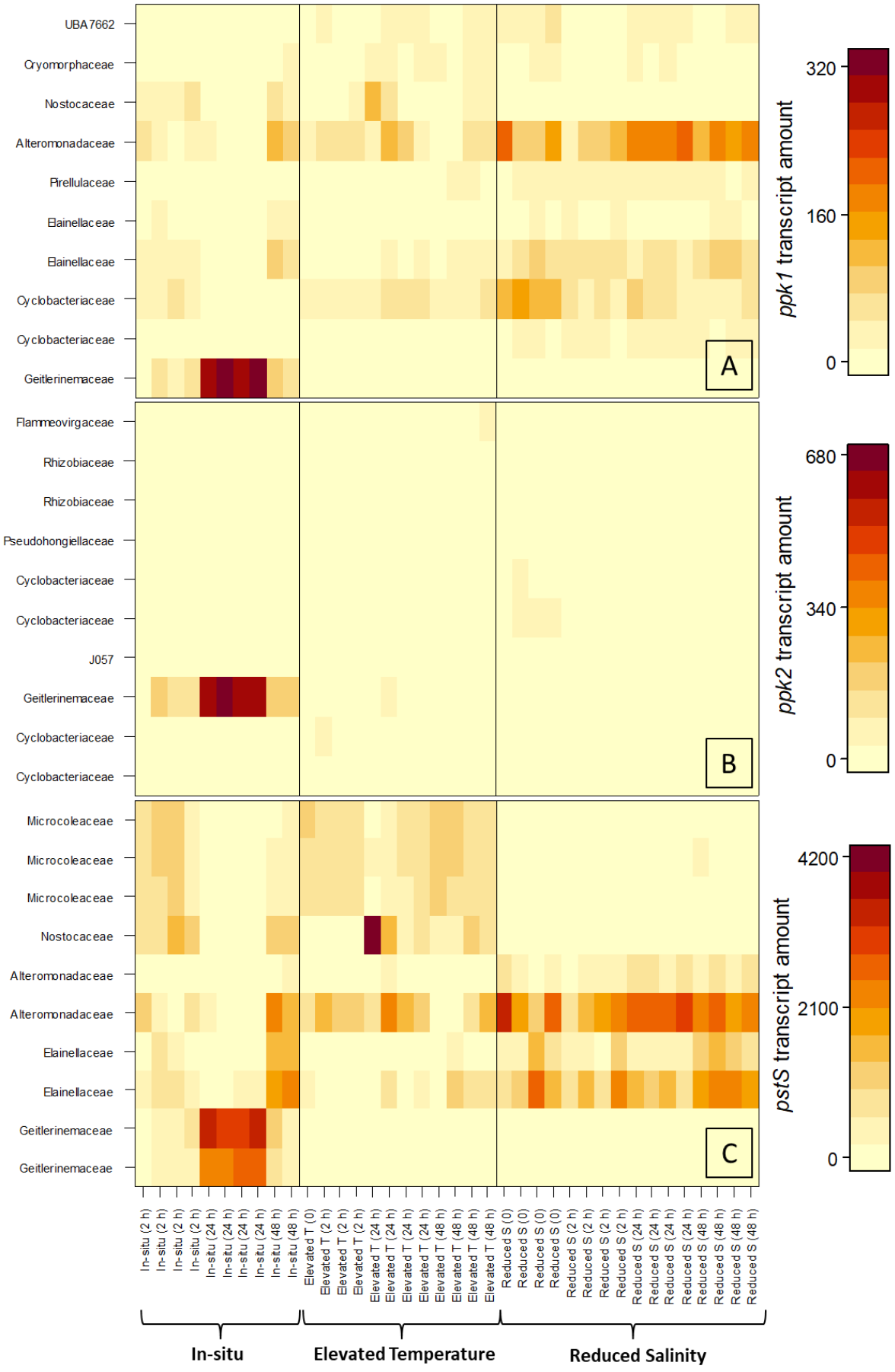

Fig. 39. Heat maps of the 10 bacteria MAGs (y-axis) contributing most to (A) *ppk1* (B) *ppk2* and (C) *pstS* gene transcript levels in general across all sequenced replicates from the 3 treatments (x-axis)

4 Discussion

4.1 Microbial-driven impact on aquatic P fluxes in a coastal peatland

4.1.1 PO_4^{3-} uptake and release in winter treatments

Our study in the winter showed distinct PO_4^{3-} release to the bottom water (Fig. 16A) and microbial polyP sequestration (Fig. 11) under elevated temperature (WinterOX15) and oxygen-depleted (WinterOD5) conditions, which greatly contrasted with the relative stability under *in-situ* conditions. The parallel increase of both bottom water Fe_{diss} and PO_4^{3-} in the first half of both incubations possibly indicated a contribution to the bottom water PO_4^{3-} pool by the redox-related dissolution of Fe oxyhydroxides and associated P (Fig. 16A & B).

Nevertheless, the parallel decrease of Fe_{diss} and PO_4^{3-} in the second half of WinterOX15 also indicated that aside from microbial PO_4^{3-} uptake and polyP accumulation, PO_4^{3-} adsorption occurred during the precipitation of Fe_{diss} as Fe oxyhydroxides in the peat layer. In the same period, the bottom water PO_4^{3-} concentration in WinterOD5 remained relatively constant despite an increase in Fe_{diss} (Fig. 16B). This might signify a depletion of Fe-bound P in the peat, resulting in a decoupling of Fe and P during the WinterOD5 incubation, as also indicated by high porewater Fe_{diss} alongside low porewater PO_4^{3-} (Fig. 19) and a lower PO_4^{3-} efflux than in WinterOX15 (Table 3). Moreover, in the porewater, the disparity that the highest Fe_{diss} was in WinterOD5 but the highest PO_4^{3-} was instead in WinterOX15 (Fig. 19B), implies that P release cannot exclusively originate from Fe oxyhydroxides.

Furthermore, the relatively low Fe_{xs}:P_{xs} molar ratio of the surface peat samples (mean: 2.6) (Table 5) was comparable to the Fe:P ratios of Fe oxyhydroxides and Fe-P mineral fractions (Dellwig et al. 2010). This might indicate that the P-adsorption sites of any Fe oxyhydroxides present in the peat were fairly saturated with PO_4^{3-}. The phosphate-sequestering ability of Fe oxyhydroxides in our peat samples further declined with increased reducing conditions during incubation under oxygen depletion and temperature elevation.

The adsorption of P on sediment particles is also pH-dependent. At a certain pH range (2 – 8), P sorption readily occurs; however, sorption rapidly declines when the threshold at both ends of this range is reached (Zhou et al. 2005). Since the winter incubations maintained a pH range of 6.3 – 7.5, the pH effect on PO_4^{3-} concentration was likely negligible.

Another factor reducing the adsorption of P on sediment particles is increasing temperature (Kleeberg & Kozerski 1997, Perkins & Underwood 2001). This increases the molar solubility

of compounds at equilibrium in the sediment, which reduces P adsorption (Eysseltová et al. 1988). An increased temperature also enhances organic matter degradation and consequently internal nutrient cycling and release, in addition to oxygen consumption (Arnosti et al. 1998). This scenario is possibly illustrated by the stronger increase of Fe_{diss} and PO_4^{3-} in WinterOX15 when compared to WinterOD5 (Fig. 16A & B), since an increased temperature-dependent degradation rate promotes both PO_4^{3-} release from organic matter and redox-related Fe oxyhydroxide dissolution.

The most significant driver of nutrient cycling is organic matter degradation, which releases biologically available components such as PO_4^{3-} and NH_4^+ (Nixon 1981). Therefore, rapidly increasing PO_4^{3-} and NH_4^+ levels in both WinterOD5 and WinterOX15 (Fig. 16A & D) point to a significant fraction of added PO_4^{3-} arising from this process, when considering that the release of both PO_4^{3-} and NH_4^+ during organic matter degradation is stoichiometrically coupled (Berner 1977, Krom & Berner 1980).

Nevertheless, a paired *t*-test comparing the bottom water NH_4^+:PO_4^{3-} ratio between the Day 5 – 10 and 0 – 5 segments in the winter treatments (Fig. 18) showed significant p-values below 0.05 (WinterOX5: 0.0003; WinterOD5: 0.003; WinterOX15: 0.003), revealing an enhanced PO_4^{3-} uptake in the latter half of the incubation. A preferential release of PO_4^{3-} in relation to NH_4^+ during organic matter degradation can also occur under reducing or even sulfidic conditions (Ingall et al. 2005), which might partly account for the low NH_4^+:PO_4^{3-} ratio in the first half of the WinterOD5 incubation. Under *in-situ* conditions (WinterOX5), a linear regression fit of the bottom water NH_4^+ trend throughout the incubation period showed a release rate of 1.95 µmol L^{-1} d^{-1} (Fig. 16D), with the rate of PO_4^{3-}, in theory, being roughly similar (Paulmier et al. 2009). *In-situ* conditions were selected for this analysis since this reduced additional NH_4^+ excretion from organisms under temperature-related or hypoxic stress (Whiles et al. 2009, Cong et al. 2009). Concurrently, NO_x^- levels (<5 µmol L^{-1}) were constantly low (Fig. 16C), implying that any loss of NH_4^+ through coupled nitrification-denitrification was negligible. Since the temperature coefficient Q_{10} typically exhibits a range of 2 – 3 in biological systems (Běhrádek 1930, Hochachka 1991), both ends of this range were used to estimate the hypothetical amount of PO_4^{3-} released on the last day of the temperature-elevated winter incubation (WinterOX15; Table 7). The estimated PO_4^{3-} concentrations were 39 µmol L^{-1} and 59 µmol L^{-1} for $Q_{10} = 2$ and $Q_{10} = 3$, respectively. These values were 24× and 37× higher than the actual PO_4^{3-} concentration of 1.6 µmol L^{-1}. Moreover, by adding the calculated change in PO_4^{3-} concentration ($C_{polyP\text{-}P}$) in WinterOX15

(Table 8) to the actual PO_4^{3-} concentration on Day 10, a value of 33 µmol L^{-1} was obtained. This amount is 85% and 60% of the hypothesized PO_4^{3-} concentrations for Q_{10} = 2 and Q_{10} = 3, respectively, indicating that polyP accumulation throughout the entire incubation period could account for a substantial portion of the difference between the actual and predicted PO_4^{3-} concentrations at the end of the incubation.

Although the difference in polyP-P content between the winter treatments on Day 10 and the freshly-collected cores on Day 0 was not statistically significant ($p > 0.05$), the large $C_{polyP\text{-}P}$ in both WinterOD5 and WinterOX15 signified that polyP accumulation could eliminate the bulk of PO_4^{3-} from the bottom water (Table 8).

Table 7. Predicted and actual PO_4^{3-} concentration under elevated temperature conditions (WinterOX15) on Day 10 of the incubation. The Q_{10} (temperature coefficient) varies mostly between 2 and 3 in biological systems and was thus used to approximate two different possibilities (Q_{10} = 2, Q_{10} = 3) of PO_4^{3-} concentration in WinterOX15 on Day 10. The PO_4^{3-} concentration of WinterOX15 on Day 0 (0.302 µmol L^{-1}) was used as the *y*-intercept value: (Predicted PO_4^{3-} concentration, last day) = (PO_4^{3-} release, 15 °C) × (No. of days)

Temperature coefficient (Q_{10})	**PO_4^{3-} release, 5 °C (µmol L^{-1} d^{-1})**	**PO_4^{3-} release, 15 °C (µmol L^{-1} d^{-1})**	**PO_4^{3-} conc., 15 °C, Day 10 (predicted) (µmol L^{-1})**	**PO_4^{3-} conc., 15 °C, Day 10 (actual) (µmol L^{-1})**
2	1.95	3.9	39	1.6
3	1.95	5.9	59	

Table 8. Change in polyP-P content from Day 0 to Day 10 in the upper 1 cm peat layer of the 3 winter treatments, and the equivalent contribution of $\Delta_{polyP\text{-}P}$ to the water column PO_4^{3-} concentration under complete hydrolysis. $\Delta_{polyP\text{-}P}$ = change in polyP-P content from Day 0 to Day 10; W_{SL} = mean weight of upper 1 cm of peat layer in the core; V_{WC} = mean volume of the water column in the core; $C_{polyP\text{-}P}$ = theoretical change in PO_4^{3-} concentration under total polyP hydrolysis

Treatment	**$\Delta_{polyP\text{-}P}$ (µmol g^{-1})**	**W_{SL} (g)**	**V_{WC} (mL)**	**$C_{polyP\text{-}P}$ (µmol L^{-1})**
Aerobic, 5 °C (WinterOX5)	-0.15	11.2	350	+4.8
Oxygen-depleted, 5 °C (WinterOD5)	+1.02	11.2	386	-29.6
Aerobic, 15 °C (WinterOX15)	+0.97	11.2	350	-31.0
Hydrolysis of entire polyP content in freshly collected cores (Day 0)	-2.23	11.2	350	+71.4

Despite our results demonstrating polyP accumulation under stressed conditions, other studies have shown conflicting and organism-specific responses to stressors. For example, studies using *Escherichia coli* strains displayed an accumulation of polyP (Yoo et al. 2018) but also remained unresponsive (Ault-Riché et al. 1998) during heat stress. In sewage treatment plants, polyP-accumulating bacteria degrade and release polyP under anoxic conditions (Cokro et al. 2017). Nevertheless, bacteria are also able to synthesize polyP under reducing conditions and/or in the absence of light (Shi et al. 2003, Goldhammer et al. 2010).

In general, the presence of an extensive mat composed of polyP-accumulating filaments in the winter treatment cores, coupled with a substantial removal of PO_4^{3-} from the bottom water, signals that polyP-accumulating organisms can affect the benthic dissolved inorganic P pool, at least at our study site. At present, the microbial polyP influence on P fluxes is not well-documented. Still, previous studies have illustrated a relationship between microbial mats and P retention in the sediment. In a stream-based study, the concentration of soluble reactive phosphorus correlated negatively with the polyP:total periphyton P ratio. Therefore, P spikes during storm events could trigger polyP accumulation by mat-like periphyton (Rier et al. 2016). On a geological time scale, fossilized microbial mats bound in phosphate-rich layers provided evidence that mat-forming bacteria were involved in phosphogenesis (Williams & Reimers 1983, Reimers et al. 1990, Diaz et al. 2008). Furthermore, in the Namibian shelf, the dissolution of microbial polyP could directly lead to apatite precipitation, resulting in the deposition of phosphorites as a long-term P sink (Schulz & Schulz 2005, Goldhammer et al. 2010).

There is growing recognition of the microbial polyP contribution being a key component of the P cycle in marine sediments. Empirical diagenetic modeling of anoxic shelf sediments showed that without a polyP-driven microbial P pump, P burial in sediments was ~30% lower when compared to the baseline model (Dale et al. 2016). This modified model included microbial-synthesized polyP as an intermediate, which could be consequently transformed into either unreactive particulate or bulk organic P such as phosphate esters and phosphonates. Although the processes in this diagenetic model are more relevant to a large time scale, the outcome indicates that microbial polyP in the sediment is essential to P sequestration.

Although polyP-P constituted only ~5% of the total P pool in the upper 1 cm peat layer of the *in-situ* treatment in winter, its complete degradation would result in a $C_{polyP\text{-}P}$ of +71.4 µmol L^{-1} (Table 8), which is 260× higher than the bottom water PO_4^{3-} concentration on Day 0 (0.3

μmol L^{-1}; Fig. 16A). Furthermore, this percentage increases when excluding e.g., refractory P components which are less involved in active nutrient cycling; hence, the contribution of polyP should not be neglected. Moreover, since microbes can potentially accumulate a large amount of polyP intracellularly, polyP-accumulating bacterial mats deserve more acknowledgment in future investigations.

4.1.2 Relationship between PO_4^{3-} uptake and microbial mats

Fluorescence microscopy (Fig. 14A) reflected the dominance of *Lyngbya* spp. filaments (Table 6) in the surface peat layer on Day 0 of the summer experiment. For the end of the summer incubation as well as the winter and fall incubations, no 16S rRNA amplicon sequencing was available. Nonetheless, both light and fluorescence microscopy provided some insight into the microbial mat community. When comparing the SummerOX25 (Fig. 14B), SummerOX15 (Fig. 14D), and SummerOD15 (Fig. 14C) samples to the Day 0 samples, the microbial community in SummerOX25 was noticeably more distinct due to the dominance of small polyP-accumulating bacteria over *Lyngbya*-like filaments. The dominance of *Lyngbya*- and *Nodularia*-like filaments in the winter treatments (Fig. 12) also corresponded to the 16S rRNA-derived community composition profile (Table 6). In contrast, the deficiency in filamentous bacteria in FallOD5 (Fig. 13) revealed a microbial community structure that was markedly different from the winter and summer treatments. Hence, it is likely that the composition of polyP-accumulating members of the microbial mat community change according to varying environmental conditions.

The potential PO_4^{3-} retention by the *Lyngbya*-dominated microbial mat could be established by comparing the oxygen-depleted fall and winter treatments, with the former displaying typically higher concentrations and release rates of PO_4^{3-} in the absence of a mat (Fig. 17A), while the difference in NH_4^+ levels between the 2 treatments was comparatively smaller (Fig. 17B). Furthermore, a linear regression over the course of the incubation showed the release rate of NH_4^+ in WinterOD5 to be 10.5 μmol L^{-1} d^{-1} (Fig. 16D), which was 130× higher than the rate of PO_4^{3-} release (0.08 μmol^{-1} d^{-1}; Fig. 17A). This assumption is also supported by the hypothetical sequestration of PO_4^{3-} from the bottom water which was calculated from the increased polyP-P content in WinterOD5 (Fig. 11). Therefore, a scenario is possible in which the polyP-accumulating microbial mat mitigates a PO_4^{3-} upsurge, since polyP can constitute >40% of the non-reactive P pool in surface lake sediments, while declining to <10% just 1 cm below the sediment surface (Hupfer et al. 2004). Considering this large variation in PO_4^{3-} concentration between the treatments, the continual removal, sequestration, and burial

of significant amounts of dissolved inorganic P in the long term (Crosby & Bailey 2012) might be a precursor for phosphogenesis along coastal wetlands of the southern Baltic Sea. However, the composition of organic matter and P fractions in the peat of both WinterOD5 and FallOD5 were not analyzed. It is possible that differences existed in the peat composition between these two treatments due to e.g., local patchiness and seasonality, thus contributing to different rates of PO_4^{3-} release. Nonetheless, these differences were regarded as minor due to the relative physical stability of our sampling site, which is only irregularly flooded during storms in winter and fall.

In the summer treatments, the removal of the surface peat layer also elucidated the role of the microbial mat in mitigating increases in bottom water PO_4^{3-} levels (Fig. 17C), especially in SummerOD15. The removal of the surface layer on Day 2 likely reduced the number of active PO_4^{3-} sorption sites and exposed porewaters below, causing an increased PO_4^{3-} efflux (Fig. 17C). However, the subsequent abrupt decline in PO_4^{3-} concentration indicated a loss of PO_4^{3-} from the water column, which was to some extent due to polyP accumulation by the re-establishing *Lyngbya*-dominated mat (Fig. 14C) (Ahern et al. 2007). The simultaneous occurrence of both PO_4^{3-} loss and mat re-establishment implies the conversion of a large amount of PO_4^{3-} into biogenic polyP. A high level of NH_4^+ in the summer treatment cores also likely contributed to a fair amount of microbial N assimilation. In SummerOD15, the PO_4^{3-} concentration at the end of the incubation was on a level similar to that before the removal of the surface peat layer (Fig. 17C). Since this treatment was oxygen-depleted, redox-sensitive compounds in the peat most likely had a limited sorption capacity for PO_4^{3-} removal. Furthermore, although aerobic conditions are optimal for organic matter degradation, oxygen depletion would have ultimately driven this degradation anaerobically, resulting in PO_4^{3-} release from organic P fractions (Holmer 1999, Bastviken et al. 2004). At the end of the SummerOX25 incubation, the dominance of tiny polyP-accumulating bacteria instead of filamentous bacteria in the surface peat layer (Fig. 14B) suggests that smaller polyP-storing microorganisms might particularly affect PO_4^{3-} removal if present in sufficient quantity. In contrast to NH_4^+, the release of PO_4^{3-} to the bottom water was much lower from Days 0 – 3 in SummerOX25 (Fig. 17C), indicating possible PO_4^{3-} retention in the surface peat layer. Like WinterOX15, the PO_4^{3-} decline in SummerOX25 from Days 3 – 8 was accompanied by a continual increase in NH_4^+ (Fig. 17D), signifying a net efflux of water column PO_4^{3-} into the peat. Nonetheless, to uncover the degree of influence that polyP-accumulating organisms have on the PO_4^{3-} flux at the peat-water interface, more data on the quantity of microbial

polyP accumulation and the various P fractions in the peat are required. The habitat at our study site was patchy and possibly encompassed various P pools as revealed by SEM-EDX analysis (Table S1), hence tracking each P pool precisely over time posed a challenge. These P-containing components would therefore comprise the remaining 95% of P in addition to polyP in the surface peat layer. The contribution of polyP metabolism to the benthic P flux has also been highlighted in earlier studies which showed polyP comprising a significant portion of the total P in the sediment, and that P release from microbial polyP degradation could account for part of the P flux under anoxic conditions (Sannigrahi & Ingall 2005, Hupfer & Lewandowski 2008). On the other hand, across different environments, redox-dependent P-binding compounds such as Fe- and Mn-bound P fractions constitute a part of the P cycle to varying degrees. Significant amounts of redox-stable P-binding compounds such as bauxites and nonreducible Fe minerals such as ilmenite might also be present in sediments, and these are potentially able to impact P release via P retention (von Gruenewaldt 1993, Hupfer & Lewandowski 2008). Accounting for these various P sources will facilitate the construction of an environmental mass-balance P budget relating the amount of accumulated polyP to the benthic dissolved inorganic P pool. To the best of our knowledge, there is still no successful record of such a mass-balance budget. Therefore, we successfully constructed mass-balance P budgets in WP 3 using lab-cultured microbial mats showing that accumulated polyP could account for the bulk of PO_4^{3-} taken up by the mat (Fig. 30, Fig. 32 & Fig. 34).

4.2 Growth progress of microbial mat during culture establishment

By determining the optimal growth condition for the microbial mat, we were able to minimize the influence of any unwanted abiotic stressors on our measurements during the incubation experiment in WP 3. The ideal growth of our cyanobacterial-dominated microbial mat in the 18 – 21 °C range is not unexpected (Fig. 21). Cyanobacteria blooms (primarily *Nodularia spumigena*) typically occur in late summer in the Baltic Sea, where ambient temperatures are consistently above 16 °C (Löptien & Dietze 2022). Moreover, this temperature range is similar to the optimal temperature for the growth of other filamentous cyanobacterial genera such as *Aphanizomenon*, *Dolichospermum,* and *Nodularia* (Munkes et al. 2021). In the north-western portion of the Baltic Sea which encompasses our study site, salinity generally ranges from 15 – 25 psu (Munkes et al. 2021). Since the intent of this study was to closely examine polyP accumulation in large bacteria, we attempted to increase the proportion of large filamentous cyanobacteria (e.g., *Anabaena* sp., *Dolichospermum* sp., *Lyngbya* sp., *Nodularia*

sp.) during the establishment of a mixed microbial culture. In the Baltic Sea, *Nodularia* spp. typically proliferate between 7 – 8 psu (Wasmund 1997); however, this rarely occurs above 13 psu (Mazur-Marzec et al. 2005). In cultivation test 3, thinner filaments at 6 and 9 psu likely outpaced large filaments in growth (Fig. 22A & B). The average diameter of these thin filaments was similar to those from the genus *Nodosilinea* (Radzi et al. 2019), which was detected during 16S rRNA analysis of the surface peat layer (Table 6) as well as the metagenomics analysis of our lab-grown microbial mat replicates (grouped within the order *Phormidesmiales*; Fig. 27). Unfortunately, not much has been documented on the salinity growth conditions of *Nodosilinea* spp.. However, our results suggest that the *Nodosilinea* sp. in our samples might have decreased salinity tolerance at 12 psu, granting *Nodulari*a sp. an increased growth advantage.

The growth of large filamentous cyanobacteria was optimal in cultures with no added ammonia, where *Lyngbya* sp. filaments were clearly more abundant than *Nodularia* sp. (Fig. 24A). On the other hand, thinner filamentous cyanobacteria were significantly more visible under ammonia addition, which might indicate a stronger affinity for ammonia assimilation as compared to larger filaments such as *Lyngbya* spp. and *Nodularia* spp.. Moreover, since filamentous cyanobacteria of all sizes still grew well under conditions without ammonia addition in our earlier cultivation tests, this signified that nitrogen-fixing bacterial species were present in the microbial mat.

The preference of microbes for an attachment substrate is also documented in other studies. The formation of biofilms on substrates is an important survival mechanism for bacteria, which includes enhancing bacterial growth by enabling more efficient nutrient uptake, strengthening interactions among bacterial cells as well as providing environmental stability (Dang & Lovell 2016, Muhammad et al. 2020). Consequently, these processes result in a thickening of the bacterial mat (Yallop et al. 1994), which was also evident in our cyano-bacterial mat cultures with an agar bottom layer (Fig. 25C). In these cultures, the mat formed on the agar substrate was also visibly thicker than that which formed on the walls of the Greiner flask, indicating that agar was a preferred attachment substrate for the filamentous cyanobacteria. Ultimately, the active proliferation of the microbial mat observed over 20 days (Fig. 6) was a testament to the success in determining a combination of ideal conditions for its growth.

4.3 Relationship between PO_4^{3-} uptake and polyP accumulation amid stressors

4.3.1 Comparison of rapid microbial PO_4^{3-} uptake with other studies

Since all replicates were already P-deficient before the start of the incubation, this likely resulted in a microbial mat that was already P-stressed at time point '0'. Thus, the rapid depletion of dissolved PO_4^{3-} within the first 2 h of incubation (*in-situ*: 14×, elevated temperature: 10×, reduced salinity: 13×) strongly indicated an "overplus response" by the microbial mat (Fig. 28) (Dyhrman 2016, Li & Dittrich 2019). This mechanism was also supported by generally high compositions of the *pstSCAB* gene transcripts (associated with PO_4^{3-} uptake and transport) in all sequenced treatment replicates (Fig. 36). The overplus response was also justified by intensified polyP synthesis within the first 2 hours of incubation (Sanz-Luque et al. 2020) in all treatments, as observed by the sizable polyP-P/PO_4^{3-} percentages (11 – 39%) by time point 2h (Fig. 30, Fig. 32 & Fig. 34). Similar responses have previously been illustrated with other bacteria communities or cultures (Table 9), where rates of PO_4^{3-} uptake higher or comparable to that in the first two hours of our incubation were observed (Shapiro et al. 1967, Fu et al. 2005, den Haan et al. 2016).

The rapid depletion of PO_4^{3-} in our culture incubations is imperative to understanding the management of PO_4^{3-} levels in coastal water bodies. In aquatic systems, PO_4^{3-} concentrations rarely surpass ~1 µmol L^{-1}, and can be as low as 0.01 – 0.1 µmol L^{-1} in pristine conditions (Boyd 2015). On the other hand, water becomes eutrophic when the PO_4^{3-} concentrations reach 0.3 – 1.0 µmol L^{-1} (epilimnion) and 10.5 µmol L^{-1} (hypolimnion) (Boyd 2015, Dodds & Whiles 2020). In surface waters of the Darß-Zingst Bodden estuary-lagoon which lies ~40 km from our study site, cyanobacterial blooms have occurred when the PO_4^{3-} concentration exceeded only 0.4 µmol L^{-1} (Wasmund 1997). The average PO_4^{3-} concentrations from short peat cores freshly collected at our study site during WP 1 were 0.24 ± 0.05 µmol L^{-1} (winter), 0.34 ± 0.12 µmol L^{-1} (summer), and 2.11 ± 0.33 µmol L^{-1} (fall) (Choo et al. 2022), which suggests that bloom events could be triggered by this seasonal variability in the level of PO_4^{3-}. In our PO_4^{3-} addition treatments as part of WP 3, the starting PO_4^{3-} concentration (~7.1 µmol L^{-1}) was well above the threshold required for eutrophication to develop. The brief period in which microbial mat replicates in all treatments were able to reduce PO_4^{3-} from a highly eutrophic to a borderline eutrophic state (2 h) and attain oligo-mesotrophic conditions (Wetzel 2001) after only 8 h (Fig. 28), highlights the mat's importance in regulating the PO_4^{3-} flux, at least at our study site.

Table 9. The PO_4^{3-} uptake rates of the microbial mat during the *in-situ*, elevated temperature, and reduced salinity treatments of the lab culture-based part of our study, compared with that of other bacterial species in published studies. The hourly PO_4^{3-} uptake rate per biomass of the strain *Trichodesmium* GBRTRLI101 was estimated from the given rate in the study (Fu et al. 2005), the generic dry weight (0.33 g) per cm^3 cell volume for bacterial cells as well as the average cell volume of strain GBRTRLI101 (~1740 μm^3)

Study	**Species of microorganism**	**Biomass concentration (g L^{-1})**	**PO_4^{3-} uptake over a duration**	**PO_4^{3-} uptake rate per biomass (µmol g^{-1} h^{-1})**
***In-situ* treatment, our study**		0.4 ± 0.2	6.6 µmol L^{-1}, 2 h	8.3
Elevated temperature treatment, our study		0.2 ± 0.03	6.4 µmol L^{-1}, 2 h	16.0
Reduced salinity treatment, our study		0.2 ± 0.03	6.5 µmol L^{-1}, 2 h	16.5
(Shapiro et al. 1967)	Activated sludge (Bacteria: *Zooglearamigera*, *Escherichia intermedium*, *Bacillus cereus*, *Flavobacterium*, *Pseudomonas*, *Sphaerotilus natans*; Protozoa: *Vorticell*a, *Opercularia*, *Epistylis*)	6	579 µmol L^{-1}, 3 h	32.0
(Fu et al. 2005)	*Trichodesmium* GBRTRLI101	-	6×10^{-15} mol $cell^{-1}$ h^{-1}	10.4
(den Haan et al. 2016)	*Lyngbya majuscula*	-	-	~4.0

Furthermore, we estimated that the presence of a microbial mat was able to reduce the PO_4^{3-} concentration in temperature-elevated cores by 96% (Table 7), while the absence of a mat (as demonstrated throughout the fall incubation FallOD5) resulted in a persistent high PO_4^{3-} concentration (Fig. 17A) (Choo et al. 2022). These results have been further justified by the rapid decline in PO_4^{3-} concentration observed in our lab incubations, and ultimately demonstrate the capability of the mat in regulating the benthic P flux and maintaining a healthy trophic level at our study site.

4.3.2 Microbial stress response to heat and reduced salinity

At time point 2 h, differential expression between *in-situ* and elevated temperature conditions showed that a 10 °C increase in temperature caused stress to the microbial mat (Fig. 37A). Half of the selected heat/general stress response genes were either significantly or noticeably upregulated under elevated temperature in relation to the *in-situ* condition, notably with heat shock genes such as *hsp17* and the Class I group (*dnaJ*, *dnaK*, *groEL,* and *grpE*) which have key roles in photosynthetic function as well as the prevention of protein misfolding and aggregation, respectively (Selby et al. 2011, Wagner et al. 2015). Nevertheless, subsequently under elevated temperature, the noticeable downregulation of 2 heat stress response genes (*groEL*, *hscA*) and significant downregulation of *rpoS* at 24 h (relative to 2 h) suggests that the microbial mat could achieve a swift post-acclimation response. The significant downregulation of the *rpoS* gene also suggested that cells exited the stationary phase (Fig. 37B) since *rpoS* expression is inhibited during exponential growth (Battesti et al. 2011).

A reduction in salinity also clearly elicited a stress response in the microbial mat, since 60% of the selected salinity stress response genes were either significantly or noticeably upregulated at 2 h, in relation to time point '0' (Fig. 38A). Furthermore, the significant downregulation of *sll1566* (encoding the enzyme glucosylglycerol-phosphate-synthase) could be explained by the lowered salt concentration in the medium, since *sll1566* is inhibited by decreasing the salinity in high salt media (Marin et al. 1998). The other significantly downregulated gene *sll1037*, which is a putative component of the TRAP transporter, might also be inhibited by declining salinity (Klähn et al. 2021); however, the metabolic function of this gene is not well-documented. Subsequently, at 24 h (relative to time point 2 h), a noticeable or significant downregulation of 70% of the same salinity stress response genes also illustrated the nearly acclimatized state of the microbial mat (Fig. 38B). Moreover, this downregulation under salinity stress was more intense, when compared to the general level of downregulation observed under elevated temperature in the same time frame (Fig. 37B). Interestingly, gene *sll0248* was significantly upregulated at time point 24 h, relative to 2 h. This gene encodes the protein flavodoxin, which functions as an electron carrier in redox-based metabolic processes. In cyanobacteria, flavodoxin accumulation is induced by increasing salinity, which enables cells to maintain photosynthetic efficiency under stress (Fulda & Hagemann 1995, Niazian et al. 2021). So far, studies have focused on flavodoxin regulation under increased salinity conditions; therefore, information on whether this molecule is also upregulated under reduced salinity conditions is critically lacking. Since

flavodoxin metabolism is closely tied to the photosynthetic pathway, its prolonged upregulation might also indicate a lingering stress effect of reduced salinity on the microbial mat after 24 h of incubation.

4.3.3 Expression of P metabolism-associated genes during stress

Abiotic stress generates physiological costs for microorganisms, and since inducing stress response mechanisms is energetically expensive, the cell is forced to divert energy-providing resources required for growth towards survival and acclimation instead (Schimel et al. 2007). This phenomenon was observed in the 2 stressed treatments (elevated temperature, reduced salinity), where despite a fairly similar expression profile of the P metabolism-associated genes among the 3 treatments at time point 24 h (relative to 2 h), the intensity of differential expression of P metabolism-associated genes in both treatments was visibly weaker than under *in-situ* conditions (Fig. 36). Although a near-acclimatized state was achieved within this period in both stressed treatments, a small fraction of stress response genes remained noticeably or significantly upregulated (*hsp17* under elevated temperature, *sll0248* under reduced salinity) (Fig. 37B & Fig. 38B), suggesting that dedicating energy and nutrients to develop stress tolerance was still critical for the microbial mat. This might thus account for both a generally weaker differential gene expression as well as a lower number of significantly upregulated genes involved in P metabolism under both elevated temperature and reduced salinity at "24 h vs. 2 h".

4.3.4 Phosphate uptake and polyP metabolism under varying conditions

In all treatments, the amount of polyP accumulated throughout the incubation successfully accounted for the main bulk of PO_4^{3-} taken up by the mat, driven in part by the PO_4^{3-} overplus response observed within the first 2 hours of incubation (Fig. 28). The polyP-linked overplus response has been observed in the cyanobacterial genus *Synechococcus*, where the polyP content in samples from the oligotrophic Sargasso Sea doubled after the addition of PO_4^{3-} (Martin et al. 2014). Following this, another study on cyanobacteria belonging to the genera *Synechococcus* and *Synechocystis* also demonstrated high polyP:TPP (total particulate phosphorus) ratios during the lag phase of the incubation with PO_4^{3-} (Li & Dittrich 2019). Moreover, the same studies also showed that cellular polyP accumulation during the overplus phenomenon (P-stressed cells) was still higher than in cells under P-replete conditions (luxury uptake), strongly indicating the relationship between stress tolerance and polyP metabolism (Rao et al. 2009).

Following WP 1 which showed polyP accumulation under both *in-situ* and abiotic stress conditions (elevated temperature, oxygen depletion) (Fig. 11) (Choo et al. 2022), polyP accumulation was also observed in lab-cultured microbial mats incubated under *in-situ* and stressed (elevated temperature, reduced salinity) conditions in WP 3 (Fig. 29). However, no substantial difference in the rate of increase in polyP-P/PO_4^{3-} between the *in-situ* treatment and the two stressed treatments was observed (between time point 2 h and the polyP-P/PO_4^{3-} peak; Fig. 30, Fig. 32 & Fig. 34), even though the differential expression of P metabolism-associated genes (including significant upregulation of *ppk1* and *ppk2*) was most intense in the *in-situ* treatment between 2 h and 24 h. Under conditions in which the microbial mat is already adapted (*in-situ*), microbial cells can dedicate a large part of their metabolism to growth by utilizing polyP as an energy resource. This was demonstrated with unicellular picocyanobacteria (*Synechococcus* sp. and *Synechocystis* sp.), which displayed increased cell growth rates upon the uptake of PO_4^{3-} from the medium in unstressed conditions (Li & Dittrich 2019). Since shorter-chain polyP molecules are preferentially hydrolyzed during cell growth (Adams et al. 2022), it is likely that they were the main form of polyP being synthesized during the significant upregulation of *ppk1* and *ppk2* under *in-situ* conditions, and then promptly degraded before further chain elongation could occur (justified by the significant upregulation of the exopolyphosphatase *ppx-gppA*) (Fig. 36). As the polyP quantification method used in this study (DAPI-based fluorescence spectroscopy) was only able to detect polyP molecules with chain lengths longer than 15 P-subunits (Christ et al. 2020), an increase in short-chain polyP ($n \leq 15$) would not have contributed to the recorded increment in polyP/PO_4^{3-} in the *in-situ* treatment (Kulakova et al. 2011), which might explain the minimal difference in the rate of increase in polyP/PO_4^{3-} between the *in-situ* and stressed conditions. On the other hand, bacterial cells possessing long-chain polyP are more resilient to stressors such as heat, oxidants, and osmotic changes (Kornberg 1995). Thus, under unstressed conditions, the urgency for cells to accumulate long-chain polyP is lower.

Furthermore, the continued upregulation of *ppk1*/*ppk2*/*pstS* (24 h vs. 2 h), despite the presence of various stressors, suggests an association with functional redundancy (Fig. 36), where multiple species of bacteria performing similar functions (in this case, *ppk*/*pstS* activity) are present in a community, therefore being able to preserve a specified function despite disturbances or changes in the community structure (Moya & Ferrer 2016). This scenario was observed at least with *ppk1* and *pstS*, where high transcript activity was observed across multiple bacterial MAGs, together with differences in MAG activity among the 3 treatments

(Fig. 39A & C). As for *ppk2*, its lack of transcript activity under stressed conditions might be partially explained by the fact that the ppk2 enzyme has a much lower affinity for polyP synthesis as compared to the ppk1 enzyme (Ishige et al. 2002), resulting in *ppk2* having a comparatively less important role in polyP accumulation. Furthermore, regarding *pstS* transcript activity, the difference in dominant MAGs was not only observed between stressed and non-stressed treatments, but also between time points, suggesting functional redundancy concerning polyP metabolism-related PO_4^{3-} uptake and transport in the microbial mat, and possibly temporal niche partitioning among bacterial species (Fig. 39C). Nonetheless, the difference in MAG activity (*ppk1*, *ppk2,* and *pstS*) among treatments might also be attributed to variations in the microbial composition of the mat across replicates (Fig. 27), as well as changes in the proliferation of certain species throughout an incubation (arising from different treatment conditions). However, the indication that various species within the mat are actively involved in polyP metabolism ultimately hints at a shared ecosystem functionality among these community members.

Fluorescence imaging of DAPI-stained filamentous cyanobacteria samples also pointed to functional redundancy within the microbial mat. The high *ppk1* activity of the MAG *Geitlerinemaceae* (which includes the genus *Lyngbya*) in the *in-situ* treatment (Fig. 39A) corresponded to the increase in polyP content in cyanobacterial filaments (Fig. 31). Nonetheless, under both elevated temperature and reduced salinity, polyP was mainly stored in thinner filaments (Fig. 33 & Fig. 35), as also indicated by noticeable *ppk1* activity from a different MAG (*Elainellaceae*) (Fig. 39A). This perceived functional redundancy suggests that the process of P accumulation is well established within the community despite changes in community composition or stressed conditions. Particularly, during periods of stress, community members that can acclimate more swiftly than the rest might increase their polyP metabolism to drive cell growth or maintain an energy reserve (Nikel et al. 2013), which might partly explain the shift in *ppk1* activity among various MAGs, across the 3 treatments (Fig. 39A).

The importance of functional redundancy during a disturbance has been observed across different environments. In an Antarctic soil microbial community, multiple microbial species could maintain carbon and nitrogen cycling levels despite temperature fluctuations (de Scally et al. 2016). In another study, a reduction in the species diversity of a soil microbial community due to cultivation had a negligible effect on the organic matter degradation process since the surviving microbes were able to acquire decomposition functions like those

in uncultivated soil (Sall et al. 2006). Functional redundancy concerning biogeochemical cycling was also seen in a subseafloor crustal aquifer microbial community, where shifts in the community structure did not lead to differences in metabolic potential in carbon fixation, and nitrogen and sulfur cycling (Tully et al. 2018). One commonality among these studies was that increased species richness played a role in maintaining specific functions within the microbial community. The assortment of bacterial orders observed in our microbial mat samples (Fig. 27), coupled with the redundancy observed with critical P cycling-associated functions within the microbial mat (dependent on stress conditions), reveals a complex system allowing the microbial mat to survive under different stressors.

4.3.5 Loss of microbial polyP during incubation

During the incubations in WP 3, the earliest decline in polyP-P content occurred under conditions of reduced salinity (Fig. 34). However, we could not clearly determine if polyP consumption was linked to increased stress since the other stressor (temperature elevation) did not cause a decline in polyP-P content within the 72-hour incubation period (Fig. 32), while *in-situ* polyP-P content declined after 64 h (Fig. 30). Nevertheless, an upregulation of the *pap* and *ppgK* genes at "48 h vs. 24 h" under both *in-situ* and reduced salinity conditions suggest an increased degradation of polyP within this timeframe (Fig. 36). The pap enzyme converts AMP to ADP, while ppgK enzyme catalyzes the phosphorylation of glucose during glycolysis, with both enzymes using polyP as a phosphoryl donor (Shiba et al. 2005). Since both these enzymes are involved in energy-producing metabolic pathways, their upregulation might be an indicator of increased metabolic requirements during a specific treatment.

Particularly, an increase in ppgK activity also suggested increased glucose metabolism by the mat (Fig. 36). This scenario is probable since enhanced glucose uptake under depleted salinity has been observed in single bacteria such as *E. coli* as well as in heterotrophic bacterial communities (Cunha et al. 2000, Li et al. 2021, Glover et al. 2022). Nevertheless, the implication of microbial polyP degradation on glucose metabolism under varying salinity conditions is still largely unknown, warranting this topic for further study.

5 Conclusion and Outlook

The polyP molecule is ubiquitous in all forms of life, ranging from microbes to humans (Rijal et al. 2020). Many polyP-accumulating organisms in the environment can sequester large amounts of polyP, yet this inorganic biopolymer remains understudied concerning its contribution to the P cycle. This thesis aimed to demonstrate the influence of a polyP-accumulating microbial mat on the benthic P flux in a coastal peatland and determine a clear relationship between microbial PO_4^{3-} uptake and polyP accumulation using a lab-cultured microbial mat.

Incubation of short peat cores from the study site showed that a microbial mat community mainly comprising filamentous cyanobacteria of the genus *Lyngbya* could regulate benthic P cycling in the short term. Under changing conditions of elevated temperature and oxygen depletion, the rise in bottom water PO_4^{3-} levels resulting from PO_4^{3-} release mechanisms such as organic matter degradation and Fe-bound P dissolution could be mitigated through PO_4^{3-} uptake by polyP-accumulating organisms within the mat in the surface peat layer. The PO_4^{3-} loss coupled with the re-establishment of a polyP-accumulating microbial mat community (after surface layer removal on Day 2) during the summer experiment indicated an uptake of PO_4^{3-} from the water column and its subsequent storage as polyP within the surface peat layer. When comparing the treatment containing a microbial mat (WinterOD5) with that where the mat was greatly reduced (FallOD5), the significantly higher bottom water PO_4^{3-} concentration in the latter revealed the role of mat-forming polyP-accumulating bacteria in mediating the benthic P flux. Although polyP-P constituted only ~5% of the total P pool in the surface peat, sequestration of this molecule can significantly affect water column PO_4^{3-} at least on short time scales, thus potentially serving as an important contributor to regulating dissolved P levels in aquatic ecosystems.

Subsequently, the treatment-specific mass-balance polyP-P/PO_4^{3-} budgets revealed a clear connection between PO_4^{3-} uptake and polyP accumulation by mat-forming polyP-accumulating organisms. Within the 72-h incubation period, the increase in polyP-P content in the microbial mat could account for the bulk of PO_4^{3-} (89 – 93%) taken up across the treatments. The P overplus response by the microbial mat was also reflected in the rapid removal of PO_4^{3-} from the medium in the P-deficient treatment replicates within 2 h from the start of incubation, thus designating it as an essential precursor mechanism to microbial polyP metabolism. Furthermore, analyses of metagenomic and metatranscriptomic data indicated

that despite stressors (elevated temperature, reduced salinity), the mechanisms of PO_4^{3-} uptake and polyP synthesis were preserved by various members of the microbial mat community through functional redundancy. From these outcomes, it is evident that microbial polyP accumulation likely has a crucial role in the PO_4^{3-} flux; however, to truly determine the polyP contribution to the P cycle at our study site, the various P pools at the site must be accounted for. Nevertheless, the ability of the microbial mat to potentially sequester a significant amount of dissolved PO_4^{3-}, coupled with the resilience of the polyP accumulation pathway under stressful conditions, is a clear indicator that microbial polyP should be considered a key component of the aquatic P cycle.

The demonstrated impact of the polyP-accumulating microbial mat on the benthic P flux has shown that the polyP pool is potentially a crucial component of aquatic P cycling, and these results will lend credible support to current P cycling models when accounting for P burial in the sediments. The low PO_4^{3-} concentrations observed despite receiving high nutrient loads from surrounding agricultural activity also point to the PO_4^{3-} sequestering capability of the microbial mats, making them potentially ideal in ecological engineering studies as a solution to managing phosphorus eutrophication in aquatic systems. Furthermore, polyP-accumulating bacteria are crucial in wastewater treatment, where they play a central role in the process of enhanced biological phosphorus removal from influent wastewater. This process is becoming increasingly important, considering a rising global need for wastewater management (Jones et al. 2021). The main bacterial MAGs actively metabolizing polyP in this study are, however, less recognized as compared to other polyP-accumulating bacteria (e.g., *Ca*. Accumulibacter, *Acinetobacter* spp., *Dechloromonas* spp., *Microlunatus* spp., *Tetrasphaera* spp.) with regards to wastewater treatment (Günther et al. 2009, Qiu et al. 2019). Our findings, therefore, present an opportunity to investigate the P sequestering potential of the putative polyP-accumulating bacteria in our samples in greater detail, which could help address challenges in the wastewater treatment process such as high costs and poor efficiency (Jiao et al. 2021). Nonetheless, not only are polyP-accumulating bacteria commercially relevant, but they ultimately form an integral part of certain environments and should deserve more attention in future research.

6 References

Adams JC, Steffen R, Chou C, Duhamel S, Diaz JM (2022) Dissolved organic phosphorus utilization by the marine bacterium *Ruegeria pomeroyi* DSS-3 reveals chain length-dependent polyphosphate degradation. Environ Microbiol 24:2259–2269.

Ahern KS, Ahern CR, Udy JW (2007) Nutrient additions generate prolific growth of *Lyngbya majuscula* (cyanobacteria) in field and bioassay experiments. Harmful Algae 6:134–151.

Ahlgren J, Reitzel K, de Brabandere H, Gogoll A, Rydin E (2011) Release of organic P forms from lake sediments. Water Res 45:565–572.

Arnosti C, Jørgensen B, Sagemann J, Thamdrup B (1998) Temperature dependence of microbial degradation of organic matter in marine sediments:polysaccharide hydrolysis, oxygen consumption, and sulfate reduction. Mar Ecol Prog Ser 165:59–70.

Arthur K, Paul V, Paerl H, O'Neil J, Joyner J, Meickle T (2009) Effects of nutrient enrichment of the cyanobacterium *Lyngbya* sp. on growth, secondary metabolite concentration and feeding by the specialist grazer *Stylocheilus striatus*. Mar Ecol Prog Ser 394:101–110.

Ault-Riché D, Fraley CD, Tzeng C-M, Kornberg A (1998) Novel assay reveals multiple pathways regulating stress-induced accumulations of inorganic polyphosphate in *Escherichia coli*. J Bacteriol 180:1841–1847.

Bastviken D, Persson L, Odham G, Tranvik L (2004) Degradation of dissolved organic matter in oxic and anoxic lake water. Limnol Oceanogr 49:109–116.

Battesti A, Majdalani N, Gottesman S (2011) The RpoS-mediated general stress response in *Escherichia coli*. Annu Rev Microbiol 65:189–213.

Běhrádek J (1930) Temperature coefficients in biology. Biological Reviews 5:30–58.

Berg P, Risgaard-Petersen N, Rysgaard S (1998) Interpretation of measured concentration profiles in sediment pore water. Limnol Oceanogr 43:1500–1510.

Berner RA (1977) Stoichiometric models for nutrient regeneration in anoxic sediments. Limnol Oceanogr 22:781–786.

Bernhardt K-G, Koch M (2003) Restoration of a salt marsh system: temporal change of plant species diversity and composition. Basic Appl Ecol 4:441–451.

Berry JP, Gantar M, Gawley RE, Wang M, Rein KS (2004) Pharmacology and toxicology of pahayokolide A, a bioactive metabolite from a freshwater species of *Lyngbya* isolated from the Florida Everglades. Comparative Biochemistry and Physiology Part C: Toxicology & Pharmacology 139:231–238.

Boudreau BP (1997) Diagenetic models and their implementation, 1st ed. Springer, Berlin.

Boyd CE (2015) Phosphorus. In: *Water Quality*. Springer International Publishing, Cham, p 243-261.

Caporaso JG, Kuczynski J, Stombaugh J, Bittinger K, Bushman FD, Costello EK, Fierer N, Peña AG, Goodrich JK, Gordon JI, Huttley GA, Kelley ST, Knights D, Koenig JE, Ley

RE, Lozupone CA, McDonald D, Muegge BD, Pirrung M, Reeder J, Sevinsky JR, Turnbaugh PJ, Walters WA, Widmann J, Yatsunenko T, Zaneveld J, Knight R (2010) QIIME allows analysis of high-throughput community sequencing data. Nat Methods 7:335–336.

Cardell C, Guerra I (2016) An overview of emerging hyphenated SEM-EDX and Raman spectroscopy systems: Applications in life, environmental and materials sciences. TrAC Trends in Analytical Chemistry 77:156–166.

Choo S, Dellwig O, Wäge-Recchioni J, Schulz-Vogt H (2022) Microbial-driven impact on aquatic phosphate fluxes in a coastal peatland. Mar Ecol Prog Ser 702:19–38.

Christ JJ, Willbold S, Blank LM (2020) Methods for the analysis of polyphosphate in the life sciences. Anal Chem 92:4167–4176.

Cokro AA, Law Y, Williams RBH, Cao Y, Nielsen PH, Wuertz S (2017) Non-denitrifying polyphosphate accumulating organisms obviate requirement for anaerobic condition. Water Res 111:393–403.

Cong H-B, Huang T-L, Chai B-B, Zhao J-W (2009) A new mixing–oxygenating technology for water quality improvement of urban water source and its implication in a reservoir. Renew Energy 34:2054–2060.

Crosby CH, Bailey J V. (2012) The role of microbes in the formation of modern and ancient phosphatic mineral deposits. Front Microbiol 3:241.

Cunha M, Almeida M, Alcântara F (2000) Patterns of ectoenzymatic and heterotrophic bacterial activities along a salinity gradient in a shallow tidal estuary. Mar Ecol Prog Ser 204:1–12.

Dale AW, Boyle RA, Lenton TM, Ingall ED, Wallmann K (2016) A model for microbial phosphorus cycling in bioturbated marine sediments: Significance for phosphorus burial in the early Paleozoic. Geochim Cosmochim Acta 189:251–268.

Dang H, Lovell CR (2016) Microbial surface colonization and biofilm development in marine environments. Microbiology and Molecular Biology Reviews 80:91–138.

Defforey D, Paytan A (2018) Phosphorus cycling in marine sediments: Advances and challenges. Chem Geol 477:1–11.

Delaney ML (1998) Phosphorus accumulation in marine sediments and the oceanic phosphorus cycle. Global Biogeochem Cycles 12:563–572.

Dellwig O, Bosselmann K, Kölsch S, Hentscher M, Hinrichs J, Böttcher ME, Reuter R, Brumsack H-J (2007) Sources and fate of manganese in a tidal basin of the German Wadden Sea. J Sea Res 57:1–18.

Dellwig O, Leipe T, März C, Glockzin M, Pollehne F, Schnetger B, Yakushev E v., Böttcher ME, Brumsack H-J (2010) A new particulate Mn–Fe–P-shuttle at the redoxcline of anoxic basins. Geochim Cosmochim Acta 74:7100–7115.

Dellwig O, Wegwerth A, Schnetger B, Schulz H, Arz HW (2019) Dissimilar behaviors of the geochemical twins W and Mo in hypoxic-euxinic marine basins. Earth Sci Rev 193.

Diaz J, Ingall E, Benitez-Nelson C, Paterson D, de Jonge MD, McNulty I, Brandes JA (2008) Marine polyphosphate: A key player in geologic phosphorus sequestration. Science (1979) 320:652–655.

Dodds WK, Whiles MR (2020) Microbes and plants. In: *Freshwater Ecology*. Elsevier, p 211–249

Dyhrman ST (2016) Nutrients and their acquisition: Phosphorus physiology in microalgae. In: *The Physiology of Microalgae*. Springer International Publishing, Cham, p 155–183

Eysseltová J, Dirkse TP, Makovicka J, Salomon M (1988) Alkali metal orthophosphates. In: *Solubility data series*. Pergamom Press

Flemming BW, Delafontaine MT (2000) Mass physical properties of muddy intertidal sediments: some applications, misapplications and non-applications. Cont Shelf Res 20:1179–1197.

Fu F-X, Zhang Y, Bell PRF, Hutchins DA (2005) Phosphate uptake and growth kinetics of *Trichodesmium* (cyanobacteria) isolates from the North Atlantic Ocean and the Great Barrier Reef, Australia. J Phycol 41:62–73.

Fulda S, Hagemann M (1995) Salt treatment induces accumulation of flavodoxin in the cyanobacterium *Synechocystis* sp. PCC 6803. J Plant Physiol 146:520–526.

Gächter R, Meyer JS (1993) The role of microorganisms in mobilization and fixation of phosphorus in sediments. Hydrobiologia 253:103–121.

Glover G, Voliotis M, Łapińska U, Invergo BM, Soanes D, O'Neill P, Moore K, Nikolic N, Petrov PG, Milner DS, Roy S, Heesom K, Richards TA, Tsaneva-Atanasova K, Pagliara S (2022) Nutrient and salt depletion synergistically boosts glucose metabolism in individual *Escherichia coli* cells. Commun Biol 5:385.

Goldhammer T, Brüchert V, Ferdelman TG, Zabel M (2010) Microbial sequestration of phosphorus in anoxic upwelling sediments. Nat Geosci 3:557–561.

Gomes FM, Ramos IB, Wendt C, Girard-Dias W, de Souza W, Machado EA, Miranda K (2013) New insights into the in situ microscopic visualization and quantification of inorganic polyphosphate stores by 4',6-diamidino-2-phenylindole (DAPI)-staining. European Journal of Histochemistry 57:34.

Gonsiorczyk T, Casper P, Koschel R (1998) Phosphorus-binding forms in the sediment of an oligotrophic and an eutrophic hardwater lake of the Baltic Lake District (Germany). Water Science and Technology 37:51–58.

von Gruenewaldt G (1993) Ilmenite-apatite enrichments in the upper zone of the Bushveld Complex: A major titanium-rock phosphate resource. Int Geol Rev 35:987–1000.

Günther S, Trutnau M, Kleinsteuber S, Hause G, Bley T, Röske I, Harms H, Müller S (2009) Dynamics of polyphosphate-accumulating bacteria in wastewater treatment plant microbial communities detected via DAPI (4′,6′-diamidino-2-phenylindole) and tetracycline labeling. Appl Environ Microbiol 75:2111–2121.

den Haan J, Huisman J, Brocke HJ, Goehlich H, Latijnhouwers KRW, van Heeringen S, Honcoop SAS, Bleyenberg TE, Schouten S, Cerli C, Hoitinga L, Vermeij MJA, Visser

PM (2016) Nitrogen and phosphorus uptake rates of different species from a coral reef community after a nutrient pulse. Sci Rep 6:28821.

Hansen HP, Koroleff F (1999) Determination of nutrients. In: *Methods of Seawater Analysis*, 3rd ed. Grasshoff K, Kremling K, Ehrhardt M (eds) Wiley-VCH Verlag GmbH, Weinheim, Germany

Harrison AF (1982) Labile organic phosphorus mineralization in relationship to soil properties. Soil Biol Biochem 14:343–351.

Hochachka PW (1991) Temperature: the ectothermy option. p 313–322

Holmer M (1999) The effect of oxygen depletion on anaerobic organic matter degradation in marine sediments. Estuar Coast Shelf Sci 48:383–390.

Hupfer M, Gächter R, Giovanoli R (1995) Transformation of phosphorus species in settling seston and during early sediment diagenesis. Aquat Sci 57:305–324.

Hupfer M, Lewandowski J (2008) Oxygen controls the phosphorus release from lake sediments - a long-lasting paradigm in limnology. Int Rev Hydrobiol 93:415–432.

Hupfer M, Ruübe B, Schmieder P (2004) Origin and diagenesis of polyphosphate in lake sediments: A 31P‡NMR study. Limnol Oceanogr 49:1–10.

Ingall E, Jahnke R (1997) Influence of water-column anoxia on the elemental fractionation of carbon and phosphorus during sediment diagenesis. Mar Geol 139.

Ingall E, Kolowith L, Lyons T, Hurtgen M (2005) Sediment carbon, nitrogen and phosphorus cycling in an anoxic fjord, Effingham Inlet, British Columbia. Am J Sci 305:240–258.

Ishige K, Zhang H, Kornberg A (2002) Polyphosphate kinase (PPK2), a potent, polyphosphate-driven generator of GTP. Proceedings of the National Academy of Sciences 99:16684–16688.

Ito F, Tamiya T, Ohtsu I, Fujimura M, Fukumori F (2014) Genetic and phenotypic characterization of the heat shock response in *Pseudomonas putida*. Microbiologyopen 3:922–936.

James WF, Barko JW, Eakin HL (2002) Labile and refractory forms of phosphorus in runoff of the Redwood River Basin, Minnesota. J Freshw Ecol 17:297–304.

Jiao G-J, Ma J, Li Y, Jin D, Ali Z, Zhou J, Sun R (2021) Recent advances and challenges on removal and recycling of phosphate from wastewater using biomass-derived adsorbents. Chemosphere 278:130377.

Jones ER, van Vliet MTH, Qadir M, Bierkens MFP (2021) Country-level and gridded estimates of wastewater production, collection, treatment and reuse. Earth Syst Sci Data 13:237–254.

Jørgensen C, Jensen HS, Andersen FØ, Egemose S, Reitzel K (2011) Occurrence of orthophosphate monoesters in lake sediments: significance of myo- and scyllo-inositol hexakisphosphate. Journal of Environmental Monitoring 13:2328.

Joshi SR, Kukkadapu RK, Burdige DJ, Bowden ME, Sparks DL, Jaisi DP (2015) Organic matter remineralization predominates phosphorus cycling in the mid-bay sediments in the Chesapeake Bay. Environ Sci Technol 49:5887–5896.

Klähn S, Mikkat S, Riediger M, Georg J, Hess WR, Hagemann M (2021) Integrative analysis of the salt stress response in cyanobacteria. Biol Direct 16:26.

Kleeberg A, Kozerski H-P (1997) Phosphorus release in Lake Großer Müggelsee and its implications for lake restoration. In: *Shallow Lakes '95*. Springer, Dordrecht, p 9–26

Kornberg A (1995) Inorganic polyphosphate: toward making a forgotten polymer unforgettable. J Bacteriol 177:491–496.

Krause J, Hopwood MJ, Höfer J, Krisch S, Achterberg EP, Alarcón E, Carroll D, González HE, Juul-Pedersen T, Liu T, Lodeiro P, Meire L, Rosing MT (2021) Trace element (Fe, Co, Ni and Cu) dynamics across the salinity gradient in Arctic and Antarctic glacier fjords. Front Earth Sci (Lausanne) 9.

Krom MD, Berner RA (1980) The diffusion coefficients of sulfate, ammonium, and phosphate ions in anoxic marine sediments. Limnol Oceanogr 25:797–806.

Kubeneck LJ, Lenstra WK, Malkin SY, Conley DJ, Slomp CP (2021) Phosphorus burial in vivianite-type minerals in methane-rich coastal sediments. Mar Chem 231:103948.

Kulakova AN, Hobbs D, Smithen M, Pavlov E, Gilbert JA, Quinn JP, McGrath JW (2011) Direct quantification of inorganic polyphosphate in microbial cells using 4′-6-diamidino-2-phenylindole (DAPI). Environ Sci Technol 45:7799–7803.

Lewin J (1966) Silicon metabolism in diatoms. v. germanium dioxide, a specific inhibitor of diatom growth. Phycologia 6:1–12.

Li F, Xiong X-S, Yang Y-Y, Wang J-J, Wang M-M, Tang J-W, Liu Q-H, Wang L, Gu B (2021) Effects of NaCl concentrations on growth patterns, phenotypes associated with virulence, and energy metabolism in *Escherichia coli* BW25113. Front Microbiol 12:705326.

Li J, Dittrich M (2019) Dynamic polyphosphate metabolism in cyanobacteria responding to phosphorus availability. Environ Microbiol 21:572–583.

Löptien U, Dietze H (2022) Retracing cyanobacteria blooms in the Baltic Sea. Sci Rep 12:10873.

Marin K, Zuther E, Kerstan T, Kunert A, Hagemann M (1998) The *ggpS* gene from *Synechocystis* sp. strain PCC 6803 encoding glucosyl-glycerol-phosphate synthase Is involved in osmolyte synthesis. J Bacteriol 180:4843–4849.

Martin P, Dyhrman ST, Lomas MW, Poulton NJ, van Mooy BAS (2014) Accumulation and enhanced cycling of polyphosphate by Sargasso Sea plankton in response to low phosphorus. Proceedings of the National Academy of Sciences 111:8089–8094.

Martin P, van Mooy BAS (2013) Fluorometric quantification of polyphosphate in environmental plankton samples: Extraction protocols, matrix effects, and nucleic acid interference. Appl Environ Microbiol 79:273–281.

Marzan L, Shimizu K (2011) Metabolic regulation of *Escherichia coli* and its *phoB* and *phoR* genes knockout mutants under phosphate and nitrogen limitations as well as at acidic condition. Microb Cell Fact 10:39.

Mazur-Marzec H, Żeglińska L, Pliński M (2005) The effect of salinity on the growth, toxin production, and morphology of *Nodularia spumigena* isolated from the Gulf of Gdańsk, southern Baltic Sea. J Appl Phycol 17:171–179.

McMahon KD, Read EK (2013) Microbial contributions to phosphorus cycling in eutrophic lakes and wastewater. Annu Rev Microbiol 67:199–219.

Moya A, Ferrer M (2016) Functional redundancy-induced stability of gut microbiota subjected to disturbance. Trends Microbiol 24:402–413.

Muhammad MH, Idris AL, Fan X, Guo Y, Yu Y, Jin X, Qiu J, Guan X, Huang T (2020) Beyond risk: Bacterial biofilms and their regulating approaches. Front Microbiol 11:928.

Munkes B, Löptien U, Dietze H (2021) Cyanobacteria blooms in the Baltic Sea: a review of models and facts. Biogeosciences 18:2347–2378.

Niazian M, Sadat-Noori SA, Tohidfar M, Mortazavian SMM, Sabbatini P (2021) Betaine aldehyde dehydrogenase (BADH) vs. flavodoxin (Fld): Two important genes for enhancing plants stress tolerance and productivity. Front Plant Sci 12:650215.

Nikel PI, Chavarría M, Martínez-García E, Taylor AC, de Lorenzo V (2013) Accumulation of inorganic polyphosphate enables stress endurance and catalytic vigour in *Pseudomonas putida* KT2440. Microb Cell Fact 12:50.

Nixon SW (1981) Remineralization and nutrient cycling in coastal marine ecosystems. In: *Estuaries and Nutrients*. Humana Press, Totowa, NJ, p 111–138

Olenina I, Hajdu S, Edler L, Andersson A, Wasmund N, Busch S, Göbel J, Gromisz S, Huseby S, Huttunen M, Jaanus A, Kokkonen P, Ledaine I, Niemkiewicz E (2006) Biovolumes and size-classes of phytoplankton in the Baltic Sea. In: *HELCOM Balt.Sea Environ. Proc. No. 106*. Baltic Marine Environment Protection Commission - Helsinki Commission, p 144

Paulmier A, Kriest I, Oschlies A (2009) Stoichiometries of remineralisation and denitrification in global biogeochemical ocean models. Biogeosciences 6:923–935.

Perkins RG, Underwood GJC (2001) The potential for phosphorus release across the sediment–water interface in an eutrophic reservoir dosed with ferric sulphate. Water Res 35:1399–1406.

Pokhrel A, Lingo JC, Wolschendorf F, Gray MJ (2019) Assaying for inorganic polyphosphate in bacteria. Journal of Visualized Experiments.

Pruesse E, Peplies J, Glöckner FO (2012) SINA: Accurate high-throughput multiple sequence alignment of ribosomal RNA genes. Bioinformatics 28:1823–1829.

Qiu G, Zuniga-Montanez R, Law Y, Thi SS, Nguyen TQN, Eganathan K, Liu X, Nielsen PH, Williams RBH, Wuertz S (2019) Polyphosphate-accumulating organisms in full-scale tropical wastewater treatment plants use diverse carbon sources. Water Res 149:496–510.

Quast C, Pruesse E, Yilmaz P, Gerken J, Schweer T, Yarza P, Peplies J, Glöckner FO (2012) The SILVA ribosomal RNA gene database project: improved data processing and web-based tools. Nucleic Acids Res 41:D590–D596.

Radzi R, Muangmai N, Broady P, Wan Omar WM, Lavoue S, Convey P, Merican F (2019) *Nodosilinea signiensis* sp. nov. (*Leptolyngbyaceae*, *Synechococcales*), a new terrestrial cyanobacterium isolated from mats collected on Signy Island, South Orkney Islands, Antarctica. PLoS One 14:e0224395.

Rao NN, Gómez-García MR, Kornberg A (2009) Inorganic polyphosphate: Essential for growth and survival. Annu Rev Biochem 78:605–647.

Reimers CE, Kastner M, Garrison RE (1990) The role of bacterial mats in phosphate mineralization with particular reference to the Monterey Formation. In: *Phosphate Deposits of the World: Vol. 3, Genesis of Neogene to Modern Phosphorites*. Riggs S.R., Burnett W.C. (eds) Cambridge University Press, p 301–311

Rier ST, Kinek KC, Hay SE, Francoeur SN (2016) Polyphosphate plays a vital role in the phosphorus dynamics of stream periphyton. Freshwater Science 35:490–502.

Rijal R, Cadena LA, Smith MR, Carr JF, Gomer RH (2020) Polyphosphate is an extracellular signal that can facilitate bacterial survival in eukaryotic cells. Proceedings of the National Academy of Sciences 117:31923–31934.

Rivas-Lamelo S, Benzerara K, Lefèvre CT, Monteil CL, Jézéquel D, Menguy N, Viollier E, Guyot F, Férard C, Poinsot M, Skouri-Panet F, Trcera N, Miot J, Duprat E (2017) Magnetotactic bacteria as a new model for P sequestration in the ferruginous Lake Pavin. Geochem Perspect Lett 5:35–41.

Sall SN, Masse D, Ndour NYB, Chotte J-L (2006) Does cropping modify the decomposition function and the diversity of the soil microbial community of tropical fallow soil? Applied Soil Ecology 31:211–219.

Sannigrahi P, Ingall E (2005) Polyphosphates as a source of enhanced P fluxes in marine sediments overlain by anoxic waters: Evidence from 31P NMR. Geochem Trans 6:52.

Santoro M, Hassenrück C, Labrenz M, Hagemann M (2023) Acclimation of *Nodularia spumigena* CCY9414 to inorganic phosphate limitation – Identification of the P-limitation stimulon via RNA-seq. Front Microbiol 13:1082763.

Santos-Beneit F (2015) The Pho regulon: a huge regulatory network in bacteria. Front Microbiol 6:402.

Sanz-Luque E, Bhaya D, Grossman AR (2020) Polyphosphate: A multifunctional metabolite in cyanobacteria and algae. Front Plant Sci 11.

de Scally SZ, Makhalanyane TP, Frossard A, Hogg ID, Cowan DA (2016) Antarctic microbial communities are functionally redundant, adapted and resistant to short term temperature perturbations. Soil Biol Biochem 103:160–170.

Schimel J, Balser TC, Wallenstein M (2007) Microbial stress-response physiology and its implications for ecosystem function. Ecology 88:1386–1394.

Schulz HD, Zabel M (2006) Marine Geochemistry, 1st ed. Schulz HD, Zabel M (eds) Springer-Verlag, Berlin/Heidelberg.

Schulz HN, Schulz HD (2005) Large sulfur bacteria and the formation of phosphorite. Science (1979) 307:416–418.

Schulz-Vogt HN, Pollehne F, Jürgens K, Arz HW, Beier S, Bahlo R, Dellwig O, Henkel J v., Herlemann DPR, Krüger S, Leipe T, Schott T (2019) Effect of large magnetotactic bacteria with polyphosphate inclusions on the phosphate profile of the suboxic zone in the Black Sea. ISME J 13:1198–1208.

Seeberg-Elverfeldt J, Schlüter M, Feseker T, Kölling M (2005) Rhizon sampling of porewaters near the sediment-water interface of aquatic systems. Limnol Oceanogr Methods 3:361–371.

Seiberling S, Stock M (2009) Renaturierung von Salzgrasländern bzw. Salzwiesen der Küsten. In: *Renaturierung von Ökosystemen in Mitteleuropa*. Spektrum Akademischer Verlag, Heidelberg

Selby K, Lindström M, Somervuo P, Heap JT, Minton NP, Korkeala H (2011) Important role of class I heat shock genes *hrcA* and *dnaK* in the heat shock response and the response to pH and NaCl stress of group I *Clostridium botulinum* strain ATCC 3502. Appl Environ Microbiol 77:2823–2830.

Shapiro J, Levin G V., Zea G. H (1967) Anoxically induced release of phosphate in wastewater treatment. J Water Pollut Control Fed 39:1810–1818.

Shi X, Yang L, Niu X, Xiao L, Kong Z, Qin B, Gao G (2003) Intracellular phosphorus metabolism of *Microcystis aeruginosa* under various redox potential in darkness. Microbiol Res 158:345–352.

Shiba T, Itoh H, Kameda A, Kobayashi K, Kawazoe Y, Noguchi T (2005) Polyphosphate:AMP phosphotransferase as a polyphosphate-dependent nucleoside monophosphate kinase in *Acinetobacter johnsonii* 210A. J Bacteriol 187:1859–1865.

Strickland JDH, Parsons TR (1968) A practical handbook of seawater analysis, 2nd ed. Bulletin of Fisheries Research Board of Canada, Ottawa.

Sulu-Gambari F, Hagens M, Behrends T, Seitaj D, Meysman FJR, Middelburg J, Slomp CP (2018) Phosphorus cycling and burial in sediments of a seasonally hypoxic marine basin. Estuaries and Coasts 41:921–939.

Sundberg C, Al-Soud WA, Larsson M, Alm E, Yekta SS, Svensson BH, Sørensen SJ, Karlsson A (2013) 454 pyrosequencing analyses of bacterial and archaeal richness in 21 full-scale biogas digesters. FEMS Microbiol Ecol 85:612–626.

Sundby B, Gobeil C, Silverberg N, Alfonso M (1992) The phosphorus cycle in coastal marine sediments. Limnol Oceanogr 37:1129–1145.

Tully BJ, Wheat CG, Glazer BT, Huber JA (2018) A dynamic microbial community with high functional redundancy inhabits the cold, oxic subseafloor aquifer. ISME J 12:1–16.

Wagner D, Rinnenthal J, Narberhaus F, Schwalbe H (2015) Mechanistic insights into temperature-dependent regulation of the simple cyanobacterial *hsp17* RNA thermometer at base-pair resolution. Nucleic Acids Res 43:5572–5585.

Wasmund N (1997) Occurrence of cyanobacterial blooms in the Baltic Sea in relation to environmental conditions. Internationale Revue der gesamten Hydrobiologie und Hydrographie 82:169–184.

Watson SJ, Cade-Menun BJ, Needoba JA, Peterson TD (2018) Phosphorus forms in sediments of a river-dominated estuary. Front Mar Sci 5:302.

Wetzel RG (2001) The phosphorus cycle. In: *Limnology*, 3rd ed. Elsevier, p 239–288

Whiles MR, Huryn AD, Taylor BW, Reeve JD (2009) Influence of handling stress and fasting on estimates of ammonium excretion by tadpoles and fish: recommendations for designing excretion experiments. Limnol Oceanogr Methods 7:1–7.

Wilfert P, Meerdink J, Degaga B, Temmink H, Korving L, Witkamp GJ, Goubitz K, van Loosdrecht MCM (2020) Sulfide induced phosphate release from iron phosphates and its potential for phosphate recovery. Water Res 171:115389.

Williams LA, Reimers C (1983) Role of bacterial mats in oxygen-deficient marine basins and coastal upwelling regimes: Preliminary report. Geology 11:267.

Yallop ML, de Winder B, Paterson DM, Stal LJ (1994) Comparative structure, primary production and biogenic stabilization of cohesive and non-cohesive marine sediments inhabited by microphytobenthos. Estuar Coast Shelf Sci 39:565–582.

Yoo NG, Dogra S, Meinen BA, Tse E, Haefliger J, Southworth DR, Gray MJ, Dahl J-U, Jakob U (2018) Polyphosphate stabilizes protein unfolding intermediates as soluble amyloid-like oligomers. J Mol Biol 430:4195–4208.

Yu J, Ding S, Zhong J, Fan C, Chen Q, Yin H, Zhang L, Zhang Y (2017) Evaluation of simulated dredging to control internal phosphorus release from sediments: Focused on phosphorus transfer and resupply across the sediment-water interface. Science of The Total Environment 592:662–673.

Zhou A, Tang H, Wang D (2005) Phosphorus adsorption on natural sediments: Modeling and effects of pH and sediment composition. Water Res 39:1245–1254.

7 Supplementary

Table S1. Automated particle analysis of 7 surface peat layer replicates during the winter showing the average weight% of Mg, Al, Si, P, Ca, and Fe in P-associated particles, using SEM-EDX. The standard deviations are displayed in brackets. n = number of particles

Replicate	Particle	*n*	Mg	Al	Si	P	Ca	Fe
1	Fe oxyhydroxide	28	0.7	0.6	2.1	3.0	0.8	55.3
			(1.1)	(1.0)	(2.7)	(1.3)	(1.0)	(5.8)
	Plagioclase	3	1.8	8.2	14.9	2.1	7.6	10.1
			(0.5)	(2.2)	(0.9)	(0.8)	(5.8)	(2.5)
	Illite	5	2.3	9.7	21.9	1.9	1.8	7.0
			(1.8)	(1.3)	(4.3)	(0.5)	(1.1)	(4.9)
	Organic	3	3.2	6.5	7.6	8.1	5.3	16.0
			(4.6)	(3.1)	(1.3)	(6.0)	(1.1)	(3.4)
2	Fe oxyhydroxide	36	0.8	0.5	2.3	3.2	1.7	55.4
			(1.1)	(0.9)	(2.0)	(0.9)	(1.3)	(5.1)
	Plagioclase	2	2.9	6.3	15.8	1.8	3.2	0.0
			(0.5)	(1.0)	(1.7)	(0.6)	(0.1)	(0.0)
	Illite	3	2.3	10.2	22.0	1.9	1.1	9.2
			(0.4)	(1.0)	(2.0)	(0.4)	(1.2)	(3.4)
	Organic	14	2.1	1.8	9.0	5.6	5.9	25.1
			(2.2)	(2.3)	(2.4)	(1.8)	(7.9)	(16.1)
3	Fe oxyhydroxide	38	1.0	0.1	2.1	3.0	1.6	55.7
			(1.2)	(0.3)	(1.5)	(1.1)	(1.2)	(3.9)
	Plagioclase	3	2.7	5.9	16.4	2.1	4.3	7.7
			(0.2)	(1.1)	(2.7)	(1.0)	(1.2)	(9.9)
	Illite	4	2.4	8.8	24.1	2.2	1.4	8.4
			(0.8)	(1.1)	(4.5)	(2.1)	(1.0)	(0.9)
	Organic	8	3.2	3.9	9.6	5.2	5.1	25.9
			(1.7)	(2.7)	(3.8)	(1.6)	(7.9)	(12.4)
4	Fe oxyhydroxide	50	0.8	0.6	2.8	3.1	1.5	54.4
			(1.0)	(0.9)	(1.6)	(1.0)	(0.9)	(4.0)
	Plagioclase	3	2.2	6.8	17.8	1.5	4.6	8.6
			(2.6)	(0.9)	(3.2)	(0.3)	(0.8)	(7.2)
	Illite	4	2.4	8.7	20.8	1.3	1.4	9.7
			(0.1)	(1.9)	(3.2)	(0.3)	(1.0)	(3.3)
	Organic	18	2.5	3.7	11.4	6.1	5.0	21.0
			(1.9)	(3.2)	(4.0)	(2.4)	(5.9)	(14.6)
5	Fe oxyhydroxide	44	0.5	0.4	2.6	2.7	1.2	56.1
			(0.7)	(0.8)	(1.7)	(0.9)	(0.7)	(4.2)
	Plagioclase	2	4.1	5.9	16.8	2.8	5.5	2.4
			(0.1)	(1.2)	(1.5)	(0.7)	(1.4)	(3.4)
	Illite	4	2.1	7.8	23.5	1.3	1.2	9.8
			(0.4)	(1.3)	(2.3)	(0.2)	(0.9)	(3.7)
	Organic	13	1.8	1.5	8.4	4.8	8.1	27.9
			(1.9)	(1.3)	(2.8)	(1.3)	(10.9)	(15.7)
6	Fe oxyhydroxide	95	0.5	0.4	2.6	2.7	1.0	56.2

			(0.8)	(0.7)	(2.0)	(1.0)	(0.7)	(4.4)
	Plagioclase	2	2.2	7.0	20.5	1.4	3.2	5.8
			(0.5)	(1.3)	(2.1)	(0.5)	(0.2)	(2.4)
	Illite	3	2.1	9.7	22.5	1.1	1.2	11.4
			(0.2)	(1.8)	(1.8)	(0.1)	(0.2)	(2.0)
	Organic	12	1.1	1.5	10.0	5.1	8.4	26.3
			(1.1)	(1.6)	(3.0)	(1.8)	(10.7)	(17.1)
7	Fe oxyhydroxide	35	1.1	0.7	2.7	3.1	1.2	54.7
			(0.9)	(1.1)	(1.6)	(1.0)	(0.7)	(4.4)
	Plagioclase	5	3.4	5.9	18.4	2.2	4.6	3.8
			(1.1)	(0.2)	(1.9)	(1.7)	(2.4)	(3.7)
	Illite	6	2.1	9.1	21.8	1.6	1.6	9.8
			(0.5)	(1.7)	(2.6)	(0.5)	(1.4)	(3.3)
	Organic	12	2.5	2.3	10.1	6.3	9.7	17.3
			(2.0)	(2.4)	(2.4)	(2.6)	(10.3)	(15.0)

Table S2. Commonly known P metabolism-associated genes in bacteria linked to polyP metabolism, derived from various literature sources (Marzan & Shimizu 2011, Santos-Beneit 2015, Santoro et al. 2023)

Gene	KEGG orthology identifier	Product
Elongation and degradation of organic P		
ppk1	K00937	polyphosphate kinase
ppk2	K22468	polyphosphate kinase
pap	K23753	polyphosphate:AMP phosphotransferase
ppx-gppA	K01524	exopolyphosphatase-guanosine pentaphosphate phosphohydrolase
ppnK	K00858	polyphosphate/ATP-dependent NAD kinase
ppgK	K00886	polyphosphate/ATP-dependent glucokinase
ppa	K01507	inorganic pyrophosphatase
surE	K03787	periplasmic acid phosphatase
Scavenging of inorganic P		
phoA	K01077	alkaline phosphatase
phoB	K07657	phosphate regulon transcriptional regulatory protein
phoD	K01113	alkaline phosphatase
phoR	K07636	histidine kinase sensor protein
$phoA^{ATP}$	K08693	2',3' cyclic nucleotide phosphodiesterase
ugpQ	K01126	glycerophosphodiester phosphodiesterase
glpQ	K17323	glycerophosphodiester phosphodiesterase
lysR	K02521	transcriptional regulator
Phosphate-specific transport		
phoU	K02039	phosphate-specific transport system accessory protein
pstA	K02038	phosphate transport system permease protein
pstB	K02036	phosphate import ATP-binding protein
pstC	K02037	phosphate transport system permease

		protein
pstS	K02040	phosphate-binding protein
Phosphonate transport		
phnC	K02041	phosphonate ABC transporter ATP-binding protein
phnD	K02044	phosphonate ABC transporter ATP-binding protein
phnE	K02042	phosphonate ABC transporter permease
phnF	K02043	component of a C-P lyase
phnG	K06166	component of a C-P lyase
phnH	K06165	component of a C-P lyase
phnJ	K06163	component of a C-P lyase
phnK	K05781	component of a C-P lyase
phnL	K05780	component of a C-P lyase
phnM	K06162	component of a C-P lyase

Table S3. Major stress-associated genes in bacteria, derived from various literature sources (Genevaux et al. 2007, Ballal & Manna 2010, Ito et al. 2014, Klähn et al. 2021)

Gene	KEGG orthology identifier	Product
Heat/general stress		
clpB	K03695	chaperone protein
htpG	K04079	chaperone protein hsp90
dnaK	K04043	chaperone protein hsp70
hscA	K04044	chaperone protein
dnaJ	K03686	chaperone protein
cbpA	K05516	curved DNA-binding protein
grpE	K03687	nucleotide exchange factor
groEL	K04077	chaperonin
hsp17	K13993	heat shock protein
rpoS	K03087	RNA polymerase sigma factor
sigB	K03090	RNA polymerase sigma factor
ggpS	K13789	glucosylglycerol-phosphate synthase
Salinity/general stress		
trxB	K00384	thioredoxin reductase
msrR	K01005	XRE family transcriptional regulator
sll1566	K03692	glucosylglycerol-phosphate synthase
stpA	K05978	curved DNA-binding protein
dnaK1	K04043	chaperone protein hsp70
dnaK2	K04043, K04046	chaperone protein hsp70
sll1037	K07080	putative component of TRAP transporter
slr0750	K04038	light-independent protochlorophyllide reductase subunit N
slr0786	K01265	methionine aminopeptidase B
sll0248	K03839	flavodoxin (IsiB)
sll1988	K04083	33 kDa chaperonin (HSP33)
sll0947	K05808	light-repressed protein A, LrpA

slr2019	K06147	putative ATP binding subunit of ABC transporter
slr1894	K04047	general stress protein MrgA/Dps
sod2	K04564	superoxide dismutase

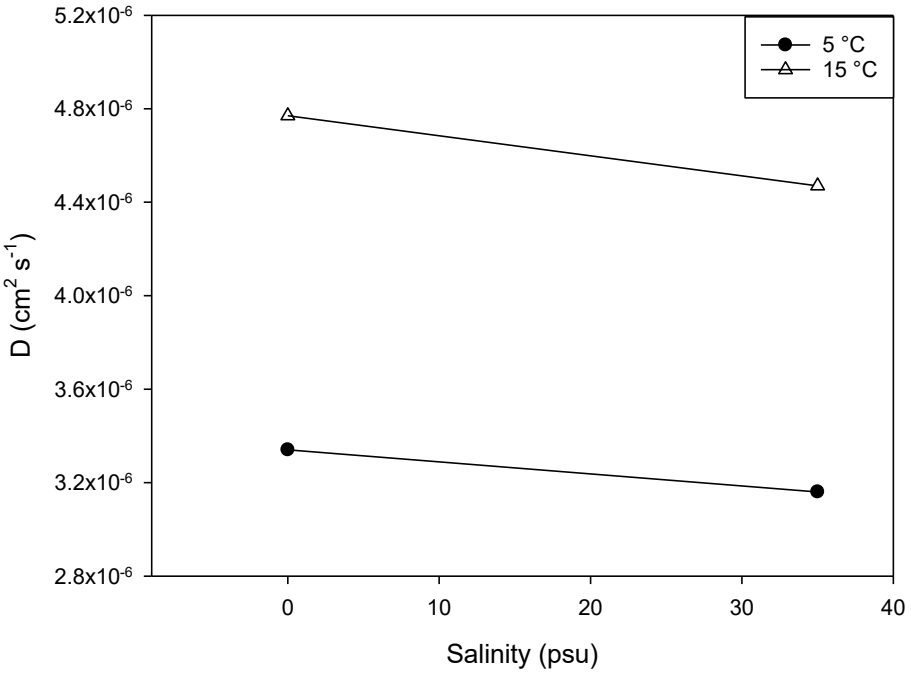

Fig. S1. Linear relations of the diffusion coefficient D with respect to salinity, approximated by 2 data points (D_0 and D_{35}) for each given temperature, with D_0 and D_{35} denoting the diffusion coefficient in pure water and water at 35 psu, respectively. Coefficient D_0 was derived from the model of Boudreau (1997), while coefficient D_{35} was derived from the model of Schulz and Zabel (2006). The D value for each given temperature was then further corrected for salinity (5.8 psu in winter cores) using the above linear relations, and finally corrected for porosity using the model of Berg et al. (1998)

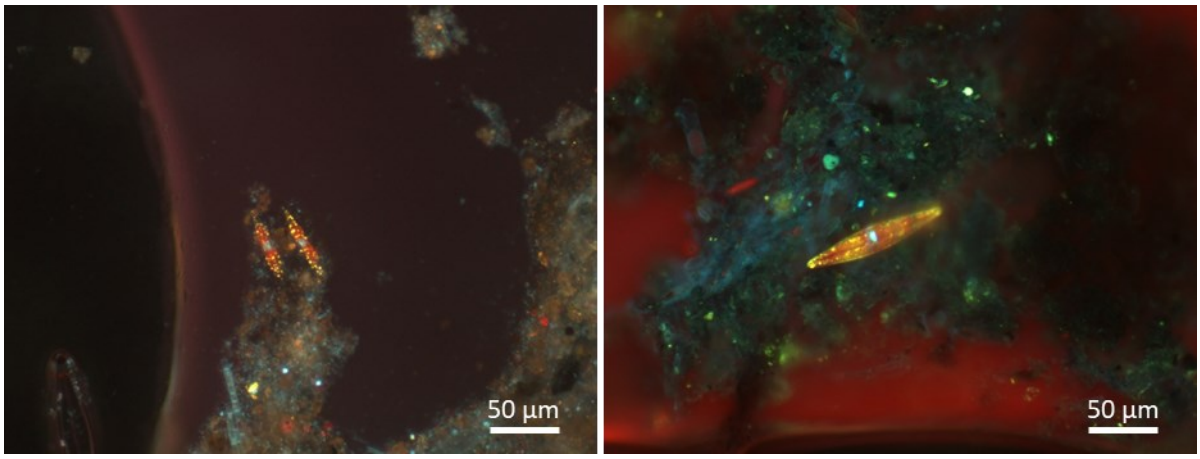

Fig. S2. PolyP inclusions were detected in diatoms with morphology like that of naviculoids, in surface peat layer samples from the winter cores on Day 0. The diatoms were extremely sparse in comparison to the number of polyP-containing filaments in the samples

8 List of Figures

10 List of Tables

11 Glossary

N1-2	Replicate 1, time point 2 h, *in-situ* treatment
N2-2	Replicate 2, time point 2 h, *in-situ* treatment
N3-2	Replicate 3, time point 2 h, *in-situ* treatment
N4-2	Replicate 4, time point 2 h, *in-situ* treatment
N1-24	Replicate 1, time point 24 h, *in-situ* treatment
N2-24	Replicate 2, time point 24 h, *in-situ* treatment
N3-24	Replicate 3, time point 24 h, *in-situ* treatment
N4-24	Replicate 4, time point 24 h, *in-situ* treatment
N1-48	Replicate 1, time point 48 h, *in-situ* treatment
N3-48	Replicate 3, time point 48 h, *in-situ* treatment
T1-0	Replicate 1, time point ‘0’, elevated temperature treatment
T2-2	Replicate 1, time point 2 h, elevated temperature treatment
T3-2	Replicate 2, time point 2 h, elevated temperature treatment
T4-2	Replicate 3, time point 2 h, elevated temperature treatment
T1-24	Replicate 1, time point 24 h, elevated temperature treatment
T2-24	Replicate 2, time point 24 h, elevated temperature treatment
T3-24	Replicate 3, time point 24 h, elevated temperature treatment
T4-24	Replicate 4, time point 24 h, elevated temperature treatment
T1-48	Replicate 1, time point 48 h, elevated temperature treatment
T2-48	Replicate 2, time point 48 h, elevated temperature treatment
T3-48	Replicate 3, time point 48 h, elevated temperature treatment
T4-48	Replicate 4, time point 48 h, elevated temperature treatment
S1-0	Replicate 1, time point ‘0’, reduced salinity treatment
S2-0	Replicate 2, time point ‘0’, reduced salinity treatment
S3-0	Replicate 3, time point ‘0’, reduced salinity treatment
S4-0	Replicate 4, time point ‘0’, reduced salinity treatment
S1-2	Replicate 1, time point 2 h, reduced salinity treatment
S2-2	Replicate 2, time point 2 h, reduced salinity treatment
S3-2	Replicate 3, time point 2 h, reduced salinity treatment

S4-2	Replicate 4, time point 2 h, reduced salinity treatment
S1-24	Replicate 1, time point 24 h, reduced salinity treatment
S2-24	Replicate 2, time point 24 h, reduced salinity treatment
S3-24	Replicate 3, time point 24 h, reduced salinity treatment
S4-24	Replicate 4, time point 24 h, reduced salinity treatment
S1-48	Replicate 1, time point 48 h, reduced salinity treatment
S2-48	Replicate 2, time point 48 h, reduced salinity treatment
S3-48	Replicate 3, time point 48 h, reduced salinity treatment
S4-48	Replicate 4, time point 48 h, reduced salinity treatment

12 Acknowledgements

Throughout this doctoral study, I have received support and guidance from several individuals. In this regard, I am especially grateful to:

Foremost, my main supervisor Prof. Dr. Heide Schulz-Vogt, with whom I could always comfortably bounce ideas off, whose door was always open when I needed advice, and who always encouraged me to push my boundaries and realize my potential,

Dr. Olaf Dellwig for believing in my study amidst the challenges, and dedicating a great amount of time and effort to deepening and sharpening my understanding of geochemistry,

Prof. Dr. Maren Voß for being a part of my thesis committee, always asking after me, and offering research advice every time I came by the office,

Dr. Christiane Hassenrück for the detailed support and guidance on the bioinformatics portion of my thesis, especially the tremendous effort, time, and patience in helping me to understand the fundamentals of the pipelines,

Dr. Janine Wäge-Recchioni and Dr. Philipp Braun, for the research and administrative advice, guidance on DNA extractions and polyphosphate measurement in the lab,

Members of the working group and biology department for the care and concern, in particular Christin Laudan for the patient guidance in the lab, and for the nice conversations we had, Dr. Jenny Fabian for the enjoyable philosophical talks, especially while working in the lab during late evenings, Christian Meeske for guidance on the entire DNA/RNA extraction and preparation process, and Christian Burmeister for readily conducting nutrient measurements of my samples,

The colleagues from Marine Geology, Anne Köhler for the measurement of my ICP-OES samples, Iris Schmiedinger for the guidance in sulfide measurements, and Sascha Plewe for the measurement of my SEM-EDX samples,

The colleagues in the Baltic TRANSCOAST project for the advice and conversations, and importantly being my home-away-from-home (you know who you are),

Fellow IOW Ph.D. colleagues from other working groups for the camaraderie, the knowledge that “we’re all in this together”, and the frank conversations (aside from the trash-talk),

And never forgetting my family and friends back home, whom I never cease thinking about, and who spurred me on through deepest doubts, so thank you for it all.

13 Declaration of Authorship

I hereby declare that I wrote this thesis independently and have not used any other sources, aside from those that I have clearly marked as citations in my reference list. All copies of this thesis are identical. I also prepared all figures and tables on my own, unless otherwise credited. Lastly, I confirm that this thesis was not previously submitted at any other institution.

Simeon Choo Rostock, 14.04.2023

14 Curriculum Vitae

Name: Simeon Choo

Contact: simeon.choo@io-warnemuende.de; simeon.choo@uni-rostock.de

EDUCATION

University of Rostock **Mar 2019 – Jul 2023**

- PhD (Dr. rer. nat) in Microbiology (Magna cum laude)
- Thesis: "Microbial-driven phosphate flux via polyphosphate accumulation in the benthic layer"
- Member of the DFG-funded Baltic TRANSCOAST Project
- In cooperation with the Leibniz Institute for Baltic Sea Research Warnemünde (IOW)

University of Kiel **Oct 2016 – Oct 2018**

- MSc Biological Oceanography
- Thesis: "*Polaribacter* spp. from marine habitats – biodiversity and biotechnological potential"
- Funded by ERA-NET Marine Biotechnology: 'ProBone - New tools for prospecting the marine bone-degrading microbiome for new enzymes' (FKZ 031B0570)
- In cooperation with the Helmholtz Centre for Ocean Research Kiel (GEOMAR)

National University of Singapore, Singapore **Aug 2010 – Jul 2014**

- BEng (Biomedical Engineering)
- Thesis: "Coral Bioengineering "
- Funded by the Evolution Innovation Lab (PI: Prof. Dr Raye Yeow)

University of Stuttgart, Germany **Mar – Aug 2013**

- Student Exchange Programme

PUBLICATIONS

Choo, S., Borchert, E., Wiese, J., Saha, M., Künzel, S., Weinberger, F., & Hentschel, U. (2020). *Polaribacter Septentrionalilitoris* sp. nov., isolated from the biofilm of a stone from the North Sea. *International Journal of Systematic and Evolutionary Microbiology*, *70*(7), 4305–4314. https://doi.org/10.1099/ijsem.0.004290

Choo, S., Dellwig, O., Wäge-Recchioni, J., & Schulz-Vogt, H. N. (2022). Microbial-driven impact on aquatic phosphate fluxes in a coastal peatland. *Marine Ecology Progress Series*, *702*, 19–38. https://doi.org/10.3354/meps14210

Li, J., Yu, Z., Choo, S., Zhao, J., Wang, Z., & Xie, R. (2020). Chemico-proteomics reveal the enhancement of salt tolerance in an invasive plant species via H2S signaling. *ACS Omega*, *5*(24), 14575–14585. https://doi.org/10.1021/acsomega.0c01275

PRESENTATIONS

Oral

Choo S., Langer, S., Schulz.Vogt, HN. Microbial life and phosphorus cycling along salinity and redox gradients. 3rd Baltic Earth Conference, virtual session, June 2020

Choo S., Dellwig O., Wäge-Recchioni J., Schulz-Vogt HN. Microbial-driven impact on aquatic phosphate fluxes in shallow coastal sediments. European Geosciences Union (EGU) General Assembly, virtual session, April 2021

Racasa ED., Kienzler J., Ahmad S., Batistel C., Choo S., Wang M., Jenner A-K., Lennartz B., Janssen M. Seasonal dynamics of submarine groundwater discharge from a rewetted coastal peatland. European Geosciences Union (EGU) General Assembly, on-site, Vienna, Austria, April 2023

Poster

Choo S., Langer S., Schulz-Vogt HN. Microbial life and phosphorus cycling along salinity and redox gradients. 16th Symposium of Aquatic Microbial Ecology (SAME16), Potsdam, Germany, September 2019

Choo S., Wiese J., Borchert E., Hentschel U. *Polaribacter septentrionalilitoris* sp. nov., isolated from the biofilm of a stone from the North Sea. Annual Conference 2020 of the Association for General and Applied Microbiology (VAAM), Leipzig, Germany, March 2020

OTHER SCIENTIFIC CONTRIBUTIONS

- Journal reviewer (2022) for Chemical Geology (ISSN 0009-2541)